Starch-Based Composites Using Mature Fine Tailings as Fillers

by

Daniel A. Moran Nava

A thesis submitted in partial fulfillment of the requirements for the degree of

Master of Science

in

Chemical Engineering

Department of Chemical and Materials Engineering
University of Alberta

Abstract

Mature fine tailings (MFT) are one of the major problems of the oil sands industry in Alberta, specifically due to the reclamation of the land filled with them. Stepping away from the most common approach of dewatering processes, this research is based on the manufacture of useful composite materials using MFT as filler to help mitigate the negative environmental effect of the oil sands industry. Thermoplastic starch was chosen as matrix because it is hydrophilic, easy to obtain, and there are several comparative studies of thermoplastic starch composites with different types of fibers and clays. Using glycerol as a plasticizer and MFT as filler for the synthesis of the composites, the morphology, water resistance and mechanical properties of the composites were studied while changing filler percentage. Changes in mechanical properties with temperature were also investigated through dynamic mechanical analysis. The MFT composites were compared to composites made with montmorillonite (MMT), cellulose nanocrystals (CNC) and Dean Stark solids (DS) as fillers. MFT composites showed a slight density increase of 0.06 g/ml after addition of 5% MFT, but the density always stayed in the same range as the rest of the composites. The water resistance of MFT and DS composites was similar and higher than the water resistance of MMT composites, but the improvement in water resistance was only 6% with the highest loading of filler. The total disruption of the starch granule after the composites preparation was proven through x-ray diffraction. Although there was not intercalation in MFT or DS composites, these showed similar and better mechanical properties than plasticized starch, with an increasing tensile and compressive modulus with increasing filler content. Despite the higher tensile modulus increase in intercalated MMT and CNC composites up to 5% filler, the MFT composites with filler contents higher than 5% achieved the same tensile modulus values, which is beneficial to MFT reduction, since more

MFT is removed from the environment to make composites this way. MFT and DS composites also showed similar and better compressive modulus and strength than MMT composites and CNC composites. The dynamic mechanical analysis of the composites determined two thermal transitions in the composites related to a plasticizer rich phase and a starch rich phase, demonstrating the heterogeneity of the composites.

Acknowledgments

I would like to acknowledge and express my gratitude to my supervisor Dr. Joao Soares for his continuous guidance, encouragement, technical and financial support. I also want to thank him for giving me the opportunity to work in such a nice area from engineering.

I would like to thank my colleagues Vahid Vajihinejad, Sarang Gumfekar and Linda Botha for their continuous support throughout my research and our discussions on the project. Especial thanks to Preetam Anbukarasu for his support on the tensile testing of the materials.

I am very grateful to my wife, my parents and brothers, since their love, support and encouragement have kept me going in good and bad moments during my studies. They are my motivation in life to achieve my goals.

Table of contents

Abstract ii
Acknowledgments iv
Table of Contents v
List of Tables viii
List of Figures x
Nomenclature xii

Chapter 1. Introduction **1**
Chapter 2. Literature Review **6**
2.1 Oil Sands Mature Fine Tailings 6
2.2 Polymer Composites 7
2.3 Starch 8
2.3.1 Starch gelatinization and retrogradation 11
2.3.2 Thermoplastic starch 11
2.3.3 Starch based polymer composites 12
2.4 Characterization of Starch-Based Polymer Composites 13
2.5 Summary 20
References 21
Chapter 3. Materials, Methods and Raw Materials Characterization **27**
3.1 General 27
3.2 Materials 27
3.3 Methods for Raw Materials Characterization 27
3.3.1 Starch characterization 27
3.3.1.1 Amylose content 28
3.3.1.2 Moisture measurement 28
3.3.1.3 Gelatinization temperature 28
3.3.1.4 X-ray diffraction (XRD) 29
3.3.2 MFT characterization 29
3.3.2.1 MFT composition 29

3.3.2.2 X-ray diffraction 30
3.3.2.3 Particle size distribution 31
3.3.3 Dean Stark solids characterization 31
3.3.3.1 Thermogravimetric analysis (TGA) 31
3.3.3.2 X-ray diffraction 31
3.4 Methods for Starch-Based Composites Preparation.....31
3.5 Methods for Starch-Based Composites Characterization 34
3.5.1 Water absorption 34
3.5.2 Scanning electron microscopy 35
3.5.3 Tensile test 35
3.5.4 Compression test 36
3.5.5 Dynamic mechanical analysis 36
3.5.6 Density 36
3.5.7 X-Ray diffraction (XRD) 37
3.6 Raw Materials Characterization 37
3.6.1 Starch characterization 37
3.6.1.1 Estimated amylose content in starch 37
3.6.1.2 Moisture content in commercial starch. 38
3.6.1.3 Determination of gelatinization temperature 38
3.6.2. Mature fine tailings characterization 39
3.6.2.1 Composition of MFT 39
3.6.2.2 Particle size distribution 40
3.6.3 Dean Stark solids characterization 40
3.7 Summary 41
References 42
Chapter 4. Mature Fine Tailings Composites Characterization 43
4.1 General 43
4.2 Morphology of Composites 43
4.3 Density 48
4.4 X-Ray Diffraction (XRD) 50
4.5 Water Absorption 54

4.6 Tensile Properties 57
4.7 Compressive Properties 61
4.8 Dynamic Mechanical Analysis (DMA) 63
4.9 Summary 70
References 70
Chapter 5. Conclusions and Recommendations **73**
5.1 Conclusions 73
5.2 Recommendations 75
Bibliography **76**
Appendix A. Determination of amylose content of Starches–Modification of ISO 6647-1...**84**
Appendix B. data for Composites Characterization **88**
Appendix C. Thermal Conductivity Measurement of MFT composites **116**

List of tables

Table 3.1. Composition of mixture for the preparation of three thin sheets (3.4 mm thickness sheets) of MFT composites 32
Table 3.2. Composition of mixture for the preparation of thick sheets (12.5 mm thickness sheets) of MFT composites 32
Table 3.3. Composition of mixture for the preparation of three thin sheets (3.4 mm thickness sheets) of Dean Stark, Na^+ Cloisite, and Cellulose Nanocrystals composites 32
Table 3.4. Composition of mixture for the preparation of thick sheets (12.5 mm thickness sheets) of Dean Stark, Na^+ Cloisite, and Cellulose Nanocrystals composites 33
Table 3.5. Estimated amylose content of commercial starch used for composites preparation 38
Table 3.6. Moisture measurement of commercial starch samples.....38
Table A.1. Mixture of amylose and amylopectin solution for calibration curve.....86
Table B.1. Measurements of sides of specimens for apparent density determination.....88
Table B.2. Measurement of thickness, mass, and calculation of average volume of specimens for apparent density determination 92
Table B.3. Calculated apparent density of specimens, average density of composites, and standard deviation 96
Table B.4. Initial weight, weight after first drying, weight after 2-hour immersion in water and final dry weight after immersion, measured according to ASTM D570-98 101
Table B.5. Initial moisture, water uptake, and mass loss of specimens with corresponding averages and standard deviations 103
Table B.6. Measured values of tensile modulus, tensile strength and strain at break 105
Table B.7. Average tensile modulus, tensile strength and strain at break for starch-based composites, with their respective standard deviation 111
Table B.8. Measured values of compressive modulus, compressive strength and compression at break 113
Table B.9. Average compressive modulus, compressive strength and compression at break for starch-based composites, with their respective standard deviation 115

List of figures

Figure 2.1. Amylose (a) and Amylopectin (b) molecules 9
Figure 2.2. a) Schematic representation of the growth rings in the starch granule, as would be observed under Scanning Electron Microscopy; b) Designation of chains present in amylopectin 10
Figure 2.3. Changes of the starch granule in the presence of water during gelatinization and retrogradation 11
Figure 2.4. Typical Stress-strain curve for brittle, ductile and rubbery materials.....16
Figure 2.5. Stress-strain curve indicating general tensile properties of materials.....17
Figure 2.6. Typical modulus vs temperature curves for amorphous (a) and semi-crystalline polymers (b) 19
Figure 3.1. Dean Stark apparatus for MFT composition determination 29
Figure 3.2. Stirrer set up for composites preparation 33
Figure 3.3. Mold used for thin (3.4 mm thickness) sheets 34
Figure 3.4. Calibration curve for amylose content determination.....37
Figure 3.5. Thermogram of commercial cornstarch, indicating the gelatinization temperature range 39
Figure 3.6. Volume density and number density of MFT particles 40
Figure 3.7. Thermogravimetric analysis of Dean Stark Solids 41
Figure 4.1. Surface, edge and transversal cut of thermoplastic starch (a,b,c) and 1% MFT composite (d,e,f) respectively 43
Figure 4.2. SEM of plasticized starch and MFT composites: a) Plasticized starch; b) 2% MFT composite; c) 5% MFT composite 44
Figure 4.3. SEM micrographs of MFT composites showing clays and bitumen: a) clay agglomerates on a 2% MFT composite; b) bright spots on clay agglomerates of a 2% MFT composite, indicating the presence of fine particles; c) clay agglomerates on a 5% MFT composite; d) fine particles on clay agglomerates of a 5% MFT composite 45
Figure 4.4. SEM of a 2% DS composite showing surface and clays: a) surface; b) clay agglomerates; c) fine particles on clay agglomerates 46

Figure 4.5. SEM micrographs of MMT composites: a) surface of a 2% MMT composite; b) clays embedded in the starch matrix of a 2% MMT composite; c) surface of a 5% MMT composite; d) edges of clays embedded in the starch matrix of a 5% MMT composite.....47
Figure 4.6. SEM micrographs of CNC composites: a) surface of a 2% CNC composite; b) bright segments and spots on the surface of a 2% CNC composite that might indicate the presence of nanocrystals; c) surface of a 5% CNC composite; d) bright segments and spots on the surface of a 5% CNC composite surface 48
Figure 4.7. Density of MFT composites as a function of filler content 49
Figure 4.8. Comparison of densities between MFT, MMT and CNC composites 49
Figure 4.9. Comparison of densities between MFT and Dean Stark composites 50
Figure 4.10. Diffractogram of raw starch and plasticized starch 51
Figure 4.11. Diffractogram of MFT, plasticized starch, and MFT composites 52
Figure 4.12. Diffractogram of Dean Stark solids, plasticized starch, and DS composites 52
Figure 4.13. Diffractogram of Na^{+}MMT, plasticized starch and MMT composites 53
Figure 4.14. Diffractogram of cellulose nanocrystals, plasticized starch, and CNC composites 54
Figure 4.15. Water uptakes of MFT and MMT composites 55
Figure 4.16. Water uptake of MFT and DS composites 55
Figure 4.17. Initial moisture of MFT, DS and MMT composites (a); Mass loss of MFT and MMT composites (b); Mass loss of MFT and DS composites (c) 56
Figure 4.18. Tensile modulus of MFT composites as a function of filler content 57
Figure 4.19. Tensile strength of MFT composites as a function of filler content 58
Figure 4.20. Strain at break of MFT composites as a function of filler content 58
Figure 4.21. Tensile properties of MFT, MMT and CNC composites: (a) Tensile Modulus; (b) Tensile strength; (c) Strain at break 59
Figure 4.22. Tensile properties of MFT and DS composites: (a) Tensile Modulus; (b) Tensile strength; (c) Strain at break 60
Figure 4.23. Compressive properties of MFT composites: (a) Compressive Modulus; (b) Compressive strength; (c) Strain at break 61
Figure 4.24. Compressive properties of MFT, DS, MMT, and CNC composites: (a) Compressive Modulus; (b) Compressive strength; (c) Strain at break 62

Figure 4.25. Storage Modulus of Plasticized Starch and MFT composites as a function of temperature 63
Figure 4.26. Loss modulus of Plasticized Starch and MFT composites as a function of temperature 64
Figure 4.27. Loss Factor Tan δ of Plasticized Starch and MFT composites with temperature 65
Figure 4.28. Storage modulus (a) and loss factor Tan δ (b) of Plasticized Starch and DS composites as a function of temperature 66
Figure 4.29. Storage modulus (a) and loss factor Tan δ (b) of Plasticized Starch and MMT composites as a function of temperature 67
Figure 4.30. Storage modulus of (a) 2% MFT, DS and MMT composites and (b) 5% MFT, DS and MMT composites as a function of temperature 68
Figure 4.31. Loss factor Tan δ of (a) 2% MFT, DS and MMT composites and (b) 5% MFT, DS and MMT composites as a function of temperature 69
Figure C.1. Thermal conductivity of MFT, DS, and MMT composites as a function of filler content 117

Nomenclature

ASTM	American Society for Testing and Materials
CNC	Cellulose Nanocrystals
CT	Consolidated Tailings
DMA	Dynamic Mechanical Analysis
DMTA	Dynamic Mechanical Thermal Analysis
DS	Dean Stark Solids
DSC	Differential Scanning Calorimetry
G’	Storage Modulus in Dynamic Mechanical Analysis
G”	Loss Modulus in Dynamic Mechanical Analysis
ISO	International Standard Organization
MDI	Methylene-dyphenyldiisocyanate
MFT	Mature Fine Tailings
MMT	Montmorillonite clay
PT	Paste Technology
SAGD	Steam Assisted Gravity Drainage
SEM	Scanning Electron Microscopy
Tan δ	Loss Factor in Dynamic Mechanical Analysis
TEM	Transmission Electron Microscopy
T_g	Glass Transition Temperature
TGA	Thermogravimetric Analysis
XRD	X-Ray Diffraction
λ	Wavelength

CHAPTER 1
Introduction

Northern Alberta in Canada has one of the largest reserves of crude bitumen in the world, estimated to be about 177 billion barrels. This bitumen is naturally mixed with sand, clays and water, forming deposits that extend up to 142,000 km^2 and are divided into three major areas: Athabasca, Peace River and Cold Lake (Masliyah, Czarnecki, and Xu, 2011).

To recover the bitumen in the oil sands deposits, companies use mainly two methods that depend on the depth of the deposit. When the thickness of the soil on top of the oil sands formation (overburden) is less than 75 m, the choice is open pit mining. In this process the vegetation and overburden are removed to expose the ore, which is extracted and goes through a grinding process. Later on, large amounts of water are used to separate the other components from the bitumen, which is finally sent to upgrading processes.

When the thickness of the overburden is too high for mining operations, the choice is In Situ bitumen recovery. This method consists mainly on the technology called Steam Assisted Gravity Drainage (SAGD), in which steam is injected into the deposit to lower the viscosity of the bitumen and make it flow through another well for recovery (Masliyah et al., 2011).

Although in-situ operations are expected to grow in the coming years, mining production has been higher than in-situ production in the past 10 years, and the forecast for year 2030 indicates that mining production will increase from 1 million barrels per day to 1.5 million barrels per day (Canadian Association of Petroleum Producers, 2016), which means open pit mining will continue having an important contribution to Alberta's oil production in the near future.

However, there are some problems associated with mining operations. Once the bitumen is extracted, large amounts of a liquid residue called oil sands tailings are sent to ponds that cover around 176 km^2 of land (Vedoy and Soares, 2015), an area so big that it can even be seen from space.

Even though they can vary in composition, fresh tailings from the process contain commonly 70 wt % water, 5 wt % bitumen and 30 wt % minerals, which include sand and clays (Botha and Soares, 2015), but when they are sent to the ponds, most of the sand and about half of the fine clays settle quickly to the bottom of the pond in what is called sand beaches. The other part of the solids settles very slowly, and after several years a suspension with about 35 wt % solids is

formed. This suspension is called mature fine tailings (MFT), and the clays present in this suspension may take decades to settle on their own (Vedoy and Soares, 2015).

Since these ponds cover big areas of land, the tailings in them have to be treated in order to reclaim the land and recover the water to reduce the intake from natural sources, but the treatment has been a challenge for the industry and researchers due to the high stability of the suspension. Different processes have been and are being studied on a laboratory scale to treat fresh tailings and MFT in terms of solids densification and water recovery by using different sets of flocculants, but currently only two processes are being used in the industry: Consolidated Tailings (CT) and Paste Technology (PT).

In the CT process, fresh tailings and MFT are mixed with gypsum to form a non-segregating mixture that is then put in a pond, where coarse sand and fine clays are expected to aggregate and form dense solids while releasing water at the surface. The problem with this process is that the addition of gypsum and other inorganic flocculants increases the ionic loading of the released water, affecting negatively the bitumen recovery if this water is re-used in bitumen extraction processes (MacKinnon, Matthews, Shaw, and Cuddy, 2001).

Paste technology uses polymeric flocculants to accelerate the natural settling of fine particles from fresh tailings, obtaining a paste with approximately 25 to 30 wt % solids (Masliyah et al., 2011). The advantage of this process is the recovery of warm water that can be reused in the process immediately, but the flaws include low dewatering performance of the flocculants in the presence of bitumen, and equipment limitations for handling the paste (Vedoy and Soares, 2015).

Due to the problems associated with solids densification and water recovery, some companies have opted for ponds capping as an alternative method for land reclamation, like coke capping in Suncor's Pond 5 (Suncor Energy, 2016), and water capping in Syncrude's test ponds (Syncrude, 2016), among others being studied by different companies.

The approach in this work is to manufacture a composite material in which MFT acts as filler. The general candidates for this purpose are polymer composites, defined as materials where a filler is dispersed and embedded in a polymer matrix. However, the first pick should be a polymer matrix that has some water compatibility or where water is used as an additive. In this way, energy would not have to be spent to remove water from the MFT prior to making the composite.

Although there are studies on the mechanical properties of a wide variety of polymer composites with clays as fillers, there is only one previous study with this work's approach, where rigid polyurethane foam composites with MFT as a filler were synthesized and their properties were compared with the same composites using sodium montmorillonite (MMT) as filler (one of the most common clay fillers used in polymer composites research). The results indicated similar mechanical properties and an improvement in thermal properties for the MFT and MMT composites (Vajihinejad and Soares, 2016).

Since this previous study showed that the composites industry can contribute to the reduction of MFT in the ponds, and even make composite materials with better properties, the objective of this work is to test a new polymer matrix with biodegradable properties to broaden the applications range of MFT composites and have more options to partially eliminate MFT and reclaim the land covered by the ponds.

Starch has proven to be a suitable material for packaging applications when combined with plasticizers (plasticized starch or thermoplastic starch), especially in the production of loose-fill packing material that works as cushion (packing peanuts).

There has been significant research done on starch-based composites for a number of different applications, such as biodegradable food packaging, bags, and boxes, but the low mechanical properties and poor water resistance of the starch matrix requires the use of different fillers, starch modifications, or blending with other polymers.

The most common fillers for thermoplastic starch are MMT, natural fibers and cellulose nanocrystals (CNC). MMT is selected due to its hydrophilicity, low cost (Xie et al., 2014), and the good dispersion in the thermoplastic starch matrix; natural fibers are common because of their availability and reinforcing properties, and cellulose nanocrystals (CNC) because they improve dramatically the mechanical properties of the composites (Cao, Chen, Chang, Muir, and Falk, 2008). On the other hand, these fillers do not increase the water resistance of the starch composites, and can only be used in small percentages because they increase the viscosity of the plasticized starch matrix, which leads to low filler dispersion.

The objectives of this work include the use MFT, a product considered as waste by the oil sands industry, as filler for thermoplastic starch, and the determination of the mechanical properties of these composites to compare them with the properties of similar composites made with MMT and cellulose nanocrystals (CNC). If the properties achieved by the MFT composites

are better, or at least in the same range of those of the other composites, MFT could be considered useful as reinforcement for thermoplastic starch. These starch/MFT composites could find applications as bags and boxes for non-edible items, mulch, and cushions, among others. This would mean an opportunity to mitigate the environmental effect of oil sands exploration by converting part of the MFT in an inexpensive product that may replace other non-biodegradable plastics. Thus, the objective of this thesis is to test the feasibility of transforming an environmentally hazardous by product of oil sands extraction into a useful and inexpensive composite material.

Additionally, a comparison will be made between starch-MFT composites and a set of composites made with the solids present in MFT once the bitumen is removed (Dean Stark solids). This comparison aims to study the effect of bitumen in the mechanical properties of the MFT composites. Dean Stark composites, however, are not proposed as a viable option for making these composites since the amount of energy required (and its associated cost) to remove bitumen from MFT does not justify making these composites.

In Chapter 2, a literature review describes the current efforts to treat MFT, the molecules present in starch and the thermal transitions in starch that allow plasticization, the main components in starch composites, and the set of properties commonly measured in starch-based composites, which include physical, mechanical and thermal properties.

Following the literature review, Chapter 3 will describe the methods used to characterize Starch, MFT, and Dean Stark solids, followed by the procedure to prepare the starch composites with the proposed fillers, and will end with the characterization results of the raw material.

Chapter 4 will show the characterization results of the starch based composites accompanied by a discussion on the variation of the properties between the composites made with different content and type of filler. The discussion will include the comparison of morphology, density, X-ray diffraction patterns, tensile properties, compressive properties and the results of a dynamic mechanical analysis.

Finally, Chapter 5 will show a series of conclusions from this work and the proposed future work related to the improvement of the Starch-MFT composites.

References

Botha, L., and Soares, J. B. P. (2015). The Influence of Tailings Composition on Flocculation. *The Canadian Journal of Chemical Engineering*, *93*(9), 1514–1523. https://doi.org/10.1002/cjce.22241

Cao, X., Chen, Y., Chang, P. R., Muir, A. D., and Falk, G. (2008). Starch-based nanocomposites reinforced with flax cellulose nanocrystals. *Express Polymer Letters*, *2*(7), 502–510. https://doi.org/10.3144/expresspolymlett.2008.60

MacKinnon, M. D., Matthews, J. G., Shaw, W. H., and Cuddy, R. G. (2001). Water Quality Issues Associated With Composite Tailings (CT) Technology for Managing Oil Sands Tailings. *International Journal of Surface Mining, Reclamation and Environment*, *15*(4), 235–256. https://doi.org/10.1076/ijsm.15.4.235.7416

Masliyah, J. H., Czarnecki, J., and Xu, Z. (2011). *Handbook on Theory and Practice of Bitumen Recovery from Athabasca Oil Sands* (Vol. I). Kingsley Publishing.

Suncor Energy. (2016). Reclamation. Retrieved from http://sustainability.suncor.com/2011/en/responsible/1794.aspx

Syncrude. (2016). Water Capping. Retrieved from http://www.syncrude.ca/environment/tailings-management/tailings-reclamation/water-capping/

Vajihinejad, V., and Soares, J. B. P. (2016). Can We Make Better Polyurethane Composite Foams with Oil Sands Mature Fine Tailing? *Macromolecular Materials and Engineering*, *301*(4), 383–389. https://doi.org/10.1002/mame.201500396

Vedoy, D. R. L., and Soares, J. B. P. (2015). Water-soluble polymers for oil sands tailing treatment: A Review. *Canadian Journal of Chemical Engineering*, *93*(5), 888–904. https://doi.org/10.1002/cjce.22129

Xie, F., Luckman, P., Milne, J., McDonald, L., Young, C., Tu, C. Y., … Halley, P. J. (2014). Thermoplastic Starch: Current development and future trends. *Journal of Renewable Materials*, *2*(2), 95–106. https://doi.org/10.7569/JRM.2014.634104

CHAPTER 2
Literature Review

This chapter starts by describing the current industrial methods used to handle MFT, then introducing polymer composites, which is the alternative approach proposed in this thesis to reduce the amount MFT in tailing ponds. Since the proposed composites are starch-based, a description of the starch molecules, their structure and thermal transitions is discussed, together with a brief literature review of plasticized starch composites with a series of fillers. Finally, a description of the most common properties of starch-based composites and a brief explanation of the purpose of each measurement is given. This information provides the knowledge necessary to understand the properties of the starch-based composites and how they are affected by filler loading and filler.

2.1 Oil Sands Mature Fine Tailings

Oil sands tailings, a mixture of water, bitumen and clays resulting from the oil sands hot water extraction process, represent one of the biggest challenges in the oil industry in Alberta. When the fresh tailings from the hot water extraction process are sent to the tailings ponds, the coarse solids and part of the fines settle in a couple of days, reaching solids content of 20%. In a period of two to five years, mature fine tailings (MFT) are formed with a solids content of approximately 30-35% (Mikula, Kasperski, Burns, and MacKinnon, 1996), after which further settling takes decades.

The current Consolidated Tailings (CT) and Paste Technology (PT) processes focus mainly on fresh tailings to improve fines settling and water recovery from the ponds, but each one has its own limitations: poor water quality for the CT process, and low dewatering performance and equipment limitations for the PT process (Vedoy and Soares, 2015). Additionally, the PT process has not been succesful for MFT treatment because researchers could not find polymers that can reach high dewatering efficiencies.

One of the most important factors when selecting a polymer is knowing the tailings composition and the minerals present in it. The composition of MFT is determined by Dean Stark extraction, the most accepted method in the industry for the determination of bitumen,

water and solids content on tailings (Cabrera, Bryan, Kantzas, and Tipm, 2010). Although the composition of MFT varies depending on the source and on the settling time, on average it is composed of 58-62% water, 1-5% of unrecovered bitumen and 37% mineral solids. (Cabrera, Bryan, Kantzas, and Tipm, 2010)

The solids present in MFT are a mixture of sand and clays, sand corresponding to about 5% of this mixture. The rest of the solids are clays and fines with particle sizes equal or less than 22 µm. Kaolinite (35 wt%) and illite (60 wt%) are the dominant clay types, with chlorite (4 wt%) and smectites (1 wt%) present in smaller amounts (Mikula et al., 1996). Aditionally, mixed layer clays are also present in MFT, including kaolinite-smectite and illite-smectite (Botha and Soares, 2015). However, these are just typical values that depend on the pond where the MFT sample was taken, and even on the depth at which the samples were collected, making it difficult to generalize the MFT composition and to create model tailings that help understand the behavior of the original mixture.

Researchers have studied a variety of polymers (Petzold, Mende, Lunkwitz, Schwarz, and Buchhammer, 2003; Yoon and Deng, 2004) to improve the flocculation of tailings in the PT process. Vedoy and Soares (2015) defined three main categories of polymers used for tailings flocculation: 1) polyacrylamide-based polymers (PAM), in anionic or cationic versions (Mcfarlane and Bremmell, 2005), 2) organic-inorganic hybrids such as Al-PAM (Alamgir, Harbottle, Masliyah, and Xu, 2012), and 3) temperature-sensitive polymers such as poly(*n*-isopropylacrylamide) (PNIPAM) (O'Shea, Qiao, and Franks, 2010). Although these polymers have potential as oil sands talings flocculants, most of the research was done on fresh tailings or clays suspensions that do not behave as MFT; as a consequence, there is still a lot of research to do to find a suitable polymer that can treat MFT efficiently.

2.2 Polymer Composites

A composite material is the result of the combination of two materials with different physical and chemical properties to achieve a new set of properties for a specific application, but maintaining a defined interface between the constituent materials. In the polymers field, they consist of a polymer matrix, or continuous polymer phase, in which other materials known as

fillers are embedded, forming a disperse phase (Josmin P. et al., 2012). These materials can be natural or synthetic fibers, particles, and even liquid inclusions.

Research on polymer composites involves a wide range of polymer matrix and filler types, depending on the target applications. The synthesis of polymer composites may be aimed at changing either thermal, chemical resistance, or mechanical properties. In some cases, the manufacture of a polymer composite follows a raw material opportunity, in which a material with no significant use and low value may be dispersed in a polymer matrix to produce a composite of higher valued to suit different applications.

Polymer composites are classified based on the type of filler: 1) fibrous, 2) particulate, or 3) laminate. If one of these fillers is a natural material, the composite would be called a bio composite. Additionally, if the filler is a natural material and the polymer matrix is a biodegradable polymer, it is said to be a green composite (Josmin P. et al., 2012). However, there is another classification in which polymer composites are separated by the size of the fillers, forming polymer nanocomposites (< 100 nm), microcomposites (< 100 μm) and macrocomposites (> 100 μm).

Even though polymer composites are used in many different applications, much recent research is aimed at making green polymer composites (Roy, Shit, Gupta, and Shukla, 2014). The most used synthetic biodegradable matrices are polyvinyl alcohol, polyvinyl acetate, polylactic acid, polyglycolic acid, and polyamides, while the most used natural polymers used as matrix are starch, chitin, cellulose, and lignin. (Josmin P. et al., 2012).

2.3 Starch

Starch is one of the most abundant natural polysaccharides. It is present in the form of granules in plants as energy reserve. It is a mixture of two macromolecules, amylose and amylopectin, in which the repeating unit is glucose (Figure 2.1). Amylose is mainly linear with α(1-4) linkages and molecular weights between 200,000 and 700,000, and amylopectin is a branched molecule in which the linear part contains α(1-4) linkages and the branching points have α(1-6) linkage, reaching molecular weights up to 200 million (Imam et al., 2012). The granule size and shape, the amount of each molecule within the granule, molecular weight, proportion and number of repeating units between branches of the amylopectin molecules will be

highly dependent on the botanical origin of the starch. The most common sources of starch are maize, potato, barley, rice, pea, wheat, tapioca and oat.

Amylose is located randomly in the amylopectin chains in the granule following a radial orientation (Perez, Baldwin, and Gallant, 2009). When amylose is in aqueous solution, it forms single helices with complexing materials or double helices with other amylose molecules. This property is what allows the formation of an iodine complex, since the iodine molecules align in the tunnel formed by the amylose helix. The deep blue color of this complex is what allows the estimation of the amylose content of starches, despite the fact that it is highly dependent on pH, temperature and mixing (Jane, 2009).

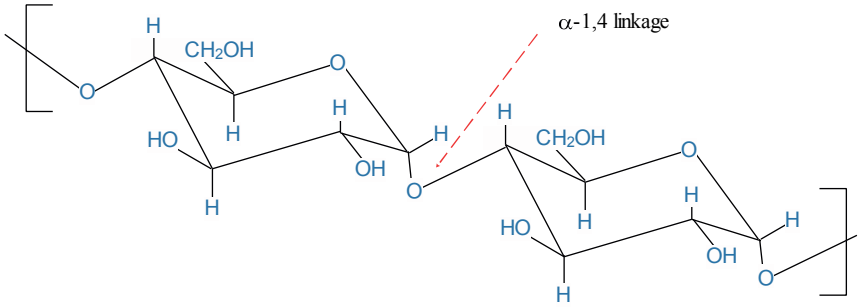

(a)

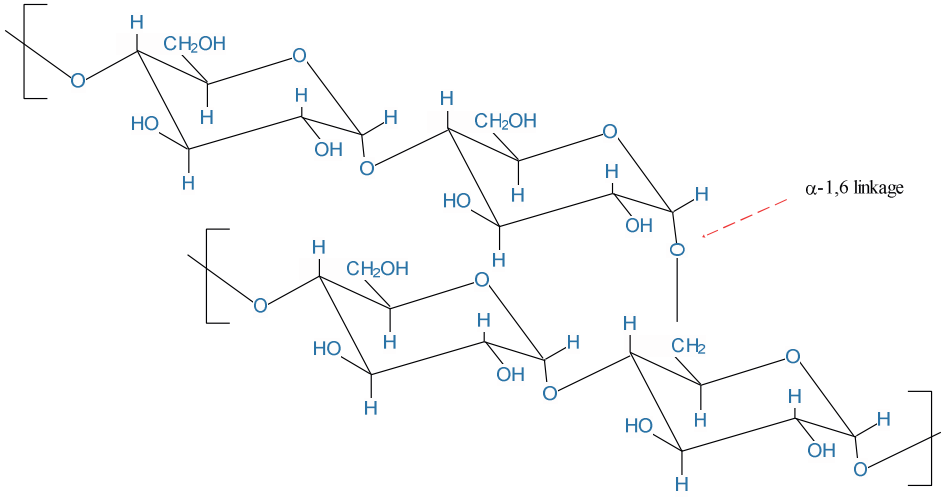

(b)

Figure 2.1. Amylose (a) and Amylopectin (b) molecules. Image modified from Lu, Xiao, and Xu, 2009.

Diverse studies of the starch granule have shown that amylose and amylopectin are organized forming growth rings made of semicrystalline and amorphous sections, as seen in Figure 2.2. The semicrystalline sections are formed by short amylopectin chains that form double helices, while the amorphous sections are formed by amylopectin amorphous segments and amylose (Imam et al., 2012).

In the amylopectin structure, the chains are classified according to their position on the granule as *A*, *B*, or *C* chain types. *A* chains have no branches, *B* chains have one or more branches, and *C* chains are known as the starch backbone. The *A* and *B* chains form the double helices present in the semicrystalline rings of the granule (Tester, Karkalas, and Qi, 2004).

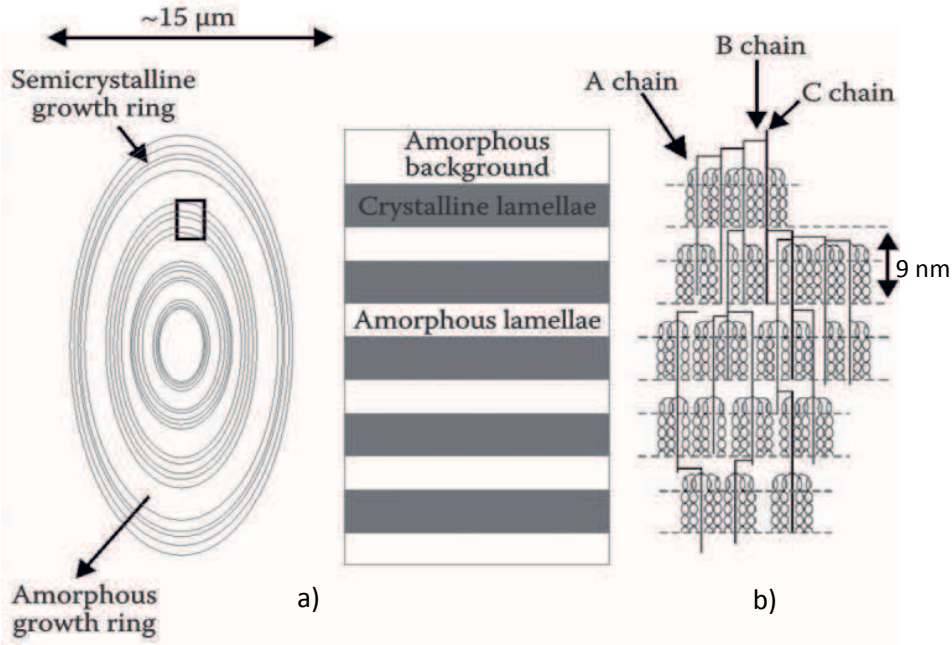

Figure 2.2. a) Schematic representation of the growth rings in the starch granule, as would be observed under Scanning Electron Microscopy. The black lines in the growth rings indicate crystalline areas, while the white areas indicate the amorphous sections; b) Designation of chains present in amylopectin. A chains with no branching and some of the branched B chains are the ones participating in the crystalline areas of the granule, while the amorphous area is occupied mainly by B chains in their branching points. C chains are considered the backbone of amylopectin, and are present in both areas. Image taken from Imam et al., 2012.

2.3.1 Starch gelatinization and retrogradation.

When starch is heated under shear in the presence of water, the original structure is disrupted and water swells the granule, breaking intermolecular and intramolecular hydrogen bonds between the starch molecules, allowing amylose to leave the granule. This process is called gelatinization, and it is an important property that allows turning starch into a thermoplastic material (Jenkins and Donald, 1998).

However, once the temperature is lowered, the disrupted starch molecules start a slow process of reassociation called retrogradation (Figure 2.3), which includes physical changes like increased viscosity, increased turbidity, and increased crystallinity with respect to the swollen starch granule. This last change in crystallinity happens because of the fast recrystallization of the amylose and the slow recrystallization of the amylopectin. (Wang, Li, Copeland, Niu, and Wang, 2015)

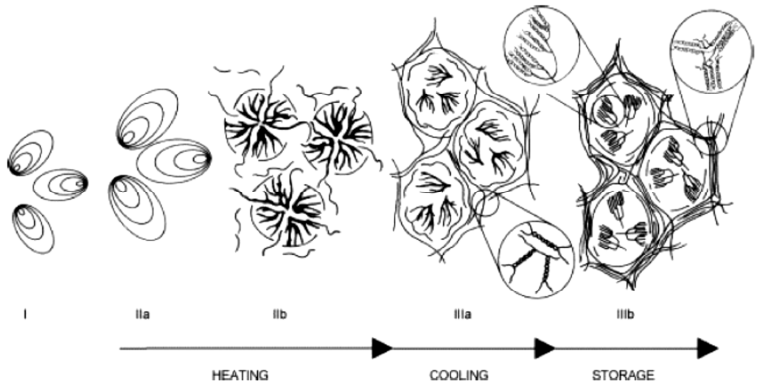

Figure 2.3. Changes of the starch granule in the presence of water during gelatinization and retrogradation: I) Representation of the starch granule; IIa) Heating in the presence of water causes the granule to swell; IIb) Complete disruption of the initial crystallinity of starch – Amylopectin is completely swollen and amylose leaches out of the granule, increasing the viscosity of the mixture and forming a paste; IIIa) Fast recrystallization of amylose due to cooling; IIIb) Slow recrystallization of amylopectin (retrogradation) during storage. Image taken from Wang, Li, Copeland, Niu, and Wang, 2015.

2.3.2 Thermoplastic starch

In order to plasticize starch, it must be gelatinized in order to break the hydrogen bonds and allow the exposed OH groups to form hydrogen bonds with water and plasticizer molecules.

After this, it becomes plasticized starch and can be processed through extrusion, compression molding, or film casting. (Ma, Chang, and Yu, 2012)

The applications of thermoplastic starch alone are limited because of its low water resistance, retrogradation due to evaporation of water, and poor mechanical properties. However, all these factors depend on the type of starch, the amount and type of plasticizer, including water, and additives.

The effect of the type of starch in the composites is due to the nature of the starch molecules and the proportions in which they are in the granule. The linear amylose molecules can form entanglements that act as physical crosslinks, giving strength to the structure, while the branched amylopectin improves flexibility and elongation of the material (Van Soest and Vliegenthart, 1997). This is why the amylose/amylopectin ratio is important and lots of research was done on how to quantify it (Nalin, Sperb-Ludwig, Venema, Derks, and Schwartz, 2015; Sak-bosnar and Gvozdi, 2012; Sargeant, 1982) and how it affects the properties of the thermoplastic starch (Liu, Yu, Xie, and Chen, 2006; Xie et al., 2009).

The plasticizer plays an important role on the properties of thermoplastic starches. Plasticizers are classified in three main categories: 1) polyols, such as glycerol, sorbitol, maltitol, and some glycols; 2) amides, such as urea, formamide, and acetamide; and 3) others, such as ethanolamine. However, glycerol is the most common plasticizer because it is not toxic, has low cost, and a high boiling point. (Ma et al., 2012)

The use of glycerol as a plasticizer overcomes the problem of retrogradation of the chains, but makes thermoplastic starches with low tensile strengths (Xie et al., 2014), while the addition of other plasticizers with low interactions with the starch molecules might improve the mechanical properties of thermoplastic starches initially, but permits retrogradation to take place, leading to the formation of brittle thermoplastic elastomers, which will be detrimental to their final application.

2.3.3. Starch based polymer composites

Since plasticized starch has its flaws related to mechanical properties and water resistance, additives or fillers may be included in the thermoplastic starch matrix to make polymer blends or composites with superior properties. Researchers have included different types of fibers

(Kaisangsri, Kerdchoechuen, and Laohakunjit, 2014; Mello and Mali, 2014; Song and Kim, 2013), clays (Coativy et al., 2015; Kaewtatip, Tanrattanakul, and Phetrat, 2013; Perotti et al., 2014), and other nanofillers (Yildirim, Shaler, Gardner, Rice, and Bousfield, 2014; Zainuddin, Ahmad, and Kargarzadeh, 2013) as reinforcements. The most common filler is phyllosilicate sodium montmorillonite (MMT), which consists of platelets with an inner layer of octahedral aluminum oxide and two outer tetrahedral silicate layers (Paul and Robeson, 2008).

The main reason for the wide use of MMT is because it is easy to disperse in the thermoplastic starch matrix due to its hydrophilicity, allowing for good interaction with the hydrogen bonds of the starch chains (Xie et al., 2014).

Additionally, cellulose nanocrystals (CNC) have been widely used lately as a potential reinforcement for polymer composites in general. Some studies in thermoplastic starch show a dramatic improvement in tensile properties of films when CNCs are used as fillers (Cao, Chen, Chang, Muir, and Falk, 2008; Zainuddin et al., 2013).

However, MMT does not improve water resistance and even though some researchers have reported a slight increase in water resistance with the addition of CNCs (Cao et al., 2008), it might not be enough for applications where high water resistance is required.

In order to improve water resistance and improve mechanical properties, starch can be blended with other polymers. The most common polymers used to enhance water resistance are polylactic acid and polycaprolactone because they maintain the biodegradability of the blend. However, since these polymers are not very compatible with starch, a compatibilizer agent with dual functionality like methylene-dyphenyldiisocyanate (MDI) or maleic anhydride is needed. Also, the chemical modification of the surface of starch particles has been proven to improve affinity with other polymers, by grafting polymer chains onto starch that can make it compatible with the other polymer in the blend (Yang, Tang, Xiong, and Zhu, 2015).

2.4 Characterization of Starch-Based Polymer Composites.

The characterization of a new material depends strongly on the application for which the material is intended, but there are some cases in which a set of properties can define a range of applications for a material. The vast majority of studies involving the synthesis of thermoplastic

starch composites include the measurement of water uptake, physical properties, thermal properties and mechanical properties.

Due to the hydrophilicity of thermoplastic starch and as a requirement for applications, almost every study related to starch composites requires the study of water uptake. The most common method to measure it is gravimetric analysis, by first completely drying the sample, then putting it in a high moisture environment or submerging it in water for a defined amount of time. Since starch is hydrophilic, the sample has to be dried again to compare the final and the initial weight and determine a potential mass loss during the measurement. Conditions like temperature, immersion time, drying temperature and drying time might vary between studies (Fabunmi, Tabil, Panigrahi, and Chang, 2011; Zainuddin et al., 2013), but standards like ASTM D570 stablish a procedure that allows to compare the results from one composite to another.

Apart from water uptake, the most common physical properties studied for starch-based composites include density and morphology. The main method for density determination is the measurement of the mass and volume of a composite sample, which yields the density of the material by dividing mass over volume. Since this method does not take into consideration the empty volume caused by voids (or cells) in the structure, the obtained result is not the real density, but the apparent density of the material. Morphology studies are covered by scanning electron microscopy (SEM), a technique used to measure the size of fillers in the plasticized starch matrix, to see how they are distributed, to check for agglomeration, and to measure the size of cells.

For some studies, especially those where the fillers are swelling clays, transmission electron microscopy (TEM) is used to study the dispersion of particles (Coativy et al., 2015) and check for signs of intercalation (the presence of the clays as stacks of several layers), or exfoliation (the presence of clays as a single layer in the starch matrix) (Chen and Evans, 2005). Intercalation and exfoliation are important processes because they affect the properties of these composites. Clays dispersed in a polymer matrix reinforce the mechanical properties of the composites, but if these clays are intercalated and/or exfoliated they disperse more effectively in the matrix, further enhancing their mechanical strength and thermal stability (J. Liu, Boo, Clearfield, and Sue, 2006). However, this measurement is not exclusive of TEM, since X-ray diffraction (XRD) is an alternative analysis that can help identify intercalation of clays in the matrix by the shifting of the peak indicating the spacing between platelets, called interlayer spacing or d-spacing. (Paul and

Robeson, 2008; Zuraida et al., 2012). This is calculated through Bragg's law, expressed in Equation (2.1),

$$2 * d * \sin\theta = \lambda \quad (2.1)$$

where λ is the wavelength of the x-ray used in the diffraction experiment, d is the interlayer distance in Armstrong, and θ is the diffraction angle (Pavlidou and Papaspyrides, 2008). If the peaks to not shift to a different angle, the interlayer spacing remain the same, no intercalation took place.

It is worth mentioning that XRD can also help identify the type of crystallinity in starches and how it is affected by plasticizers and fillers. XRD analysis on different type of starches reveals that there are different crystallinity patterns related to the organization of the double helices formed by amylopectin branches and by amylose chains. The crystallinity patterns are A, for short chain length (weight average chain length between 19-28), B for long chain length (weight average chain length between 29-31), and C for a mixture of short and long chains (Jane, 2009), but different physical treatments like gelatinization may change the crystallinity pattern of starches. An additional crystallinity pattern is V, related to the crystallinity of amylose complexes mentioned in section 2.3.

The main thermal analysis made on starch composites is through thermogravimetric analysis (TGA). Since the addition of clays as inorganic materials may improve the thermal stability of polymer composites (Zuraida et al., 2012), TGA is the right option to determine this effect by measuring the mass loss with temperature increase. However, the addition of cellulose nanocrystals, which are organic fillers, does not improve significantly the thermal stability of the composites (Zainuddin et al., 2013).

Although thermal conductivity is not a property commonly measured in starch based materials, one study found similar thermal conductivity values between starch based microcellular foams and commercial insulation materials (Glenn and Irving, 1995), and another one found similar values in thermal conductivity with the previous study when making a composite with cellulose nanofibrils (Yildirim et al., 2014); in both studies, however, freeze drying was used to remove all the water from the structure. This last treatment is necessary because if water acts as a plasticizer, the thermal conductivity might be higher.

The improvement of the mechanical properties of thermoplastic starch with the addition of fillers, or with any other modification, is the main object of study in most research work in the area. The most common test made on films and foams is to measure tensile properties, followed by compression properties, and impact properties. Additionally, some researchers perform dynamic mechanical thermal analysis (DMTA) of these materials, in which mechanical properties are studied as a function of temperature.

The tensile properties are measured by putting a material under stress (load divided by the original cross-section of the material) to cause strain (deformation related to the initial length) and study the behavior of the curve. The shape of the stress-strain curves characterizes the material. Typical curves can be seen on Figure 2.4, where different shapes indicate a distinct behavior for brittle, ductile and rubbery materials. Brittle materials have a low strain before breaking at high stress, while ductile and rubbery materials have higher strain with low stress, which means they are not as stiff.

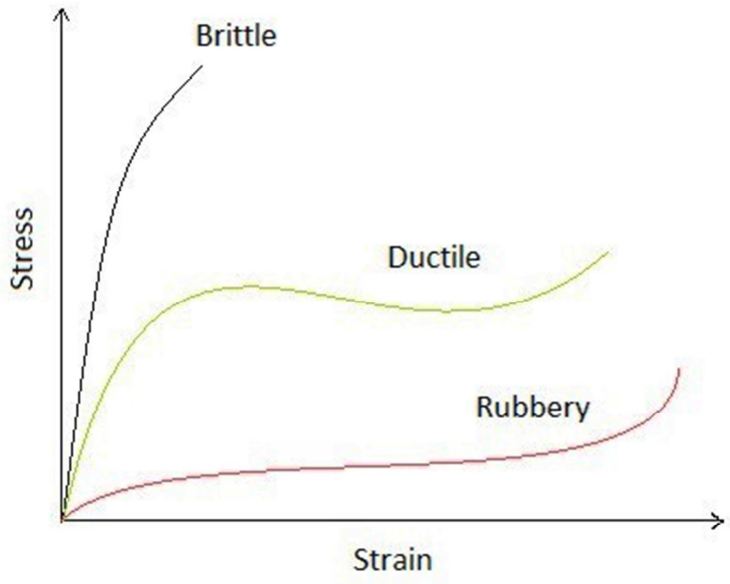

Figure 2.4. Typical Stress-strain curve for brittle, ductile and rubbery materials. Image redrawn from Painter and Coleman, 2009.

The importance of knowing this behavior relies on the properties that can be defined by the shape and values of this curve. Young's modulus, calculated as the slope of the initial linear or

almost linear part of the curve, is an indicative of the stiffness of a material and sets a limit for its elastic deformation, as seen in Figure 2.5. After the point in which the linearity stops, called yield point, the plastic deformation starts until the breaking point, at which the maximum strain is measured. The maximum value of stress required to break the material and form two new surfaces is the tensile strength. (Painter and Coleman, 2008)

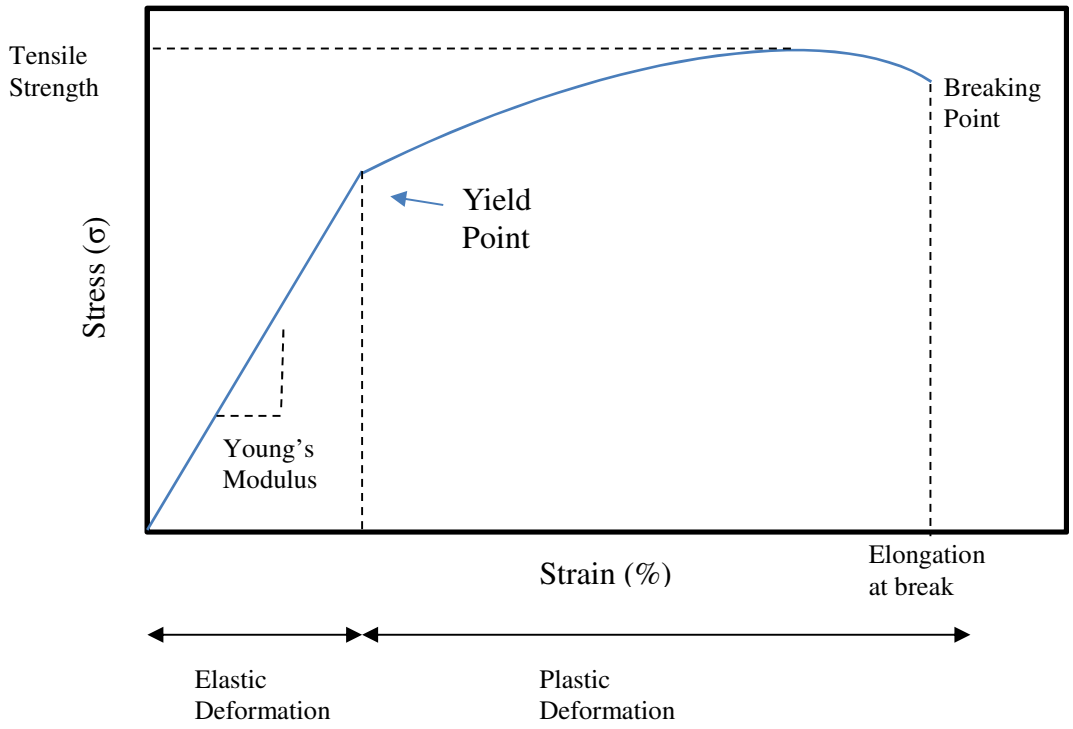

Figure 2.5. Stress-strain curve indicating general tensile properties of materials.

In the case of compressive properties, the stress strain curve has a similar behavior. Although the strain will be negative since there is a shortening of the initial length of the material, it can be easily understood if the sign is changed to yield a curve with the same trend as the tensile curve.

Generally, well dispersed clays in a polymer matrix have been proven to increase the stiffness or modulus of the polymer, and may also increase the tensile strength, but there are cases in which it may decrease it. Although there are some exceptions, the elongation at break decreases when fillers are loaded (Paul and Robeson, 2008).

For starch based composites, multiple studies have found improvements in tensile modulus and tensile strength, with loss of elongation at break (Karimi, Abdulkhani, Tahir, and Dufresne, 2016; López, Mutjé, Carvalho, Curvelo, and Gironès, 2013; Zainuddin et al., 2013), but others

have found a decrease or no change in tensile strength, and even improvements in elongation (Polat, Uslu, Aygün, and Certel, 2013; Then, Ibrahim, and Wan Yunus, 2011). Similar results have been found for compressive properties of starch composites (Kaisangsri et al., 2014; Yildirim et al., 2014), but the results depend strongly on the type and amount of fillers, their interaction with starch chains, type and amount of plasticizer, number of defects on the structure, polymer used for blending and their compatibility with starch chains, among other factors than might affect the behavior.

For polymers, the glass transition temperature (T_g) – or glass transition region since it happens in a narrow temperature range depending on the heating or cooling rate (Rudin and Choi, 2013) – plays an important role on the behavior of the material, since it is the temperature at which, upon cooling, the amorphous domains of a polymer take the characteristic brittleness and stiffness of a glassy state (Odian, 2004). Below this temperature, a semi-crystalline polymer may behave as a brittle material, while above T_g it may behave as a ductile or rubbery material. Whether it is an amorphous polymer or a semi-crystalline polymer, there are notable changes in the mechanical properties in the glass transition region (Rudin and Choi, 2013).

Because of these changes, a study of the mechanical properties of the polymers at different temperatures reveals how it will behave in different applications. For a completely amorphous polymer, a typical curve of modulus versus temperature is shown in Figure 2.6-a, where at sufficiently low temperature the modulus is high, but in the glass transition range it drops significantly. Below the glass transition, there are no large-scale movements of polymer segments because the energy is not enough to allow rotation of single bonds, but after this range, the thermal energy allows the movement of segments and the modulus drops to a point in which the material behaves as a rubber. In this region, there are still restrictions for the movement of the whole macromolecules due to entanglements, which means that the higher the molecular weight, the longer the rubbery section will be. At higher temperatures, the modulus keeps dropping and the polymer behaves as a rubbery liquid, unless the polymer chains are crosslinked, in which case the rubbery section continues until the degradation temperature of the polymer, with a less significant drop in modulus depending on the crosslinking density. When it comes to semi-crystalline polymers, the movements of segments occur only on amorphous regions; as the crystallinity increases there is less segmental movement (Rudin and Choi, 2013), resulting in the behavior seen on Figure 2.6-b.

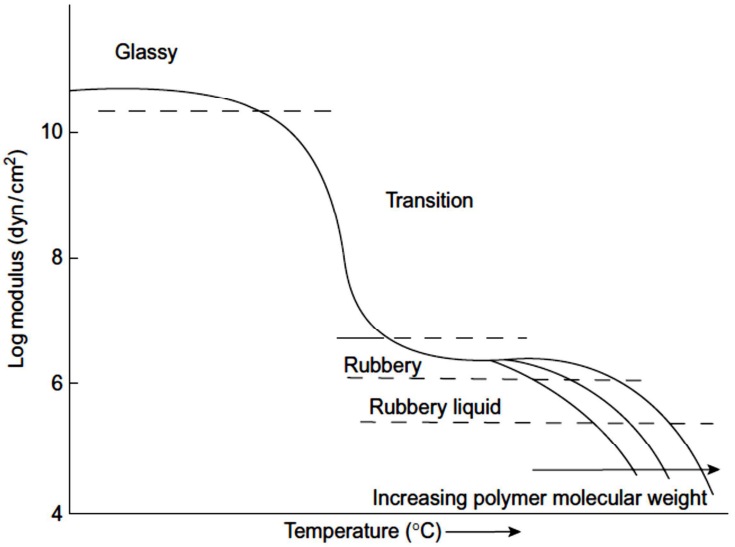

(a)

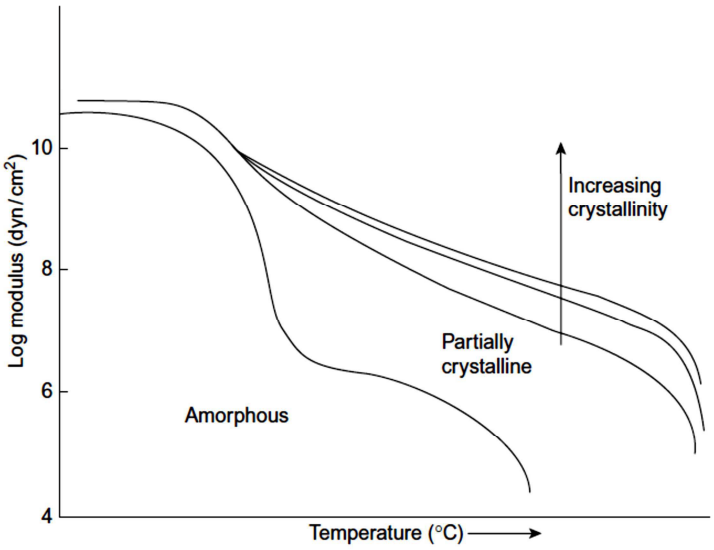

(b)

Figure 2.6. Typical modulus vs temperature curves for amorphous (a) and semi-crystalline polymers (b). Images taken from Rudin and Choi, 2013.

Polymers can behave in elastic, viscous or, as in most cases, viscoelastic manner and these responses will vary with the time scale of the stress or strain applied. There are experiments like creep, where a constant load is put in a polymer and the change in elongation is measured, and

stress relaxation, where an instant strain is put in a polymer sample and the change in stress is measured. However, the study of the viscoelastic behavior requires the measurement in very long times, which means creep and stress relaxation have limitations (Rudin and Choi, 2013). Dynamic mechanical analysis is the best option to study viscoelasticity, which measures the response of the polymer to a sinusoidal stress as a function of temperature (Sinha Ray, 2013), and it allows the comparison of curves likes the ones showed in Figure 2.6.

The experiment measures the storage modulus G', associated with the stiffness of the polymer; the loss modulus G", associated with the internal friction between macromolecules (Sinha Ray, 2013), which indicates the energy that is lost to cause flow in the specimen (Rudin and Choi, 2013); and finally the damping factor Tan δ or the ratio of the energy lost and the energy stored in the specimen, which is useful for the determination of thermal transitions like T_g.

For starch-based composites using glycerol as a plasticizer, many authors have studied the dynamic mechanical behavior with a common result, which is the heterogeneity of the composites defined by two Tan δ peaks, one related to a glycerol rich phase and other related to a starch rich phase (Karimi et al., 2016; López et al., 2013; Vallejos et al., 2011). Despite this common finding, there are changes in the peaks magnitude and temperature shifting depending on the same factors that affect the tensile and compression properties.

2.5 Summary

Polymer composites may represent a viable option to reduce the amount of MFT in tailing ponds, and the use of plasticized starch might be one of the best options due to its low cost and availability. The properties of starch molecules, their organization, the plasticizer, and the fillers play an important role in the properties that the composites might have, along with the filler dispersion and preparation methods. The information available from previous studies on starch composites serves as a guide to infer what changes to expect in morphology, water uptake, and mechanical and thermal properties as a function of filler type and content, allowing to make a comparison of the most common starch composites with MFT composites, which include bitumen as an additional parameter that may affect the properties, but might be a cheaper and environmentally friendly option.

References

Alamgir, A., Harbottle, D., Masliyah, J., and Xu, Z. (2012). Al-PAM assisted filtration system for abatement of mature fine tailings. *Chemical Engineering Science*, *80*, 91–99. http://doi.org/10.1016/j.ces.2012.06.010

Botha, L., and Soares, J. B. P. (2015). The Influence of Tailings Composition on Flocculation. *The Canadian Journal of Chemical Engineering*, *93*(9), 1514–1523. http://doi.org/10.1002/cjce.22241

Cabrera, S. C. M., Bryan, J., Kantzas, A., and Tipm, C. (2010). Estimation of Bitumen and Solids Content in Fine Tailings Using Low-Field NMR Technique. *Journal of Canadian Petroleum Technology*, *49*(7), 8–19.

Cao, X., Chen, Y., Chang, P. R., Muir, A. D., and Falk, G. (2008). Starch-based nanocomposites reinforced with flax cellulose nanocrystals. *Express Polymer Letters*, *2*(7), 502–510. http://doi.org/10.3144/expresspolymlett.2008.60

Chen, B., and Evans, J. R. G. (2005). Thermoplastic starch–clay nanocomposites and their characteristics. *Carbohydrate Polymers*, *61*(4), 455–463. http://doi.org/10.1016/j.carbpol.2005.06.020

Coativy, G., Gautier, N., Pontoire, B., Buléon, A., Lourdin, D., and Leroy, E. (2015). Shape memory starch – clay bionanocomposites. *Carbohydrate Polymers*, *116*, 307–313. http://doi.org/10.1016/j.carbpol.2013.12.024

Fabunmi, O. O., Tabil, L. G., Panigrahi, S., and Chang, P. R. (2011). Effects of Incorporating Polycaprolactone and Flax Fiber into Glycerol-Plasticized Pea Starch, 841–848. http://doi.org/10.1007/s10924-011-0374-5

Glenn, G. M., and Irving, D. W. (1995). Starch-Based Microcellular Foams. *American Association of Cereal Chemists*, *72*(2), 155–161.

Imam, S. H., Wood, D. F., Abdelwahab, M. A., Chiou, B., Williams, T. G., Glenn, G. M., and Orts, W. J. (2012). Chapter 2 Starch Chemistry, Microstructure, Processing, and Enzymatic

Degradation. In J. Ahmed, B. K. Tiwari, S. H. Imam, and M. A. Rao (Eds.), *Starch-Based Polymeric Materials and Nanocomposites* (pp. 5–32). CRC Press Taylor and Francis Group.

Jane, J. lin. (2009). *Chapter 6 Structural Features of Starch Granules II*. *Starch* (Third Edit). Elsevier Inc. http://doi.org/10.1016/B978-0-12-746275-2.00006-9

Jenkins, P. J., and Donald, A. M. (1998). Gelatinisation of starch: A combined SAXS/WAXS/DSC and SANS study. *Carbohydrate Research*, *308*(1–2), 133–147. http://doi.org/10.1016/S0008-6215(98)00079-2

Josmin P., J., Sant, K. M., Sabu, T., Kuruvilla, J., Koichi, G., and Meyyarappallil, S. S. (2012). Advances in Polymer Composites: Macro- and Microcomposites – State of the Art, New Challenges, and Opportunities. In *Polymer Composites: Volume 1* (Vol. 1, pp. 3–16). http://doi.org/10.1002/9783527645213

Kaewtatip, K., Tanrattanakul, V., and Phetrat, W. (2013). Preparation and characterization of kaolin/starch foam. *Applied Clay Science*, *80–81*, 413–416. http://doi.org/10.1016/j.clay.2013.07.011

Kaisangsri, N., Kerdchoechuen, O., and Laohakunjit, N. (2014). Characterization of cassava starch based foam blended with plant proteins, kraft fiber, and palm oil. *Carbohydrate Polymers*, *110*, 70–77. http://doi.org/10.1016/j.carbpol.2014.03.067

Karimi, S., Abdulkhani, A., Tahir, P. M., and Dufresne, A. (2016). Effect of cellulosic fiber scale on linear and non-linear mechanical performance of starch-based composites. *International Journal of Biological Macromolecules*, *91*, 1040–1044. http://doi.org/10.1016/j.ijbiomac.2016.06.061

Liu, H., Yu, L., Xie, F., and Chen, L. (2006). Gelatinization of cornstarch with different amylose / amylopectin content, *65*, 357–363. http://doi.org/10.1016/j.carbpol.2006.01.026

Liu, J., Boo, W.-J., Clearfield, A., and Sue, H.-J. (2006). Intercalation and Exfoliation: A Review on Morphology of Polymer Nanocomposites Reinforced by Inorganic Layer Structures. *Materials and Manufacturing Processes*, *21*(2), 143–151. http://doi.org/10.1080/AMP-200068646

López, J. P., Mutjé, P., Carvalho, a. J. F., Curvelo, a. a S., and Gironès, J. (2013). Newspaper fiber-reinforced thermoplastic starch biocomposites obtained by melt processing: Evaluation of the mechanical, thermal and water sorption properties. *Industrial Crops and Products*, *44*, 300–305. http://doi.org/10.1016/j.indcrop.2012.11.020

Lu, D. R., Xiao, C. M., and Xu, S. J. (2009). Starch-based completely biodegradable polymer materials. *Express Polymer Letters*, *3*(6), 366–375. http://doi.org/10.3144/expresspolymlett.2009.46

Ma, X., Chang, P. R., and Yu, J. (2012). Chapter 4 Plasticized Starch. In J. Ahmed, B. K. Tiwari, S. H. Imam, and M. A. Rao (Eds.), *Starch-Based Polymeric Materials and Nanocomposites Chemistry, Processing and Applications* (pp. 69–83). CRC Press Taylor and Francis Group.

Mcfarlane, A. J., and Bremmell, K. E. (2005). Optimising the dewatering behaviour of clay tailings through interfacial chemistry , orthokinetic flocculation and controlled shear, *160*, 27–34. http://doi.org/10.1016/j.powtec.2005.04.046

Mello, L. R. P. F., and Mali, S. (2014). Use of malt bagasse to produce biodegradable baked foams made from cassava starch. *Industrial Crops and Products*, *55*(2014), 187–193. http://doi.org/10.1016/j.indcrop.2014.02.015

Mikula, R. J., Kasperski, K. L., Burns, R. D., and MacKinnon, M. D. (1996). Nature and fate of oil sands fine tailings. *Suspensions: Fundamentals and Applications in the Petroleum Industry*, *251*, 677–723.

Nalin, T., Sperb-Ludwig, F., Venema, K., Derks, T. G. J., and Schwartz, I. V. D. (2015). Determination of amylose/amylopectin ratio of starches. *Journal of Inherited Metabolic Disease*, *38*(5), 985–986. http://doi.org/10.1007/s10545-015-9850-8

O'Shea, J. P., Qiao, G. G., and Franks, G. V. (2010). Solid-liquid separations with a temperature-responsive polymeric flocculant: Effect of temperature and molecular weight on polymer adsorption and deposition. *Journal of Colloid and Interface Science*, *348*(1), 9–23. http://doi.org/10.1016/j.jcis.2010.04.063

Odian, G. (2004). *Principles of Polymerization* (Fourth Edi). Wiley-Interscience.

Painter, P., and Coleman, M. (2009). *Essentials of polymer science and engineering*. DEStech Publications, Inc. Retrieved from http://books.google.com/books?hl=enandlr=andid=CL7O_hH0aw4Candoi=fndandpg=PR15anddq=Essentials+of+Polymer+Science+and+Engineeringandots=PCan_QdRW4andsig=FkrBTN-RpgAxfz6MObqKcWiYav4

Paul, D. R., and Robeson, L. M. (2008). Polymer nanotechnology: Nanocomposites. *Polymer*, *49*(15), 3187–3204. http://doi.org/10.1016/j.polymer.2008.04.017

Pavlidou, S., and Papaspyrides, C. D. (2008). Progress in Polymer Science A review on polymer – layered silicate nanocomposites, *33*, 1119–1198. http://doi.org/10.1016/j.progpolymsci.2008.07.008

Perez, S., Baldwin, P. M., and Gallant, D. J. (2009). Chapter 5 Structural Features of Starch Granules I. In *Starch Chemistry and Technology* (Third Edit, pp. 149–192). Elsevier Inc. http://doi.org/10.1016/B978-0-12-746275-2.00005-7

Perotti, G. F., Tronto, J., Bizeto, M. A., Izumi, C. M. S., Temperini, M. L. A., Lugao, A. B., Parra, Duclerc F., and Constantino, V. R. L. (2014). Biopolymer-Clay Nanocomposites: Cassava Starch and Synthetic Clay Cast Films. *Journal of Brazilian Chemical Society*, *25*(2), 320–330. http://doi.org/http://doi.org/10.5935/0103-5053.20130300

Petzold, G., Mende, M., Lunkwitz, K., Schwarz, S., and Buchhammer, H. (2003). Higher efficiency in the flocculation of clay suspensions by using combinations of oppositely charged polyelectrolytes, *218*, 47–57. http://doi.org/10.1016/S0927-7757(02)00584-8

Polat, S., Uslu, M. K., Aygün, A., and Certel, M. (2013). The effects of the addition of corn husk fibre, kaolin and beeswax on cross-linked corn starch foam. *Journal of Food Engineering*, *116*(2), 267–276. http://doi.org/10.1016/j.jfoodeng.2012.12.017

Roy, S. B., Shit, D. S. C., Gupta, D. R. a Sen, and Shukla, D. P. R. (2014). A Review on Bio-Composites: Fabrication, Properties and Applications. *International Journal of Innovative Research in Science, Engineering and Technology*, *3*(10), 16814–16824. http://doi.org/10.15680/IJIRSET.2014.0310058

Rudin, A., and Choi, P. (2013). *The Elements of Polymer Science and Engineering* (Third). Academic Press - Elsevier.

Sak-bosnar, M., and Gvozdi, V. (2012). Determination of the botanical origin of starch using direct potentiometry and PCA, *87*, 2619–2623. http://doi.org/10.1016/j.carbpol.2011.11.038

Sargeant, J. G. (1982). Determination of Amylose: Amylopectin Ratios of Starches. *Starch - Stärke*, *34*(3), 89–92. http://doi.org/10.1002/star.19820340306

Sinha Ray, S. (2013). *Environmentally Friendly Polymer Nanocomposites*. *Environmentally Friendly Polymer Nanocomposites*. http://doi.org/10.1533/9780857097828.2.269

Song, K. H., and Kim, I. S. (2013). Effects of plasticizer on the mechanical properties of kenaf/starch bio-composites. *Fibers and Polymers*, *14*(12), 2135–2140. http://doi.org/10.1007/s12221-013-2135-7

Tester, R. F., Karkalas, J., and Qi, X. (2004). Starch - Composition, fine structure and architecture. *Journal of Cereal Science*, *39*(2), 151–165. http://doi.org/10.1016/j.jcs.2003.12.001

Then, Y. Y., Ibrahim, N. A., and Wan Yunus, W. M. Z. (2011). Enhancement of Tensile Strength and Flexibility of Polycaprolactone/Tapioca Starch Blends by Octadecylamine Modified Clay. *Journal of Polymers and the Environment*, *19*(2), 535–539. http://doi.org/10.1007/s10924-011-0284-6

Vallejos, M. E., Curvelo, A. A. S., Teixeira, E. M., Mendes, F. M., Carvalho, A. J. F., Felissia, F. E., and Area, M. C. (2011). Composite materials of thermoplastic starch and fibers from the ethanol–water fractionation of bagasse. *Industrial Crops and Products*, *33*(3), 739–746. http://doi.org/10.1016/j.indcrop.2011.01.014

Van Soest, J. J. G., and Vliegenthart, J. F. G. (1997). Crystallinity in starch plastics: Consequences for material properties. *Trends in Biotechnology*, *15*(6), 208–213. http://doi.org/10.1016/S0167-7799(97)01021-4

Vedoy, D. R. L., and Soares, J. B. P. (2015). Water-soluble polymers for oil sands tailing treatment: A Review. *Canadian Journal of Chemical Engineering*, *93*(5), 888–904.

http://doi.org/10.1002/cjce.22129

Wang, S., Li, C., Copeland, L., Niu, Q., and Wang, S. (2015). Starch Retrogradation: A Comprehensive Review. *Comprehensive Reviews in Food Science and Food Safety*, *14*(5), 568–585. http://doi.org/10.1111/1541-4337.12143

Xie, F., Luckman, P., Milne, J., McDonald, L., Young, C., Tu, C. Y., … Halley, P. J. (2014). Thermoplastic Starch: Current development and future trends. *Journal of Renewable Materials*, *2*(2), 95–106. http://doi.org/10.7569/JRM.2014.634104

Xie, F., Yu, L., Su, B., Liu, P., Wang, J., Liu, H., and Chen, L. (2009). Rheological properties of starches with different amylose / amylopectin ratios. *Journal of Cereal Science*, *49*(3), 371–377. http://doi.org/10.1016/j.jcs.2009.01.002

Yang, Y., Tang, Z., Xiong, Z., and Zhu, J. (2015). Preparation and characterization of thermoplastic starches and their blends with poly(lactic acid). *International Journal of Biological Macromolecules*, *77*, 273–279. http://doi.org/10.1016/j.ijbiomac.2015.03.053

Yildirim, N., Shaler, S. M., Gardner, D. J., Rice, R., and Bousfield, D. W. (2014). Cellulose nanofibril (CNF) reinforced starch insulating foams. *Cellulose*, *21*(6), 4337–4347. http://doi.org/10.1007/s10570-014-0450-9

Yoon, S., and Deng, Y. (2004). Flocculation and reflocculation of clay suspension by different polymer systems under turbulent conditions, *278*, 139–145. http://doi.org/10.1016/j.jcis.2004.05.011

Zainuddin, S. Y. Z., Ahmad, I., and Kargarzadeh, H. (2013). Cassava starch biocomposites reinforced with cellulose nanocrystals from kenaf fibers. *Composite Interfaces*, *20*(3), 189–199. http://doi.org/10.1080/15685543.2013.766122

Zuraida, A., Yusliza, Y., Nurizan, O., Anuar, H., Zahurin, H., and Noorasikin, S. (2012). Properties of Montmorillonite-Reinforced Thermoplastic Sago Starch Composites, *445*, 469–474. http://doi.org/10.4028/www.scientific.net/AMR.445.469

CHAPTER 3
Materials, Methods and Raw Materials Characterization

3.1 General

This chapter describes the methods for raw materials characterization, starch composites preparation, and composites characterization. Initially, the procedures for the characterization of starch, mature fine tailings, and dean stark solids are described. After that, polymer composites preparation and their characterization in terms of physical, mechanical and thermal properties are explained. Finally, the results of the raw material characterization will be discussed.

3.2 Materials

The materials used for the synthesis of the starch were a commercial cornstarch grade, glycerol from Sigma-Aldrich, deionized water, mature fine tailings from Suncor's Oil sands plant, sodium cloisite from BYK additives, and cellulose nanocrystals from Celluforce. The materials used for characterization will be mentioned in each section. The equipment for composites preparation consisted on an AND FX-4000 balance, a Caframo BDC6015 stirrer with a Rushton turbine type impeller, and a Carver Laboratory Press 4186 with heated platens.

3.3 Methods for Raw Materials Characterization

3.3.1 Starch characterization

Since the used cornstarch comes from a commercial source, characterization was required to determine if there was significant variation in the amylose content and moisture. Additionally, the preparation of the composites required heating of a mixture of starch, glycerol, water, and fillers, in proportions that will be shown later, above the gelatinization temperature of starch; therefore, differential scanning calorimetry (DSC) was also used to characterize the cornstarch sample.

3.3.1.1 Amylose content

The determination of amylose content was performed following a modification of the standard method ISO 6647-1, which takes advantage of the blue colored iodine complex formed by the amylose double helices.

For this method, a calibration curve was prepared by measuring the absorbance at 620 nm (λ_{620}) and 510 nm (λ_{510}) wavelengths of standard amylose and amylopectin solutions in different proportions, with the addition of an iodine solution to achieve different tones of blue (Kaufman, Wilson, Bean, Herald, and Shi, 2015). The difference λ_{620}-λ_{510} was plotted as a function of concentration of the standard solutions. Finally, three samples of starch from different lots were used to prepare solutions with iodine and measure the absorbance, which was read in the calibration curve to determine the estimated amylose content. The detailed procedure can be found on Appendix A.

3.3.1.2 Moisture measurement

To determine the moisture content, an approximate amount of 2 grams of starch were put in an aluminum pan specifically designed to fit in an Ohaus MB 45 moisture meter. The equipment heated the sample up to a temperature of 105 °C and recorded the mass loss with time. Once the mass loss curve became a horizontal line, which happened in about forty minutes and meant there was no more water loss, the moisture weight percentage was recorded.

3.3.1.3 Gelatinization temperature

The gelatinization temperature of the starches was determined by DSC. Initially, 5 grams of starch were combined with 10 grams of water in a closed vial, and mixed for 10 minutes to disperse the starch in water. After mixing, between 5 and 10 mg of the mixture were weighed in a 40 µl aluminum crucible and capped with a crucible press. Finally, the sealed crucible was put in a Mettler Toledo DSC 3 at a heating rate of 10 °C/min to obtain the corresponding thermogram, which showed the heat flow in the sample from 25 °C to 100 °C.

3.3.1.4 X-ray diffraction (XRD)

A commercial starch sample was dried in an oven for 24 hours at 60°C and analyzed as a powder in an Ultima IV XRD machine with CuK_α (λ = 1.54 Å) radiation to later compare the diffractogram with the one resulting from plasticized starch. The range for the angle was between 5 and 45 degrees.

3.3.2 MFT characterization

3.3.2.1 MFT composition

The composition of MFT was measured using a Dean Stark extraction process, which allows the separation of the bitumen from the solids using toluene as a solvent for bitumen. The apparatus can be seen in Figure 3.1.

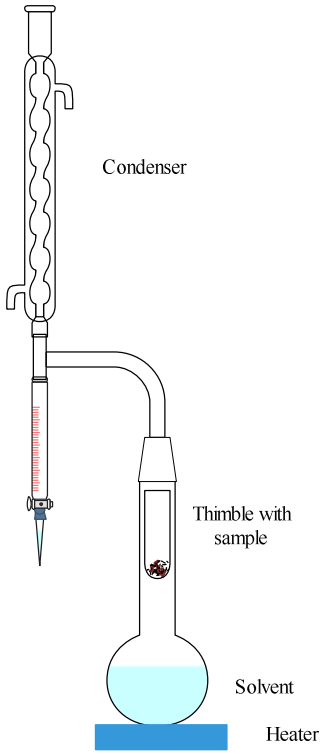

Figure 3.1. Dean Stark apparatus for MFT composition determination.

In this extraction process, about 130 g of MFT were put in a pre-weighed thimble for water and bitumen extraction. The toluene boiled in the round bottom glass and its vapors went from the top condenser to the collection tip, but after overfilling it the toluene fell back in the thimble to dissolve the bitumen present in the MFT sample. The heating continued for at least 10 hours, and water was collected from the collection tip valve to avoid it from falling back into the thimble.

Once the toluene falling to the round bottom glass was completely clear, the heating mantle was turned off and the system was left to cool down. The toluene in the collection tip valve was recovered in a beaker, the thimble with the solids was left in the fume hood to dry, and the bitumen-toluene mixture was put in a pre-weighed aluminum pan to let toluene evaporate, also inside the fume hood.

All the toluene in the mixture was considered to be evaporated after 24 hours in the fume hood, which is when the water, thimble, and bitumen pan were weighed to determine the weight percentage of each component from the MFT using the equations below,

$$Water\ wt\% = \frac{Recovered\ water\ from\ side\ valve\ (g)}{Initial\ mass\ of\ MFT\ (g)} * 100 \quad (3.1)$$

$$Bitumen\ wt\% = \frac{Mass\ of\ aluminum\ Pan\ (g) - Mass\ of\ empty\ pan\ (g)}{Initial\ Mass\ of\ MFT\ (g)} * 100 \quad (3.2)$$

$$Solids\ wt\% = \frac{Mass\ of\ thimble\ with\ solids\ (g) - Mass\ of\ empty\ thimble\ (g)}{Initial\ mass\ of\ MFT\ (g)} * 100 \quad (3.3)$$

$$Lost\ material\ (\%) = \frac{Sum\ of\ Water, Bitumen\ and\ Solids\ (g)}{Initial\ mass\ of\ MFT\ (g)} * 100 \quad (3.4)$$

Once all the results were calculated, they were normalized so their summation reached 100%. The solids were recovered from the thimbles in each extraction, crushed in a ring and puck pulverizer, and left to dry in an oven for 24 hours at 65 °C to be used as fillers in the composites.

3.3.2.2 X-ray diffraction

A MFT sample was dried in an oven for 24 hours at 60°C and ground with a ring and puck pulverizer to then be analyzed as a dry powder in an Ultima IV XRD spectrometer with CuK_{α} (λ

= 1.54 Å) radiation, with the objective of comparing the diffractogram with the one from MFT composites. The range for the angle was between 5 and 45 degrees.

3.3.2.3 Particle size distribution

An MFT sample was put in a **Malvern Mastersizer 3000 particle sizer** to determine the volume density, number density, and the diameter at which 50% of the sample volume is comprised of smaller particles (D_{50}). The laser obscuration was set between 10 and 11%.

3.3.3 Dean Stark solids characterization

3.3.3.1 Thermogravimetric analysis (TGA)

A sample of Dean Stark solids was sent for thermogravimetric analysis (TGA) in order to quantify the amount of organic material left in the solids after toluene extraction. A mass of 7 mg of solids were put in a crucible in the sample holder of a Mettler Toledo TGA/DSC1, covering a range that goes from 25 °C to 900 °C at a heating rate of 10 °C/min. A duplicate sample was run to confirm repeatability.

3.3.3.2 X-ray diffraction

A Dean Stark solids sample was dried in an oven for 24 hours at 60°C and analyzed as a dry powder in an Ultima IV XRD machine with CuK_{α} (λ = 1.54 Å) radiation to later compare the diffractogram with the Dean Stark solids composites. The range for the angle was between 5 and 45 degrees.

3.4 Methods for starch-based composites preparation

A fixed amount of starch, glycerol, filler and water were weighed in a 400-mL beaker in the proportions shown in Tables 3.1 and 3.2 for MFT composites, and in the proportions shown in

Tables 3.3 and 3.4 for Dean Stark, montmorillonite (MMT) and cellulose nanocrystals (CNC) composites.

Table 3.1. Composition of mixture for the preparation of three thin sheets (3.4 mm thickness sheets) of MFT composites.

Sample Tag	T0	T1	T2	T3	T5	T10	T20
Filler (%)*	0	1	2	3	5	10	20
Starch (g)	135	135	135	135	135	135	135
Glycerol (g)	65.1	65.1	65.1	65.1	65.1	65.1	65.1
Water (g)	81.00	78.52	76.05	73.57	68.62	56.23	31.46
MFT (g)	0	3.87	7.74	11.61	19.35	38.7	77.4

*Weight percentage with respect to the starch content.

Table 3.2. Composition of mixture for the preparation of thick sheets (12.5 mm thickness sheets) of MFT composites.

Sample Tag	T0	T1	T2	T3	T5	T10	T20
Filler (%)*	0	1	2	3	5	10	20
Starch (g)	200	200	200	200	200	200	200
Glycerol (g)	96.4	96.4	96.4	96.4	96.4	96.4	96.4
Water (g)	120.00	116.29	112.58	108.87	101.44	82.89	45.77
MFT (g)	0	5.71	11.42	17.13	28.55	57.10	114.20

*Weight percentage with respect to the starch content.

Table 3.3. Composition of mixture for the preparation of three thin sheets (3.4 mm thickness sheets) of Dean Stark, Na^+ Cloisite, and Cellulose Nanocrystals composites.

Sample Tag*	XX-1	XX-2	XX-3	XX-5	XX-10	XX-20
Filler (%)**	1	2	3	5	10	20
Starch (g)	135	135	135	135	135	135
Glycerol (g)	65.1	65.1	65.1	65.1	65.1	65.1
Water (g)	81.00	81.00	81.00	81.00	81.00	81.00
Filler (g)	1.35	2.7	4.05	6.75	13.5	27

*XX is DS for Dean Stark solids composites, MMT for Na^+ Cloisite composites and CNC for cellulose nanocrystals composites.

**Weight percentage with respect to the starch content.

Table 3.4. Composition of mixture for the preparation of thick sheets (12.5 mm thickness sheets) of Dean Stark, Na^+ Cloisite, and Cellulose Nanocrystals composites.

Sample Tag*	XX-1	XX-2	XX-3	XX-5	XX-10	XX-20
Filler (%)**	1	2	3	5	10	20
Starch (g)	200	200	200	200	200	200
Glycerol (g)	96.4	96.4	96.4	96.4	96.4	96.4
Water (g)	120	120	120	120	120	120
Filler (g)	1.35	2.7	4.05	6.75	13.5	27

*XX is DS for Dean Stark solids composites, MMT for Na^+ Cloisite composites and CNC for cellulose nanocrystals composites.

**Weight percentage with respect to the starch content.

Tables 3.1 and 3.2 show that there are two types of sheet for characterization purposes, thin (3.4 mm thickness) and thick (12.5 mm thickness). Glycerol and starch amounts stay constant for each type of sheet and in the same proportion, and water content varies to compensate for the water present in MFT to achieve an overall constant water content. The case is similar for the rest of the composites in Tables 3.3 and 3.4, with the exception of water compensation.

After the components were weighed in the same beaker, they were mixed by hand until the solids lumps were not detected visually. The mixture was then put in the stirrer at 600 rpm for 180 minutes, as seen in Figure 3.2.

Figure 3.2. Stirrer set up for composites preparation.

The mixture was then removed from the stirrer and 75 g were poured in 130 mm x 130 mm x 3.4 mm carbon steel molds with the caps covered with a Teflon sheet, as seen in Figure 3.3. In the case of the thick sheets, 380 g of the mixture were poured into a 13 cm x 13 cm x 1.25 cm molds. The mold was pressed at 2.36 metric tons and heated at 110 °C for one minute in the case of thin sheets and 3 minutes in the case of thick sheets, and then it was left to cool under pressure until the temperature was less than 60 °C, which happened in a period of 45 minutes.

Finally, the pressure was released, the mold was removed from the press, and the composite removed from the mold to dry it at room temperature for 48 hours. During this time, there was retrogradation of the starch molecules. After the drying period, the pieces were put in sealed plastic bags until the conditioning process.

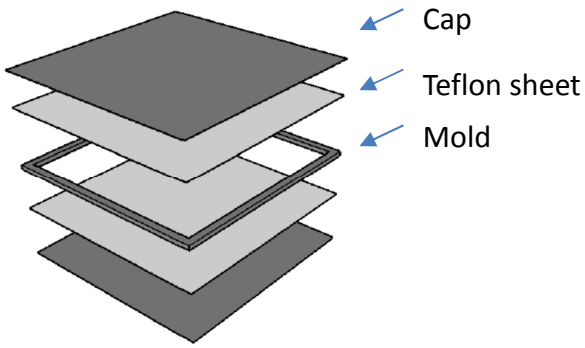

Figure 3.3. Mold used for thin (3.4 mm thickness) sheets.

3.5 Methods for Starch-Based Composites Characterization

3.5.1 Water absorption

Water absorption on the composites was measured following the 2-hour immersion experiment described in ASTM D570-98. Three 1-inch x 3-inch pieces from the thin sheets of each composite were cut and left in a desiccator for 48 hours at a controlled relative humidity of 58%, achieved with the use of sodium bromide. The samples were then weighed and dried in an oven at 60 °C for 24 hours to determine the initial moisture by weight difference using equation 3.5. After that, the samples were immersed in water for 2 hours and then weighed to determine water uptake with equation 3.6. Finally, the samples were dried in an oven at 60 °C for 24 hours to

determine mass loss with equation 3.7. The data calculated from the water absorption measurement can be seen on tables B.4 and B.5 in Appendix B.

$$Initial\ Moisture\ (wt\%) = \frac{Initial\ weight\ (g) - Weight\ after\ 1st\ drying\ (g)}{Initial\ weight\ (g)} * 100 \quad (3.5)$$

$$Uptake\ (wt\%) = \frac{Weight\ after\ 2h\ immersion\ (g) - Weight\ after\ 1st\ drying\ (g)}{Weight\ after\ 1st\ drying\ (g)} * 100 \quad (3.6)$$

$$Mass\ loss\ (wt\%) = \frac{Weight\ after\ 1st\ drying\ (g) - Final\ dry\ weight\ (g)}{Weight\ after\ 1st\ drying\ (g)} * 100 \quad (3.7)$$

3.5.2 Scanning electron microscopy

To study the morphology of selected starch composites and visualize clay dispersion in the starch matrix, thin films of less than 150 μm were cut with a scalpel, gold coated in a Delton Gold Sputter unit, and examined under a Zeiss EVO MA10 scanning electron microscope.

3.5.3 Tensile test

The tensile test followed the procedure of ASTM D638 using twelve Type IV specimens. Two bone-shaped specimens were cut from each of six thin sheets coming from two batches of mixture using a stainless-steel cutter. The specimens were conditioned in a desiccator for 48 hours at a controlled relative humidity of 58%. They were tested in an Instron 5943 machine with a speed of 10 mm/min and setting the report to include tensile modulus, tensile strength and elongation at break. The software of the machine automatically calculated the modulus by dividing the stress-strain curve in six sections going from the zero-strain point to the point of maximum stress, applying a square fit algorithm to each region to determine their slope, determining the pair of consecutive regions with the highest slope sum, and assigning the value of the highest slope of the pair to the modulus. Random curves were checked by determining the slope in the section around 3% strain, obtaining similar values of modulus as the ones reported from the software. The tensile strength was reported by the software as the stress at the highest point of the stress-strain curve. The elongation at break was calculated manually at the point after the maximum stress when the curve becomes linear with a negative slope, indicating a rapid

linear decrease of the load. The tensile modulus and tensile strength used for characterization of the composites were the ones reported by the software. The tensile test data for each specimen tested is shown on Table B.6 of Appendix B.

3.5.4 Compression test

The compressive modulus, strength, and strain at break were determined following ASTM D695-15 using four standard 12.7 mm x 12.7 mm x 25.4 mm specimens. Two specimens were cut from each of two thick sheets and conditioned in a desiccator for 48 hours at a relative humidity of 58%. The test was performed on an ElectroForce 3510 universal testing machine with a compression speed of 1.3 mm/min. The stress and strain were calculated with the measurement of the specimens and the reported load and displacement from the machine. The compression modulus was calculated as the slope of the curve around 5% strain; the compressive strain was recorded as the highest value of stress, and the strain at break was calculated at the point at which the curve becomes almost linear with a negative slope. The compression test data for each specimen tested is shown on Table B.8 of Appendix B.

3.5.5 Dynamic mechanical analysis

The DMA was performed using a TA Q800 analyzer with a one-point bending set-up in a range from -100 °C and 60 °C and a frequency of 1 Hz in the Lipids Chemistry Laboratory of the Faculty of Agricultural, Life and Environmental Sciences of the University of Alberta. The required 12.5 mm x 35.4 mm x 2.8 mm specimens were cut from thin pieces using a knife and a ruler and conditioned in a desiccator for 48 hours at a relative humidity of 58% before testing.

3.5.6 Density

The samples cut for water absorption and DMA were measured on each side with a caliper to determine an average volume of each piece, and were then weighed to determine the density as mass/volume in g/cm^3. The measurement of mass, volume and density for each specimen can be seen on tables B.1, B.2 and B.3 of Appendix B.

3.5.7 X-Ray diffraction (XRD)

For each composite, 18 mm x 16 mm sized pieces were cut from thin sheets for testing in an Ultima IV XRD machine with CuK_α (λ = 1.54 Å) radiation to determine any angle displacement in the peaks related to the clays present in each composite. The range for the angle was between 5 and 45 degrees. If the peak shifted, indicating a change in the interlayer clay spacing, the latter was calculated with Equation (2.1), using θ and λ to determine *d*.

3.6 Raw Materials Characterization

3.6.1 Starch characterization

3.6.1.1 Estimated amylose content in starch

As shown in Figure 3.4, the plot λ_{620}-λ_{510} versus amylose weight percentage follows a linear trend, which can then be used to determine the amylose content of any starch sample by measuring the absorbance at the mentioned wavelengths.

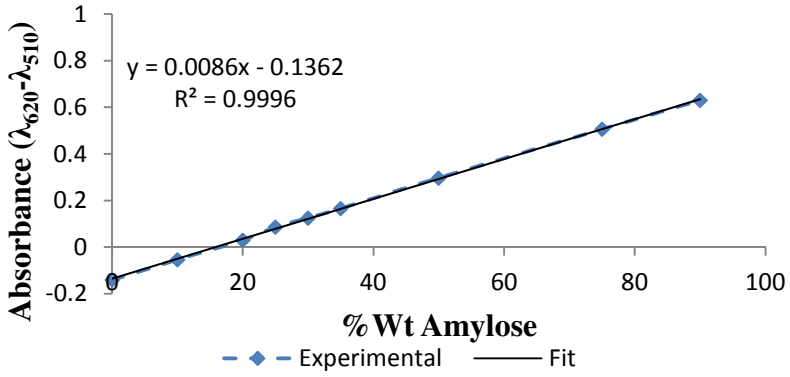

Figure 3.4. Calibration curve for amylose content determination.

The samples of commercial starch from different batches gave the results showed in Table 3.5 for amylose content estimation. The measurement of the amylose content is important since

its crystallization during the retrogradation process of starch may affect the mechanical properties of the composites.

The results indicate that the amylose values are close and the small variation might be due to experimental error. It is also worth mentioning that the amylose content reported in table 3.5 as 18.63 ± 1.21 wt % is an estimated value and not the real one, since the amylose can also form a complex with the lipids present in starch.

Table 3.5. Estimated amylose content of commercial starch used for composites preparation.

Sample	λ_{620}-λ_{510}	Estimated Amylose Content (wt %)	Average Amylose content (wt %)	Standard Deviation
1	0.03	19.33		
2	0.012	17.23	18.63	1.21
3	0.03	19.33		

3.6.1.2 Moisture content in commercial starch.

As with the amylose content, the moisture content of the starch has to be measured to determine the variability of water content in the composites. As shown in Table 3.6, the moisture content of the commercial starch is 9.87% ± 0.3 wt %, which is around the same value found in literature for similar starch samples (Ma, Chang, and Yu, 2012). The standard deviation indicates that it is not necessary to adjust the water content of starch before preparing the composites.

Table 3.6. Moisture measurement of commercial starch samples.

Sample	Moisture Content (wt %)	Average Moisture Content (wt %)	Standard Deviation
1	9.55		
2	10.14	9.87	0.30
3	9.92		

3.6.1.3 Determination of gelatinization temperature

The thermogram resulting from the differential scanning calorimetry made on the commercial starch is shown in Figure 3.5. The onset of the peak indicates the gelatinization

temperature, which is within the range of 62-72 °C found in literature for cornstarch (Eckhoff and Watson, 2009).

The gelatinization temperature is important for the preparation of starch composites, since it allows picking a temperature high enough for the composites preparation to achieve a disruption of the hydrogen bonds and allow the formation of new bonds with plasticizer. The preparation of the composites was made at 110 °C, a value higher than the gelatinization range, to guarantee the complete gelatinization of the starch granules.

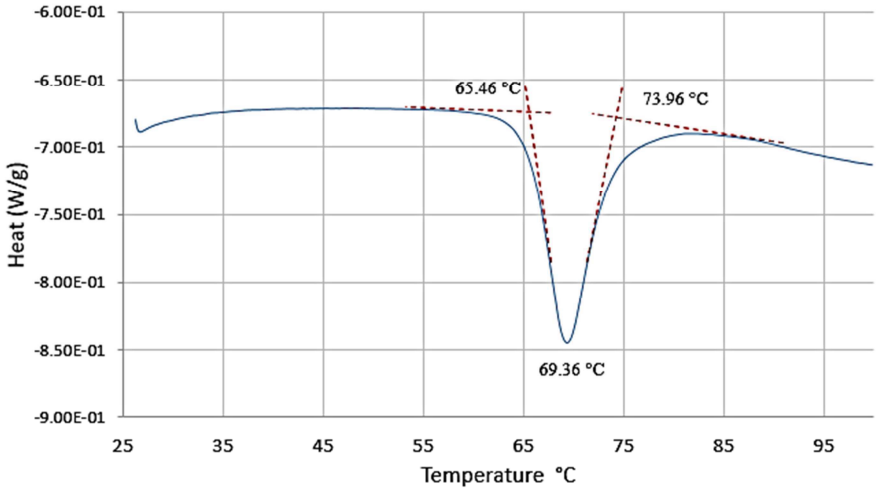

Figure 3.5. Thermogram of commercial cornstarch, indicating the gelatinization temperature range.

3.6.2 Mature fine tailings characterization

3.6.2.1 Composition of MFT

The composition of MFT determined by Dean Stark extraction yielded a 35.08 wt% of solids, 4.17 wt % of bitumen, and 60.75 wt % of water, which agrees with the range of values reported for most MFT samples. The MFT used for composites preparation was stored in the same bottle used for composition measurement.

3.6.2.2 Particle size distribution

The particle size distribution of MFT is valuable information when studying the mechanical properties of composites. Figure 3.6 shows that the particle size distribution ranges from 0.2 to 211 µm, with a volume D_{50} of 16.1 µm. Volume D_{50} is defined as the median value of the volume distribution, and it indicates that 50% of the volume is occupied by particles with a size of D_{50} = 16.1 µm or less. This value is important for comparison purposes, as the D_{50} of sodium cloisite is 25 µm, around the same range of magnitude as the MFT particles. When looking at the number density, Figure 3.6 shows that most particles are less than 1 µm in size, even though fewer big particles occupy more volume in the sample.

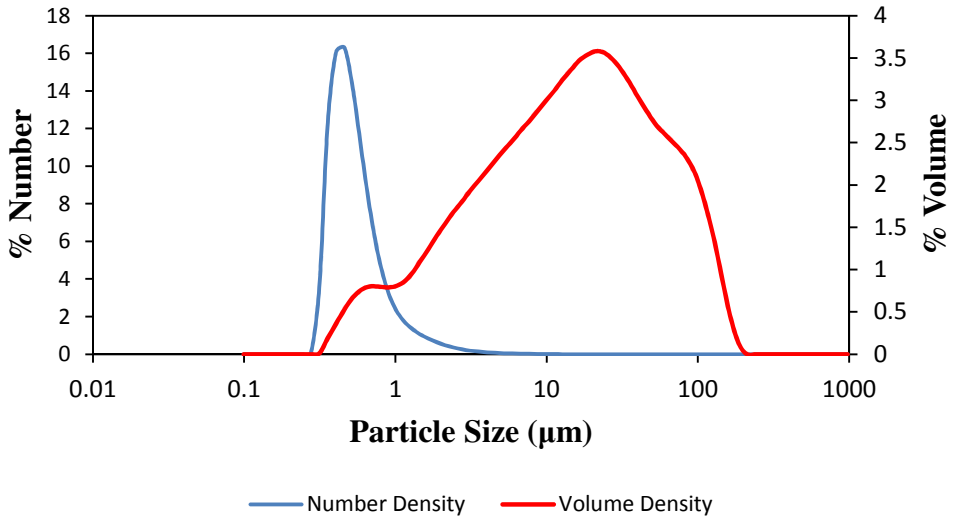

Figure 3.6. Volume density and number density of MFT particles.

3.6.3 Dean Stark solids characterization

Although many essays may be done on the solids present in MFT, the focus of this characterization was the thermogravimetric analysis (TGA). Figure 3.7 shows a significant mass loss of 11.01 wt % between 360 and 550 °C, indicating that there still are organic compounds present in the solids after Dean-Stark extraction. These are tightly bound organics that have been reported before as part of the clays coming from the Athabasca oil sands (Kaminsky, Etsell, Ivey, and Omotoso, 2006; Oladipo Omotoso, 2004; Oladipo Omotoso, Mikula, and Stephens, 2002).

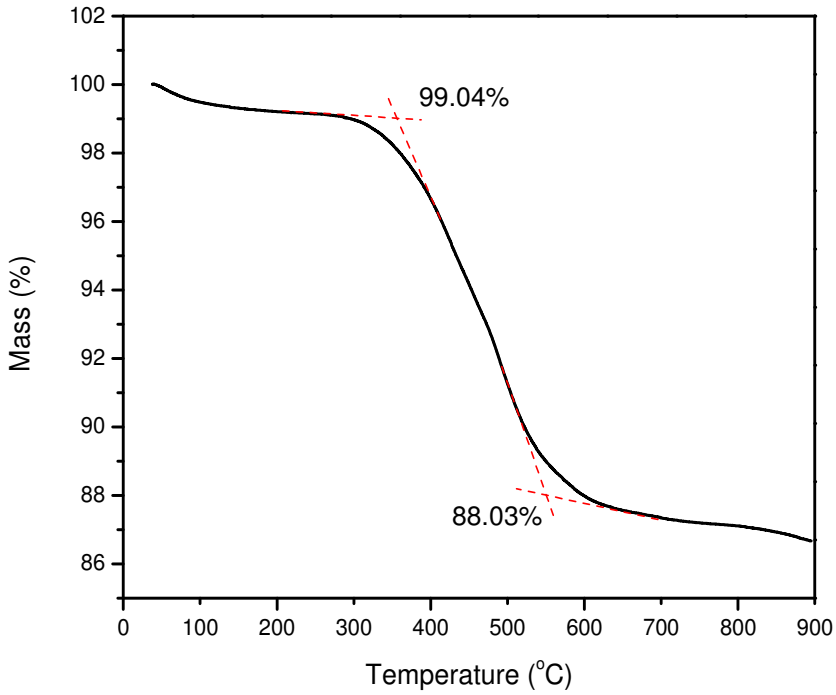

Figure 3.7. Thermogravimetric analysis of Dean Stark solids.

3.7 Summary

This chapter provided detailed information on techniques used to characterize corn starch, MFT and Dean Stark solids, as well as for starch based composites, including morphology and x-ray diffraction patterns, density, water absorption, tensile properties, compression properties, and dynamic mechanical thermal analysis. Additionally, a discussion on the characterization of raw materials was presented, including the results of amylose, moisture and gelatinization temperature for starch, composition and particle size distribution for MFT, and finally the thermal gravimetric analysis of Dean Stark solids. The results from these methods, plus the characterization of the raw materials, set the basis for the discussion on the properties of the composites in the following chapter.

References

Eckhoff, S. R., and Watson, S. A. (2009). Chapter 9 Corn and Sorghum Starches: Production. In *Starch* (Third Edit, pp. 373–439). Elsevier Inc.

Kaminsky, H., Etsell, T., Ivey, D. G., and Omotoso, O. (2006). Fundamental Particle Size of Clay Minerals in Athabasca Oil Sands Tailings. *Clay Science*, *12*(Supplement 2), 217–222.

Kaufman, R. C., Wilson, J. D., Bean, S. R., Herald, T. J., and Shi, Y.-C. (2015). Development of a 96-well plate iodine binding assay for amylose content determination. *Carbohydrate Polymers*, *115*, 444–447. https://doi.org/10.1016/j.carbpol.2014.09.015

Ma, X., Chang, P. R., and Yu, J. (2012). Chapter 4 Plasticized Starch. In J. Ahmed, B. K. Tiwari, S. H. Imam, and M. A. Rao (Eds.), *Starch-Based Polymeric Materials and Nanocomposites Chemistry, Processing and Applications* (pp. 69–83). CRC Press Taylor and Francis Group.

Omotoso, O. (2004). High surface areas caused by smectitic interstratification of kaolinite and illite in Athabasca oil sands. *Applied Clay Science*, *25*(1–2), 37–47. https://doi.org/10.1016/j.clay.2003.08.002

Omotoso, O., Mikula, R. J., and Stephens, P. W. (2002). Surface Area of Interstratified Phyllosilicates in Athabasca Oil Sands From Synchrotron XRD. *Advances in X-Ray Analysis*, *45*, 391–396.

CHAPTER 4

Mature Fine Tailings Composites Characterization

4.1 General

This chapter will cover the main physical, mechanical, and thermal properties of starch based composites using mature fine tailings (MFT) as a filler, and compare them with composites made with sodium montmorillonite (MMT), cellulose nanocrystals (CNC), and Dean Stark solids (DS).

4.2 Composite morphologies

The optical photographs of plasticized starch and MFT composites with 1% filler are shown in Figure 4.1. The surfaces are smooth, with a pattern imprinted by the teflon sheet used to prepare the pieces. In addition, the MFT composite is darker than the plasticized starch because of the clay particles embedded in the starch matrix.

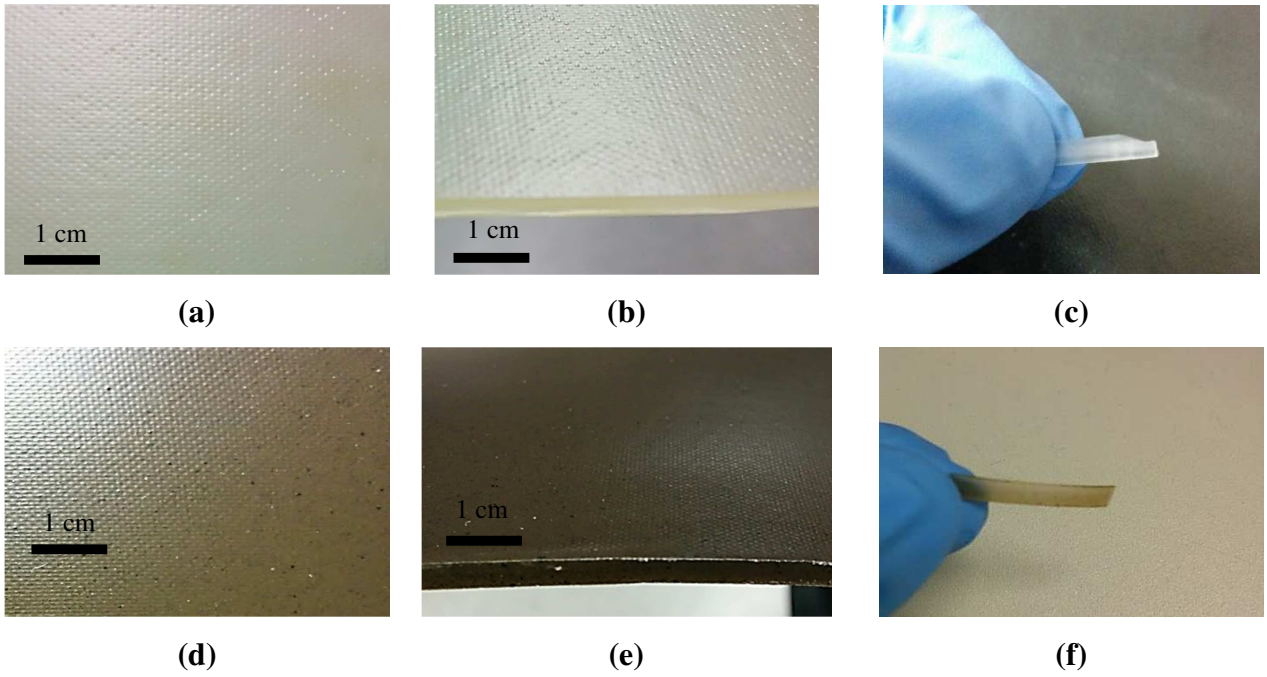

Figure 4.1. Surface (a.d), edge (x,y) and transversal cut (x,y) of thermoplastic starch (a,b,c) and 1% MFT composite (d,e,f) respectively.

From the transversal area of the sheets, a small film of less than 150 µm was cut for SEM imaging in order to investigate the microstructure of each piece in more depth. The surface of the plasticized starch is compared to those of MFT composites with two MFT loadings in Figure 4.2, showing that voids in the surface of the structure are formed by the evaporation of water during the making of the composites. As the MFT content goes from 2 to 5%, the surface becomes rougher and the number of voids increases. A decrease in strength and elasticity of the material is also expected.

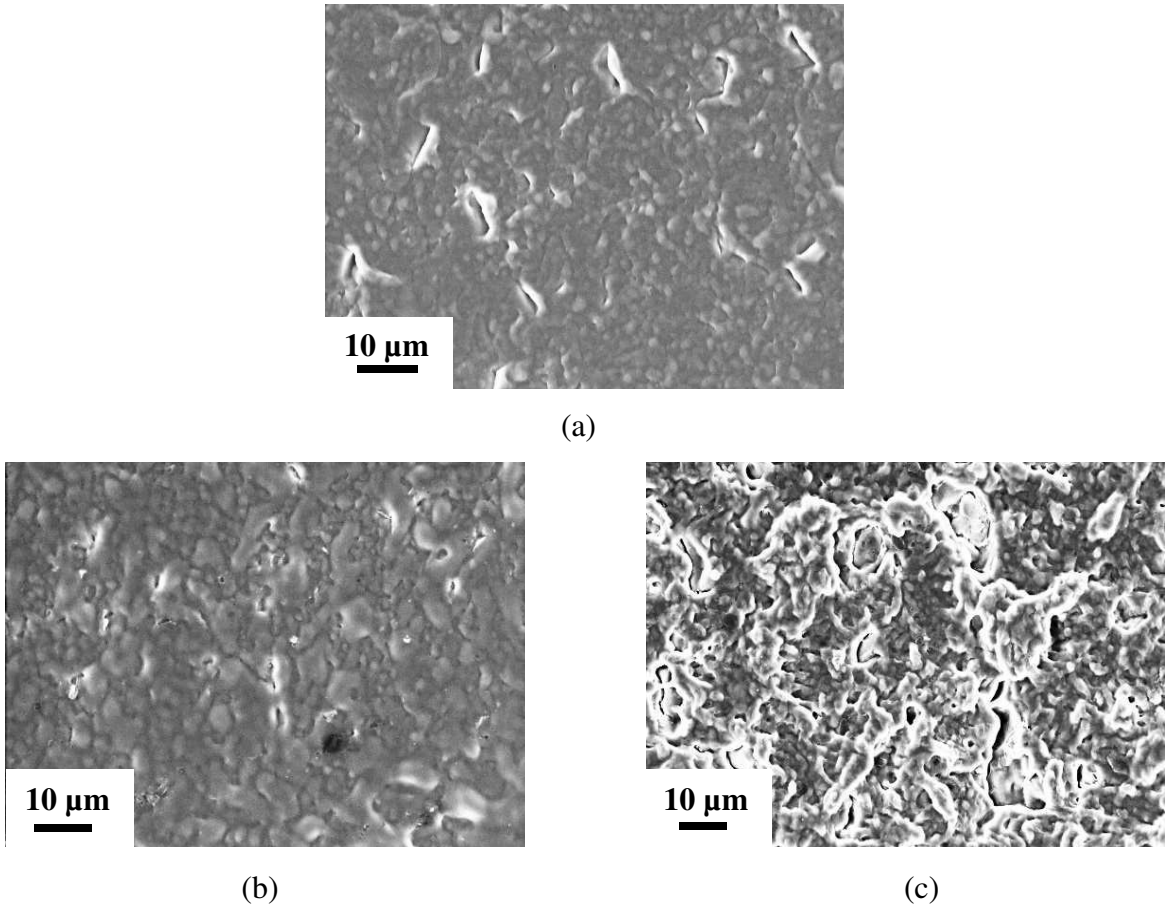

(a)

(b)

(c)

Figure 4.2. SEM of plasticized starch and MFT composites: a) Plasticized starch; b) 2% MFT composite; c) 5% MFT composite.

A close up in some of the structural voids of the MFT composites shows the presence of the clays, and black stains indicate the presence of bitumen, as seen in Figure 4.3. Even though clay seems to be well dispersed in the starch matrix, a few agglomerates can also be seen in the SEM

micrographs. Figure 4.3 (left column) shows that the size of the clay agglomerates seems to be larger for 5% MFT than for 2% MFT, and that fine particles are scattered all over the clay agglomerates (right column).

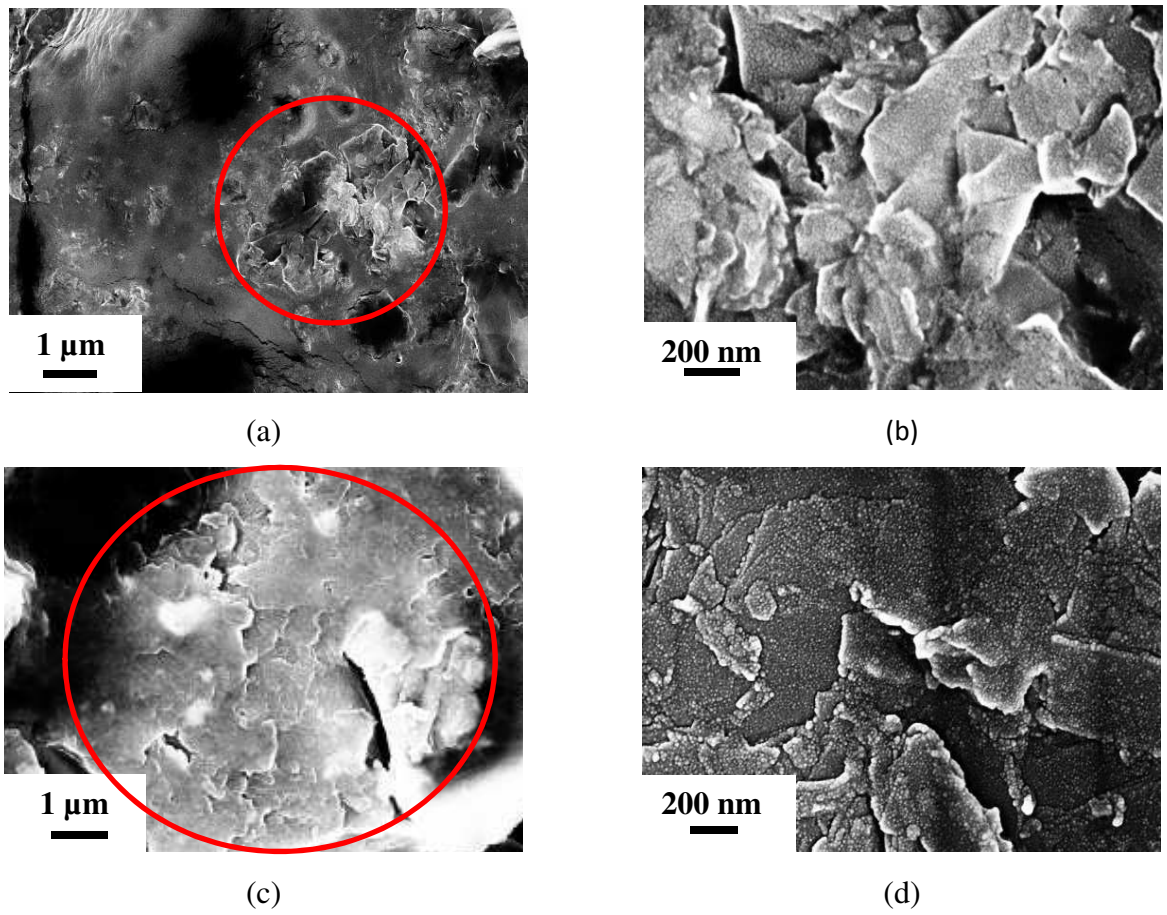

Figure 4.3. SEM micrographs of MFT composites showing clays and bitumen: a) clay agglomerates on a 2% MFT composite; b) bright spots on clay agglomerates of a 2% MFT composite, indicating the presence of fine particles; c) clay agglomerates on a 5% MFT composite; d) fine particles on clay agglomerates of a 5% MFT composite.

When comparing to Dean Stark composites, the same morphology without the presence of bitumen is expected. The SEM micrograph for 2% DS composites shown in Figure 4.4 confirms the expectation, as the surface looks similar to the one with 2% MFT, except that there are no black areas due to the absence of bitumen, and the clays can be seen together with the scattered fines.

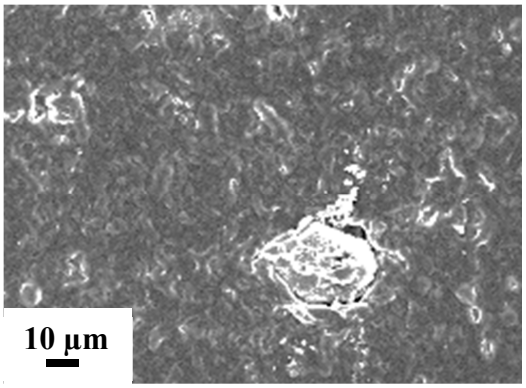

(a)

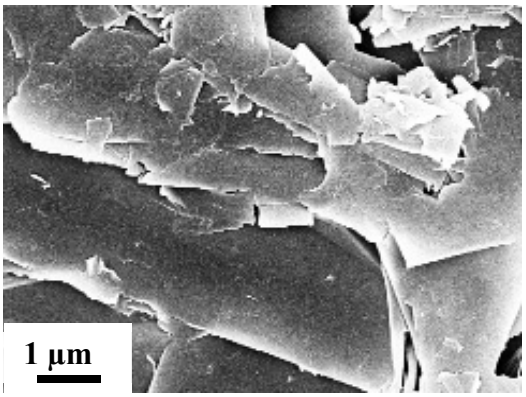

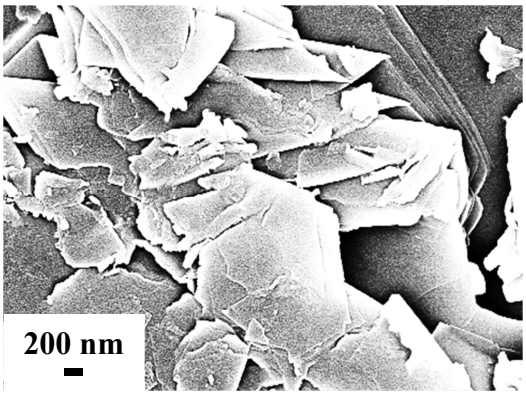

(b) (c)

Figure 4.4. SEM of a 2% DS composite showing surface and clays: a) surface; b) clay agglomerates; c) fine particles on clay agglomerates.

In the case of MMT composites, the surface of the composites is similar to the surface of MFT and DS composites, but it was harder to find a good spot where the clays were exposed. Figure 4.5 shows the surface of MMT composites on the left and the clays identified by the sharp edges on the right side. Although SEM is not the proper analysis to confirm intercalation or exfoliation of the clays, the fact that they look completely covered by the starch matrix on the right side of Figure 4.5 leads us to think that MMT may be intercalated. This hypothesis was proven later via X-ray diffraction, as discussed below.

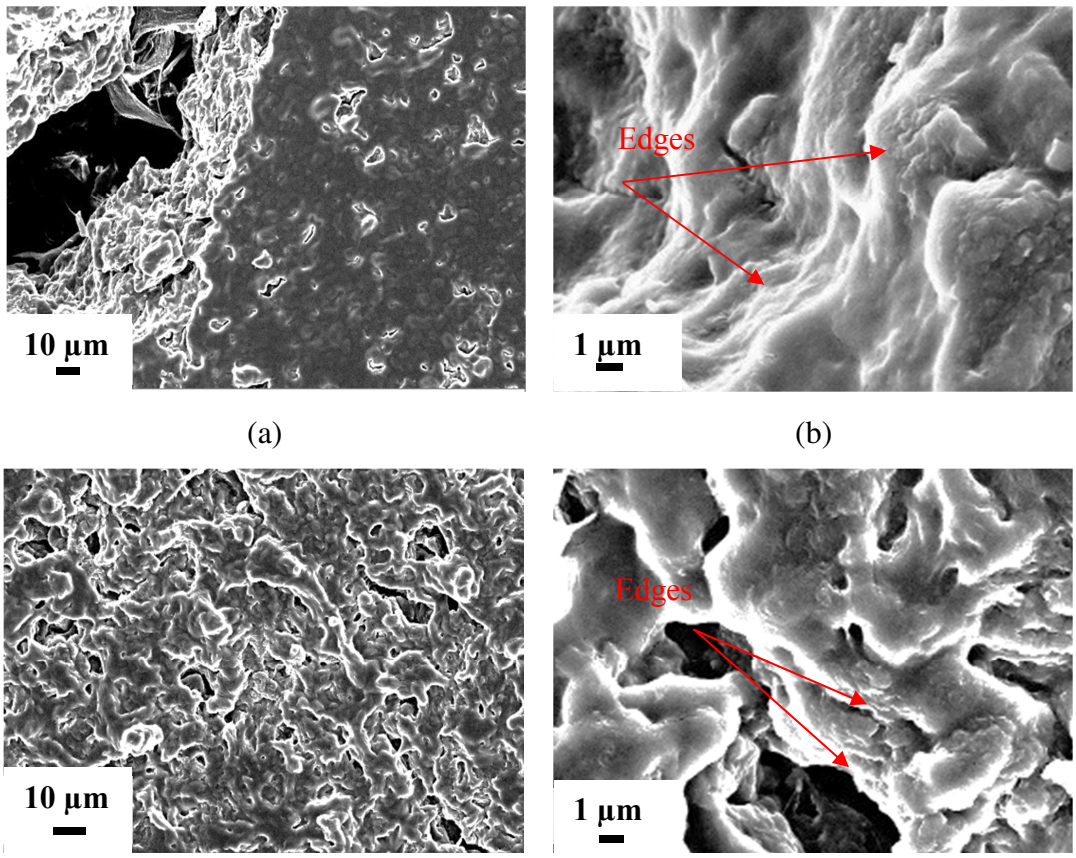

Figure 4.5. SEM micrographs of MMT composites: a) surface of a 2% MMT composite; b) clays embedded in the starch matrix of a 2% MMT composite; c) surface of a 5% MMT composite; d) edges of clays embedded in the starch matrix of a 5% MMT composite.

The same difficulties to visualize the filler under SEM was faced when analyzing the CNC composites in Figure 4.6, as the surface was smoother, with no salient details other than bright small segments and dots that might indicate the presence of CNC nanocrystals, contrary to the results reported by Zainuddin, Ahmad, and Kargarzadeh (2013) that showed clear bright spots in the cassava starch matrix. This lack of surface details is a good sign of strong starch-CNC interactions, but it has to be further studied with a different imaging technique.

The SEM micrographs shown in Figure 4.2 to 4.6 indicate that the morphology of composites made with MFT, MMT and CNC differ drastically, and that one could expect their properties to also vary significantly. Composites made with MFT and DS solids have closer morphologies,

differing mainly on the presence or absence of bitumen, and will provide an interesting comparison on the effects to fugitive bitumen in the properties of these composites.

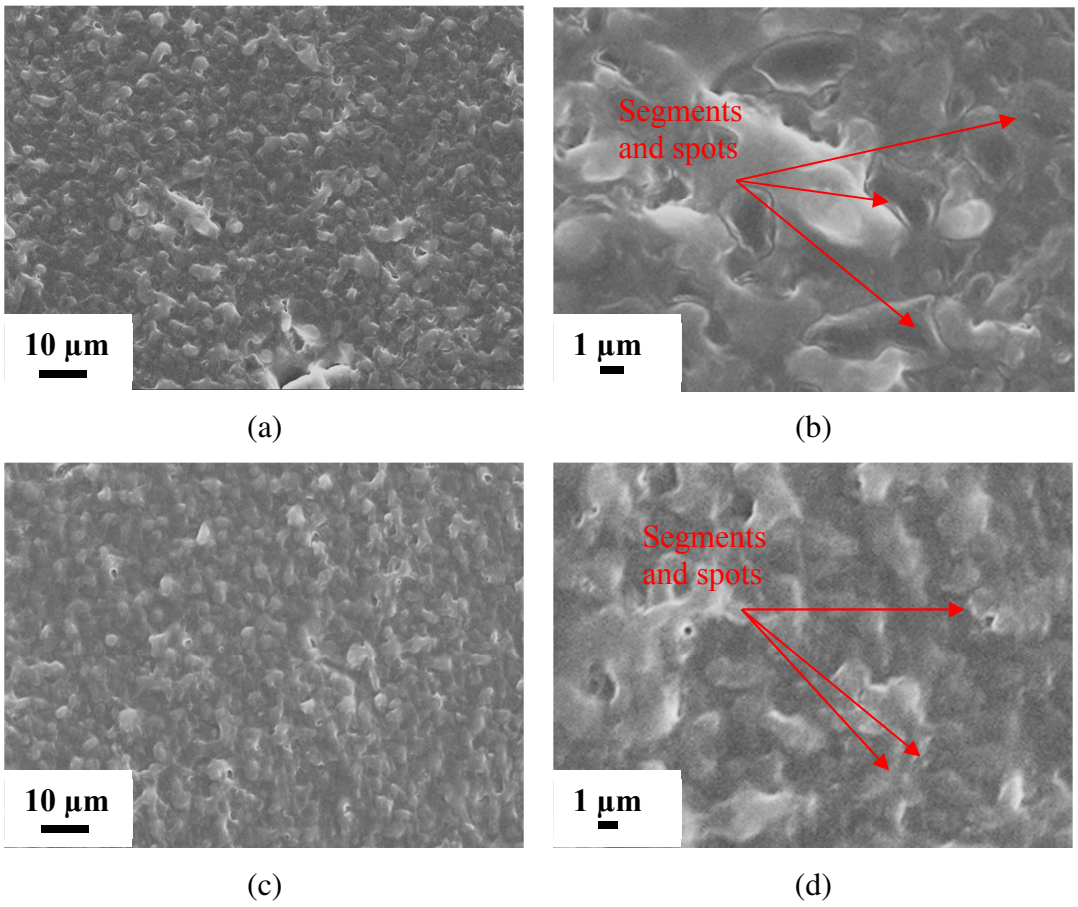

Figure 4.6. SEM micrographs of CNC composites: a) surface of a 2% CNC composite; b) bright segments and spots on the surface of a 2% CNC composite that might indicate the presence of nanocrystals; c) surface of a 5% CNC composite; d) bright segments and spots on the surface of a 5% CNC composite surface.

4.3 Density

The density of MFT composites as a function of MFT loading is shown in Figure 4.7. The density is relatively flat for up to about 10% MFT loading (considering the experimental error), but starts increasing for filler loadings higher than 10%. The increase in density is likely due to the higher solids loading and reduced expansion of the starch matrix due to the higher viscosity of the composite at high filler loadings (Kaewtatip, Tanrattanakul, and Phetrat, 2013).

Additionally, during cooling, retrogradation and water loss causes the composite to shrink, but composites with higher MFT content shrink less, which also explains the observations shown in Figure 4.7.

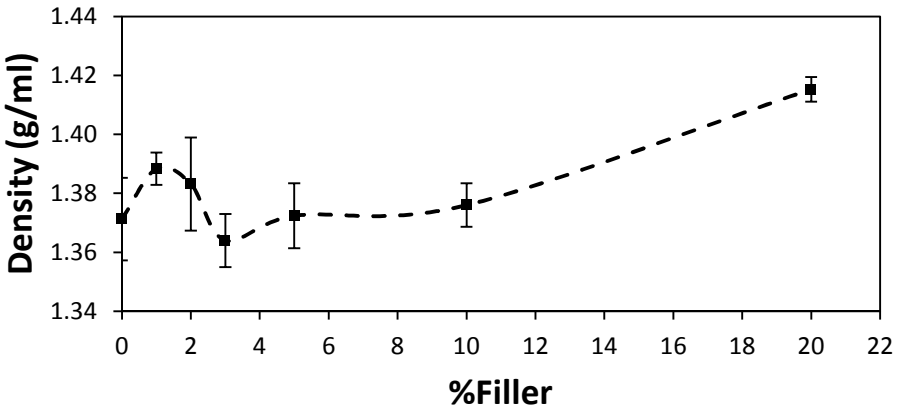

Figure 4.7. Density of MFT composites as a function of filler content.

Figure 4.8 compares the densities of MFT, MMT, and CNC composites. Densities differences in all composites are minor, and considering the experimental error associated with this measurement, they may be undistinguishable. It is worth mentioning that for MMT and CNC composites, the highest filler content achievable in this work was 5%, since higher loadings of filler led to higher viscosities of the mixture used to make the composites, causing mixing problems and the formation of bubbles in the final piece.

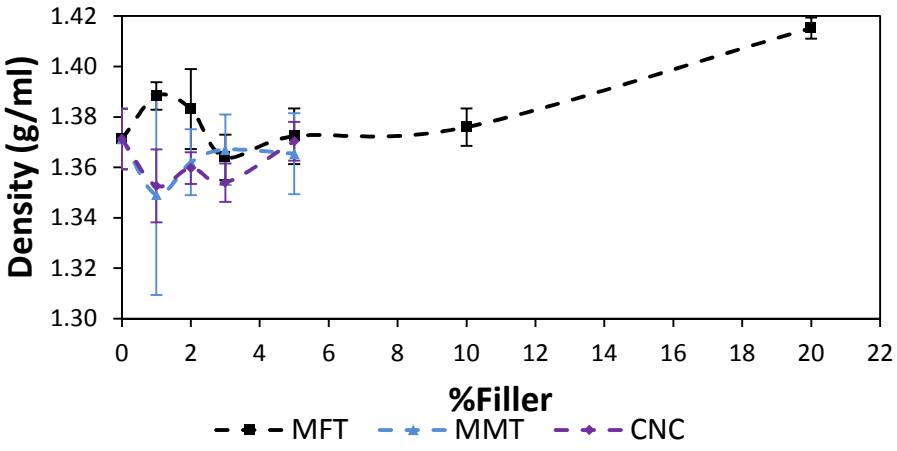

Figure 4.8. Comparison of densities between MFT, MMT and CNC composites.

Finally, Figure 4.9 compares the apparent densities of MFT and the Dean Stark solids composites. Considering the experimental uncertainties in these methods, one can conclude that the type of filler has no effect on the density of these composites. Therefore, the residual bitumen present in MFT does not affect the density of the composites.

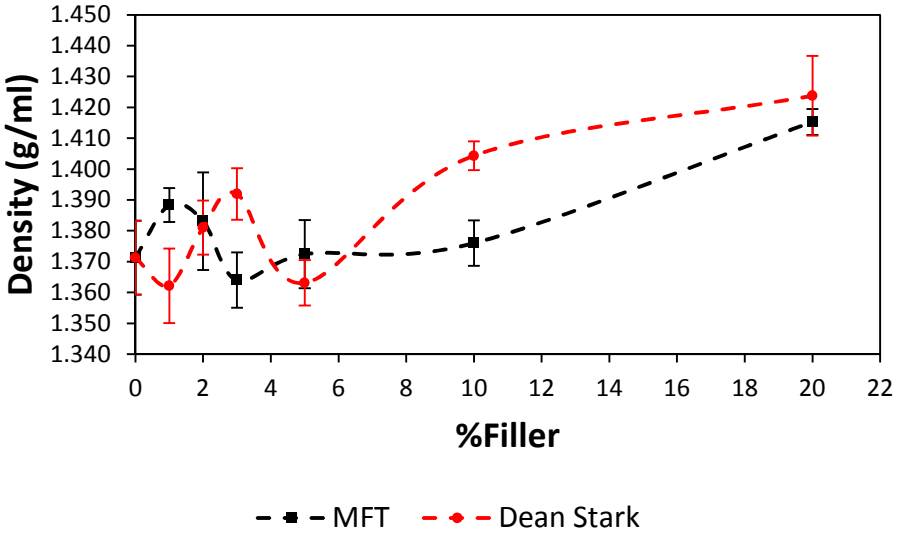

Figure 4.9. Comparison of densities between MFT and Dean Stark composites.

4.4 X-Ray Diffraction (XRD)

It is important to compare first the raw starch with glycerol-plasticized starch to observe the change in crystallinity through XRD. Depending on the length and how the amylopectin molecules are in the granule, starch can have A, B or C-type crystallinity patterns, and the amylose may also make the starch have a V-type crystallinity pattern, as explained in section 2.4.

Figure 4.10 shows that the main peaks in raw cornstarch appear at 2θ = 15.20, 17.17, 18.13 and 23.07°, which correspond to the values reported for A-type starches (Lin and Tung, 2009). In the case of plasticized starch, the main peaks appear at different angles (2θ = 16.9, 20.81 and 21.9) from those detected for raw starch, demonstrating that the introduction of glycerol disrupted the original crystallinity of the starch granule. According to the work of Lin and Tung (2009), the peaks at 16.9 and 21.9 correspond to B-type crystallinity, and the work of Huang, Yu,

and Ma (2005) shows that the peak at 20.81 corresponds to a V-type crystallinity, due to recrystallization after gelatinization, where amylose forms a single helix complex with glycerol. In summary, gelatinization disrupts the original crystallinity of starch creating an amorphous structure, but after cooling retrogradation creates a new crystallinity structure.

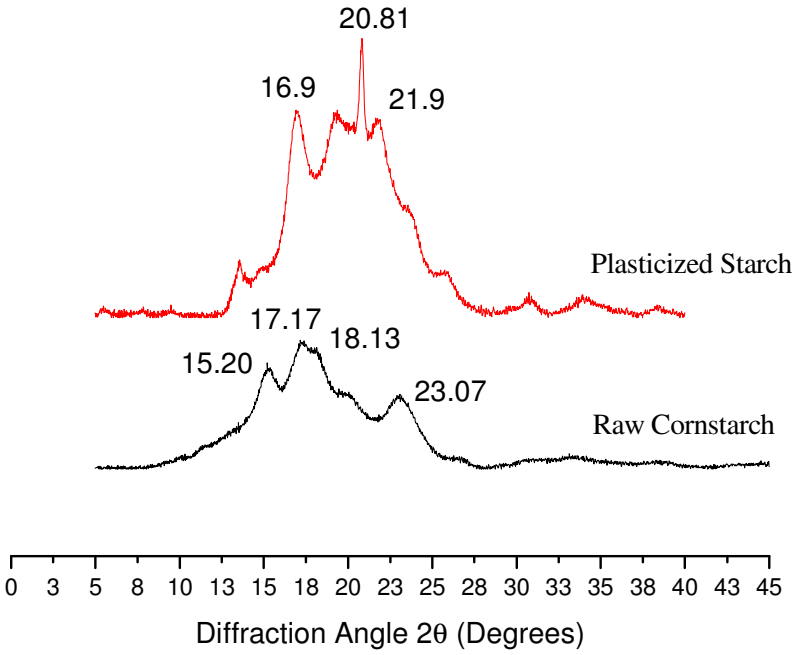

Figure 4.10. Diffractogram of raw starch and plasticized starch.

For MFT composites the comparison has to be made with plasticized starch and with dry MFT. The diffractogram in Figure 4.11 shows the main peaks of MFT at $2\theta = 8.8$, 20.8, and 26.6 (illite), 24.9 (quartz), and 12.3, and 27.1 (kaolinite) (Omotoso, 2004).

The addition of MFT to the plasticized starch makes the peaks appear on top of the plasticized starch curve, and the height of the peaks increase with the increase in filler content. By comparing each MFT composite diffractogram with the MFT diffractogram, we notice that none of the peaks shift positions, meaning there is no change in the interlayer spacing of any of the clays particles, and no sign of intercalation or exfoliation. A similar behavior is observed by comparing the diffractograms of DS composites in Figure 4.12.

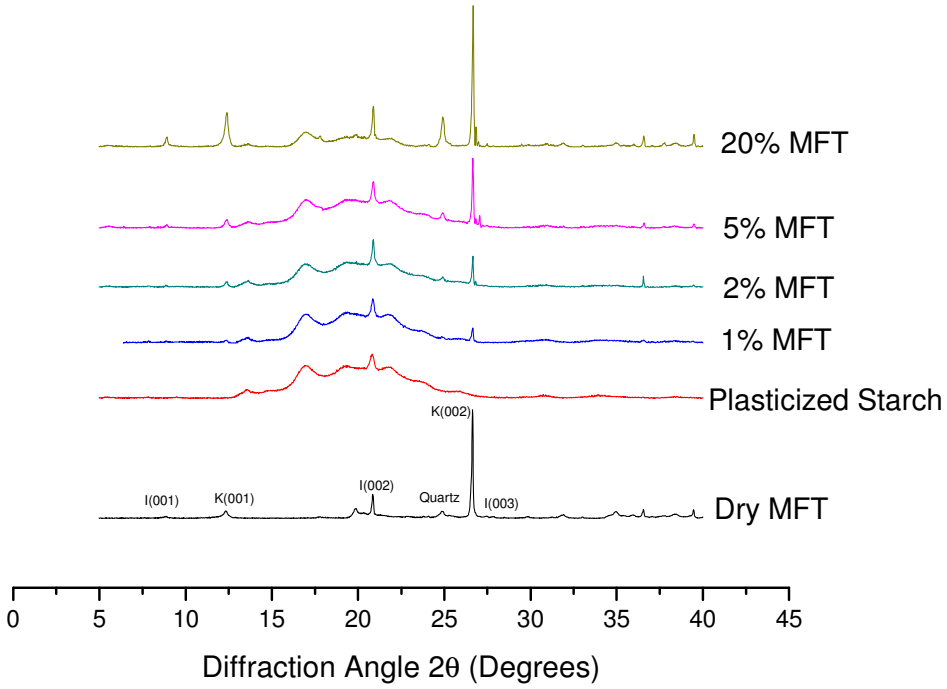

Figure 4.11. Diffractogram of MFT, plasticized starch, and MFT composites.

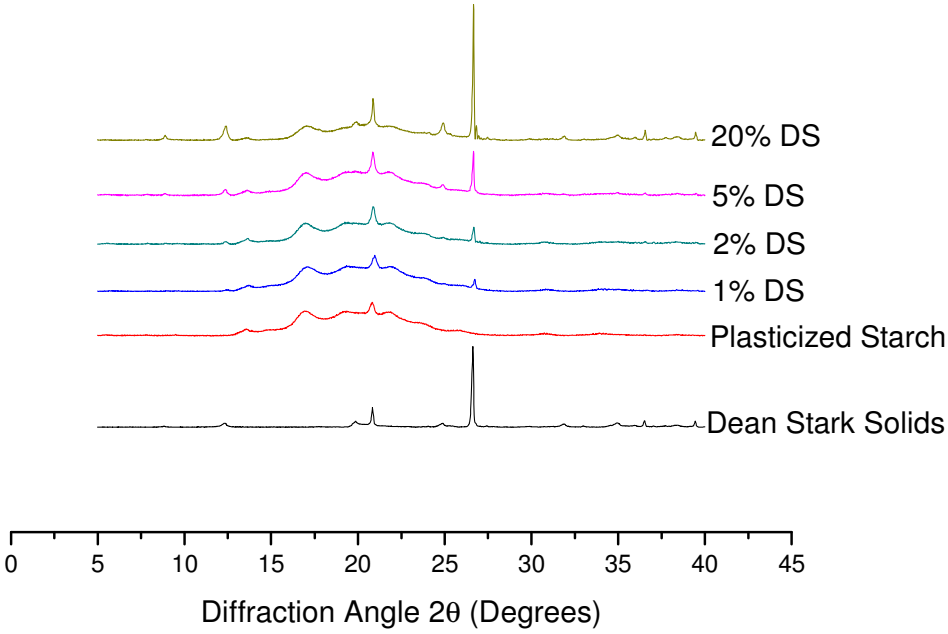

Figure 4.12. Diffractogram of Dean Stark solids, plasticized starch, and DS composites.

On the other hand, MMT composites have a substantially different behavior than the ones observed for MFT and DS composites. MMT is a swelling clay, which means the interlayer spacing changes easily, and it is possible for polymer molecules to diffuse in between the layers

of the clay (intercalation), and even sometimes push them apart (exfoliation). The diffractogram of MMT composites, seen in Figure 4.13, shows that the MMT crystalline peaks are mostly absent in their composites, proving that starch disrupts the crystalline order of pristine MMT, and also confirming the hypothesis we raised above when discussing the SEM micrographs of these composites in Figure 4.5.

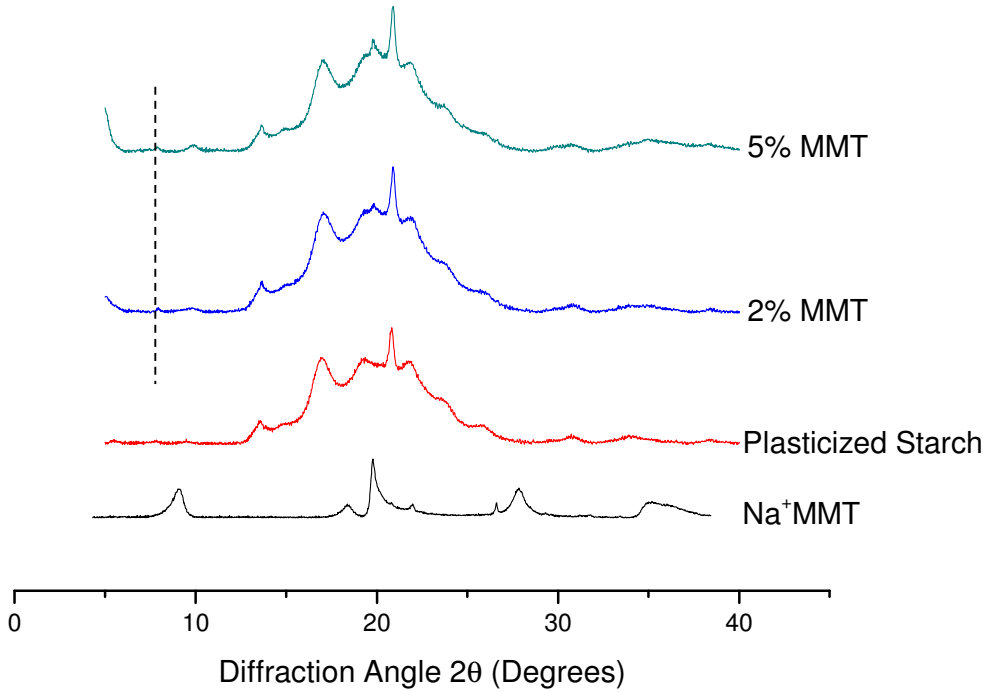

Figure 4.13. Diffractogram of Na^{+}MMT, plasticized starch and MMT composites.

In most studies of starch composites with MMT, special attention is paid to the peak at $2\theta =$ 9°, used to determine the interlayer distance (Min, Zhou and Xu, 2015). By using Bragg's law, the interlayer spacing in the MMT used for our composites is 9.8 Å. If the peak shifts to the left, it means the interlayer distance increased because the clay layers separated due to intercalation, but if they disappear, it means there is no distance to measure and complete exfoliation was achieved. This peak did not completely disappear in the MMT composites made in this work, but it shifted to $2\theta =$ 7°, indicating that the interlayer spacing increased to 12.61 Å through starch intercalation without achieving complete exfoliation. These intercalation results have also been reported by other researchers, to an even greater interlayer distance of 2.73 nm (Cyras, Manfredi, Ton-That, and Vázquez, 2008; Ming Zhou, Zhao, and Zhou, 2011).

In the case of CNC, Figure 4.14 shows three main peaks at 2θ = 15, 16.8 and 22.8, corresponding to the cellulose crystal planes ($1\bar{1}0$), (110) and (200), respectively (Echeverria, Almeida, Feio, Figueirinhas, and Godinho, 2015; Poletto, Pistor, and Zattera, 2013).

However, the diffractograms of CNC composites do not show any of the peaks present in neat CNC. Da Silva et al. (2013) studied thermoplastic starch-bacterial cellulose composites, and showed that while bacterial cellulose had the same crystalline patterns as CNCs, their composites with thermoplastic starch had no remaining cellulose crystallinity. They explained their observations by the melting of cellulose crystallites due to the baking process needed to make the composite. This same melting may happen in the preparation of our CNC composites, which would explain the results depicted in Figure 4.14.

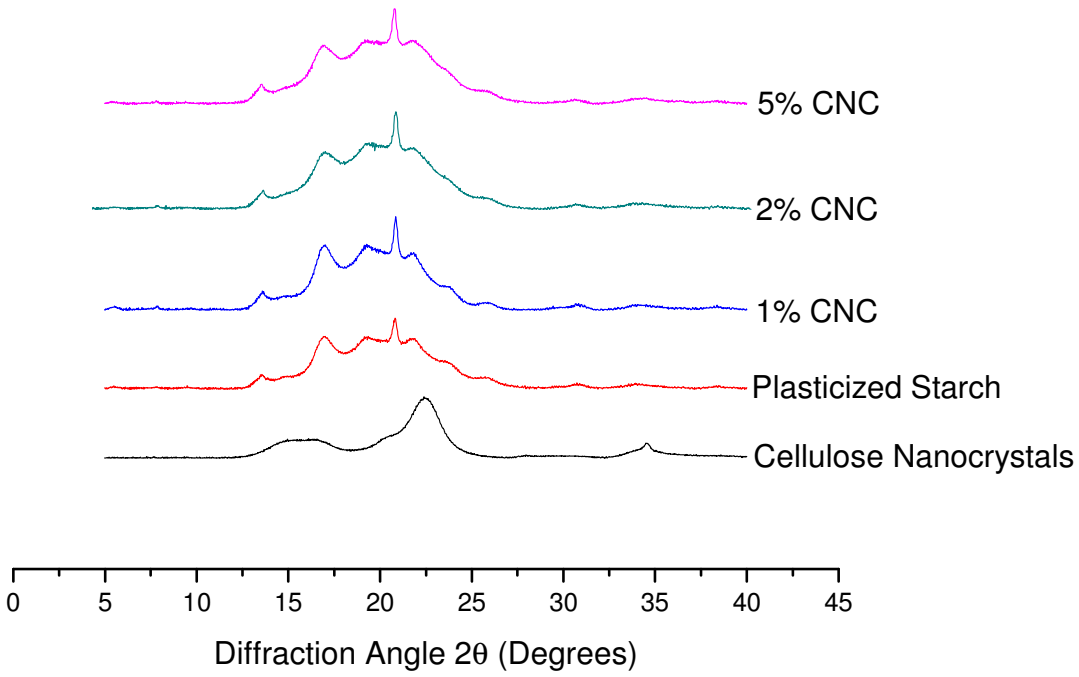

Figure 4.14. Diffractogram of cellulose nanocrystals, plasticized starch, and CNC composites.

4.5 Water Absorption

One of the limitations of starch-based materials is their hydrophilicity. The water uptake of MFT and MMT composites differ dramatically, as shown Figure 4.15. The higher water uptake of MMT composites is likely favored by the swelling ability of MMT, in comparison with the

poor swelling of clays present in MFT. More interestingly, while the water uptake of MMT composites increases with increasing MMT loading up to about 5%, the water uptake of MFT composites decreases slightly as the filler content increases. It is important to note that the large error bars in water uptake of MMT composites are due to experimental error, since part of the specimens broke during immersion and was hard to recover, going into the mass loss percentage that is shown in Figure 4.17.

One is tempted to attribute the MFT composites decreasing water uptake as a function of filler content to bitumen present in MFT, but when comparing the water uptake with DS composites (Figure 4.16), we observe a similar trend. Therefore, we may speculate that the tightly bound organics present in both MFT and DS fillers are the ones playing an important role on the enhanced water resistance of these composites.

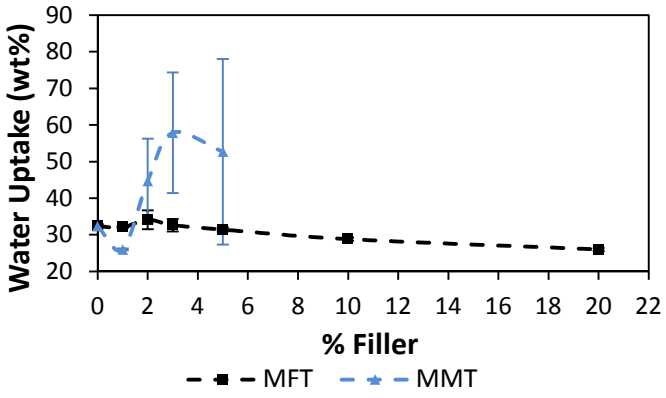

Figure 4.15. Water uptakes of MFT and MMT composites.

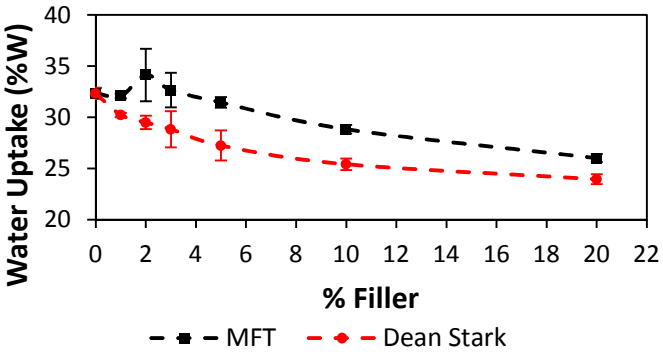

Figure 4.16. Water uptake of MFT and DS composites.

Figure 4.16 also shows that the water uptake of the MFT composites is slightly higher than of the DS composites, but one would expect it to be the same or lower, due to the presence of bitumen in the MFT filler. However, Figure 4.17.a shows that the initial moisture content of the MFT composites was also higher; therefore, after the drying period, they should have a higher capacity to absorb water. It is possible that the initial moisture content on MFT composites was higher than on DS composites because the 48-hour conditioning period might not be long enough to stabilize the water content of these composites, but further experiments would be needed to verify these assertions. For the purpose of this investigation, it suffices to note that the water uptake of both MFT and DS composites decreases with increasing solids content, in stark contrast with MMT composites.

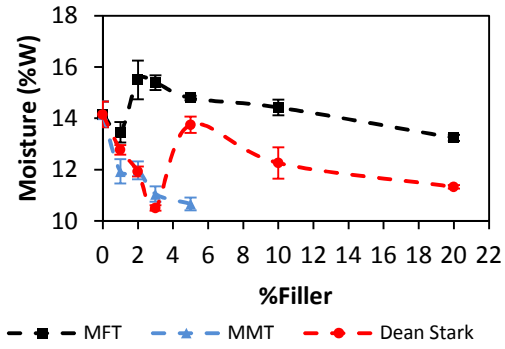

(a)

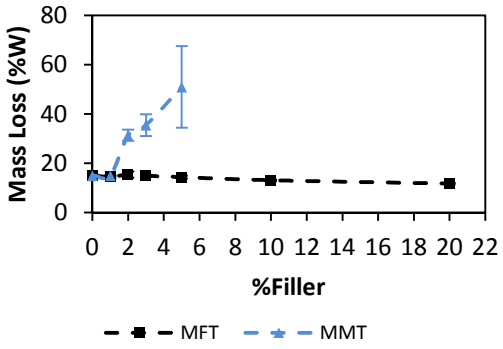

(b)

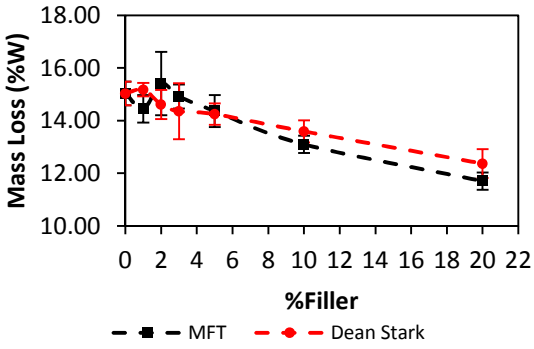

(c)

Figure 4.17. Initial moisture of MFT, DS and MMT composites (a); Mass loss of MFT and MMT composites (b); Mass loss of MFT and DS composites (c).

Figures 4.17.b and 4.17.c show that the mass loss during water immersion for MFT, MMT, and DS composites follow the same trend of water uptake, with the exception that after 10% solids loading, the mass loss is slightly higher for DS composites than for MFT composites.

4.6 Tensile Properties

The tensile properties of the investigated composites were quantified through Young's modulus, maximum strength, and maximum strain. Figure 4.18 shows that the Young's modulus of the MFT composites increases with increasing filler content, although this increase does not seem to be statistically significant for loadings varying from 0 to 3% MFT. This increase in Young's modulus may be attributed to the reinforcing effect caused by strong interactions between MFT clay and starch chains in the composite.

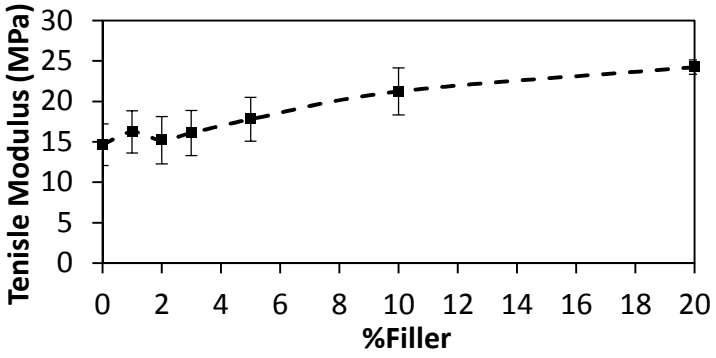

Figure 4.18. Tensile modulus of MFT composites as a function of filler content.

The tensile strength of the MFT composites decreased slightly after 2% filler content, but remained constant up to 20% filler content (Figure 4.19). Although an increase in tensile strength should be the expected outcome when the filler content was increased, the presence of bitumen and air bubbles in the structure of the composite (caused by the increased viscosity of the mixture) might explain this behavior. On the other hand, Figure 4.20 shows how the strain at break decreases with increasing MFT content, due mainly to the decreased mobility of the starch chains as the MFT content in the composite increases.

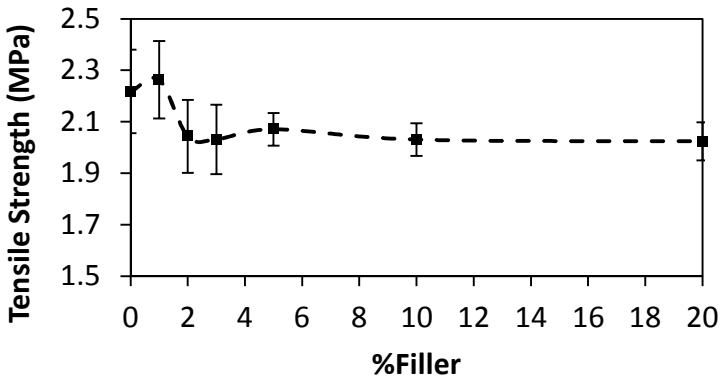

Figure 4.19. Tensile strength of MFT composites as a function of filler content.

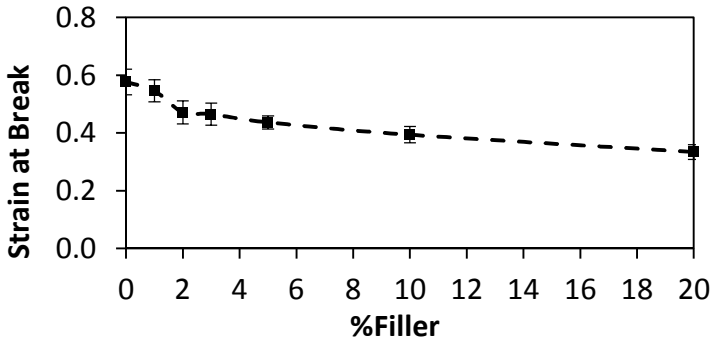

Figure 4.20. Strain at break of MFT composites as a function of filler content.

The tensile properties of MMT and CNC composites deviates from that of the MFT composites. Figure 4.21 compares the tensile modulus, tensile strength, and strain at break of MFT, MMT and CNC composites. The tensile modulus of all composites increase with increasing filler content, but the magnitude of the increase follows the relation MMT > CNC > MFT. We may attribute the stronger response of the MMT composites to the intercalation of starch chains in MMT platelets, and the better performance of the CNC composites (compared to the MFT composites) to the strong interfacial interaction between cellulose and starch chains (Zainuddin et al., 2013).

Despite the higher modulus of MMT and CNC composites, it is important to note that the Young's modulus of the MMT composites approached the same values of MMT and CNC composites at higher MFT loading (5% for MMT and CNC versus 20% for MFT). Since our objective is to use as much MFT as possible as a way to mitigate their environmental impact, this may be seen as a positive property of MFT composites.

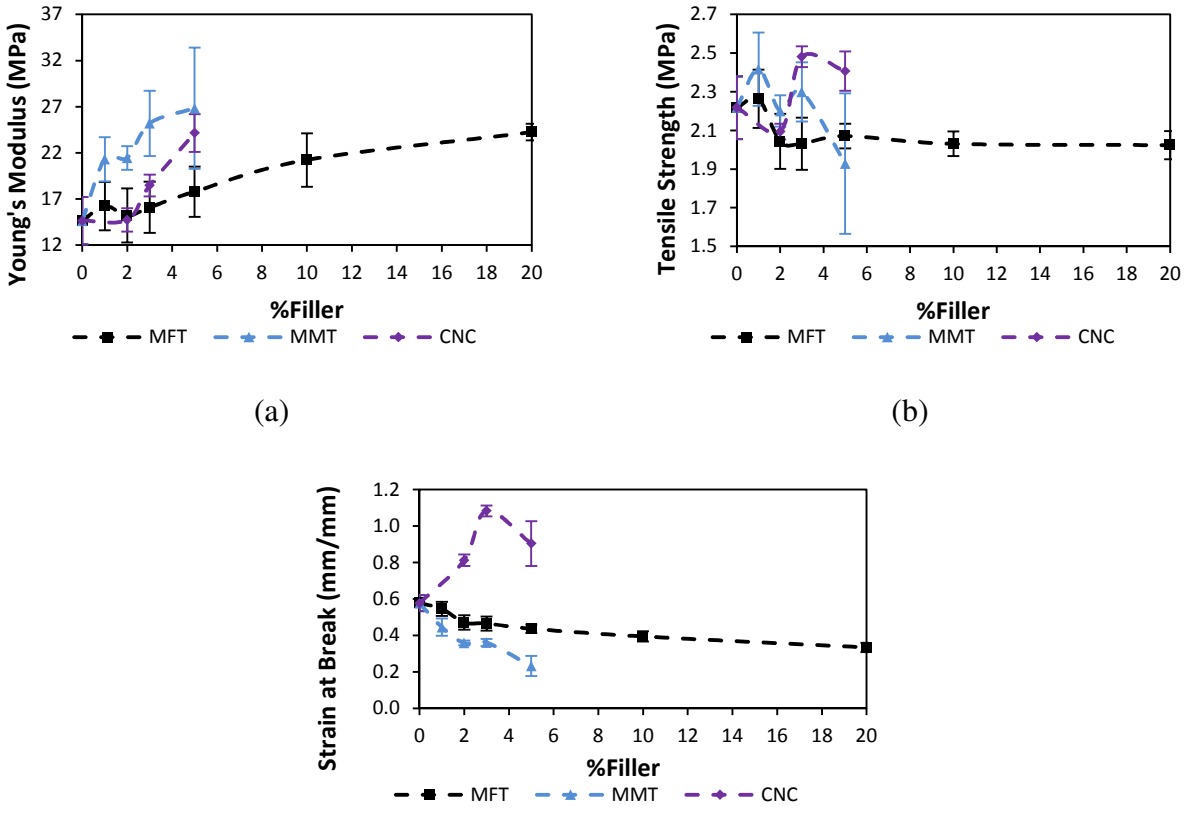

Figure 4.21. Tensile properties of MFT, MMT and CNC composites: (a) Tensile Modulus; (b) Tensile strength; (c) Strain at break.

MMT composites have a tensile strength that initially increases due to the reinforcing effect of the clay (Figure 4.21.b), but then decreases as the filler content becomes higher, caused by an increasing number of defects in the structure resulting from the presence of air bubbles and high viscosity of the mixture. The data for the CNC composites is relatively noisy, but it seems that the tensile strength tends to increase up to about 3 to 5% filler. However, we expected that if higher loadings were attempted, the tensile strength would start decreasing as well, due to more imperfections caused by the high viscosity of the mixture.

Figure 4.21.c shows that MFT composites are more ductile than MMT composites, since there is a more pronounced decrease in the strain at break for the latter. Contrarily, CNC composites have a higher strain at break, reaching a maximum value when the CNC loading is 3%.

In general, when comparing the tensile properties of MFT composites with MMT and CNC composites, the most important fact is that the properties, slightly better or slightly worse, are

around the same magnitude, allowing the use of MFT composites for certain applications in which the other composites may also be used, with the advantage that MFT are much less expensive than CNC or MMT.

Finally, to study the effect of bitumen, Figure 4.22 compares the tensile properties of MFT and DS composites.

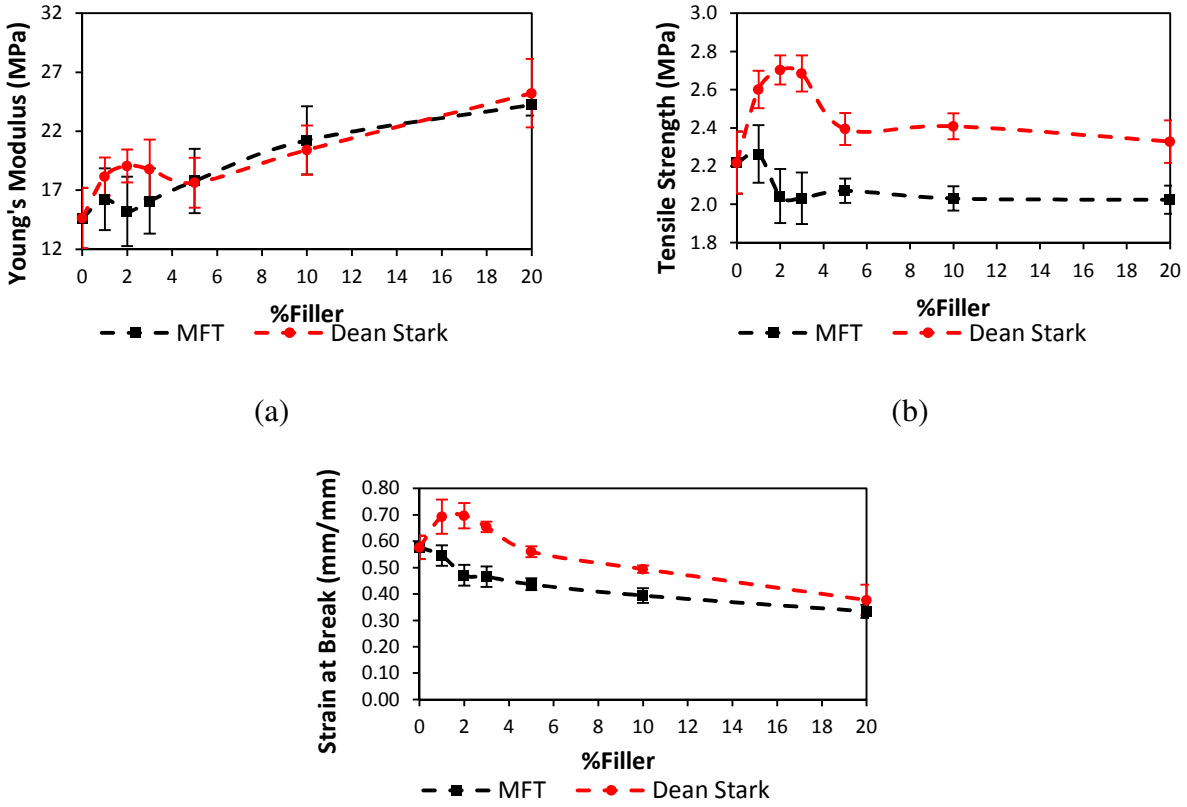

Figure 4.22. Tensile properties of MFT and DS composites: (a) Tensile Modulus; (b) Tensile strength; (c) Strain at break.

Figure 4.22.a shows that the modulus of DS composites is slightly higher for low solids loadings, but the magnitudes for both composites are very similar throughout the whole range investigated in this study. The tensile strength of DS composites (Figure 4.22.b) increases up to 3% filler and then decreases to reach a plateau after 5% filler. The tensile strength of the DS composites is higher than the tensile strength of the MFT composites, showing that bitumen does not have a good interaction with the hydrophilic starch chains, and seems to weaken the composite structure. The elongation at break of the composites (Figure 4.22.c) proves once more

the adverse effect of bitumen on the tensile properties of the MFT composites, but the differences are small in all tensile properties of MFT and DS composites.

4.7 Compressive Properties

The compressive properties of MFT composites can be seen in Figure 4.23. Tensile and compressive moduli have a similar behavior, increasing as the filler content gets higher. (The sudden decrease in modulus for the 2% MFT composite is attributed to experimental error, since the specimens for testing only came from one thick piece instead of two like the other composites, due to problems during testing.)

The compressive strength reaches a maximum for 5% MFT, falling for higher loadings because of the imperfections in the structure of the composite (Figure 4.23.b). A similar maximum is observed for elongation at break (Figure 4.23.c).

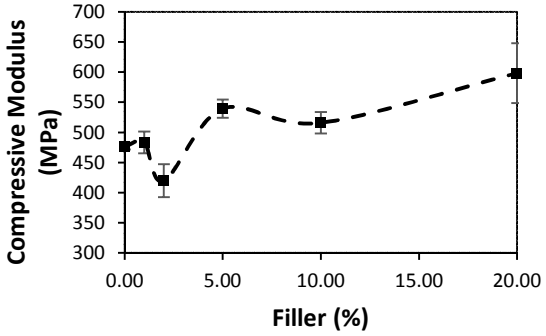

(a)

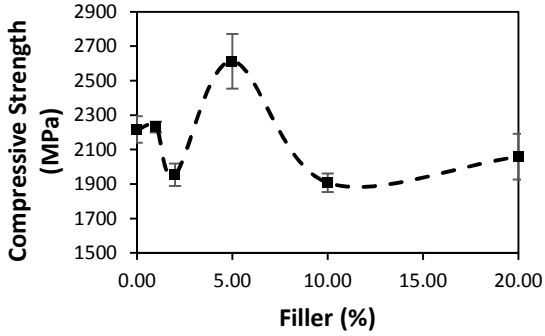

(b)

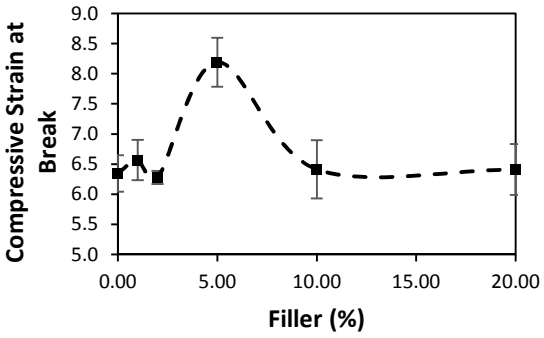

(c)

Figure 4.23. Compressive properties of MFT composites: (a) Compressive Modulus; (b) Compressive strength; (c) Strain at break.

It is noticeable how the compressive modulus of MFT, DS and MMT composites are in the same range, but the modulus of CNC composites is much lower (Figure 4.24.a). Compressive strength follows a similar trend for MFT and DS composites, but is much lower for MMT and CNC composites, meaning that bitumen is not causing any harm on compressive properties as it seems to do to tensile properties. The decrease in compressive strength in MMT and CNC composites is caused by stress concentration points on the imperfections resultant from the high viscosity of the mixture, which also explains the strain at break in Figure 4.24.c, showing substantially higher compression strains for MFT and DS composites than for CNC and MMT.

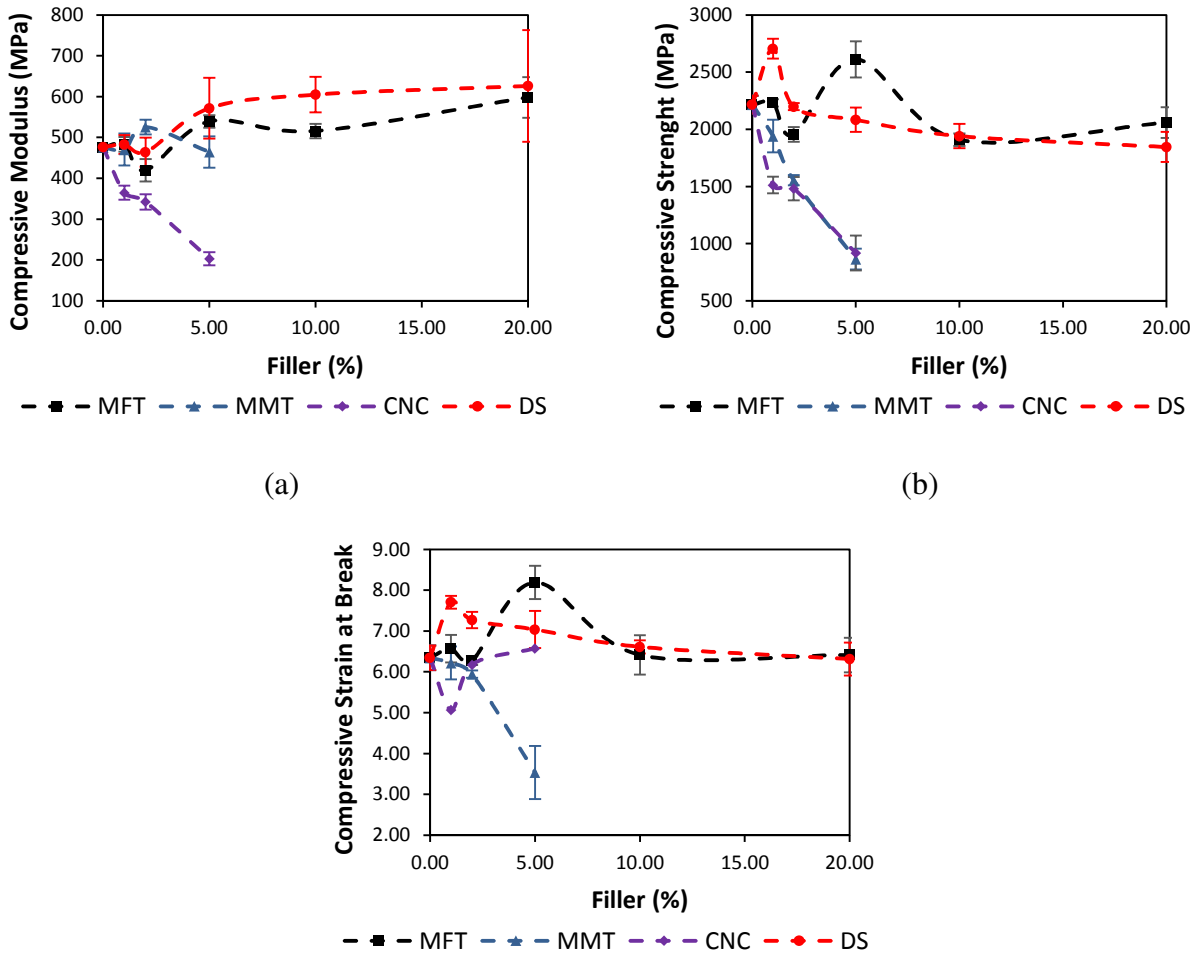

Figure 4.24. Compressive properties of MFT, DS, MMT, and CNC composites: (a) Compressive Modulus; (b) Compressive strength; (c) Strain at break.

The analysis presented in this section shows that the compression properties of MFT composites are better than those of MMT and CNC composites. However, to quantify these effects more precisely, improvements in making thick test pieces for compressive testing have to be made. The thick pieces in this work were made specifically for compression testing, and despite the change in mixing conditions and pressing time to match the procedure used for thin pieces, there might be differences in the dispersion of fillers and the degree of plasticization of starch, which can cause deviations in the properties of the materials. Additionally, the cutting of the specimens for compression testing left different thicknesses and heights on the specimens, which is an additional cause for experimental error.

4.8 Dynamic Mechanical Analysis (DMA)

Dynamic mechanical analysis shows the viscoelastic behavior of the polymer composites in a wide range of temperatures. For MFT composites, the change in storage modulus, loss modulus and loss factor Tan δ as a function of temperature at 1 Hz is shown in Figures 4.25, 4.26 and 4.27, respectively.

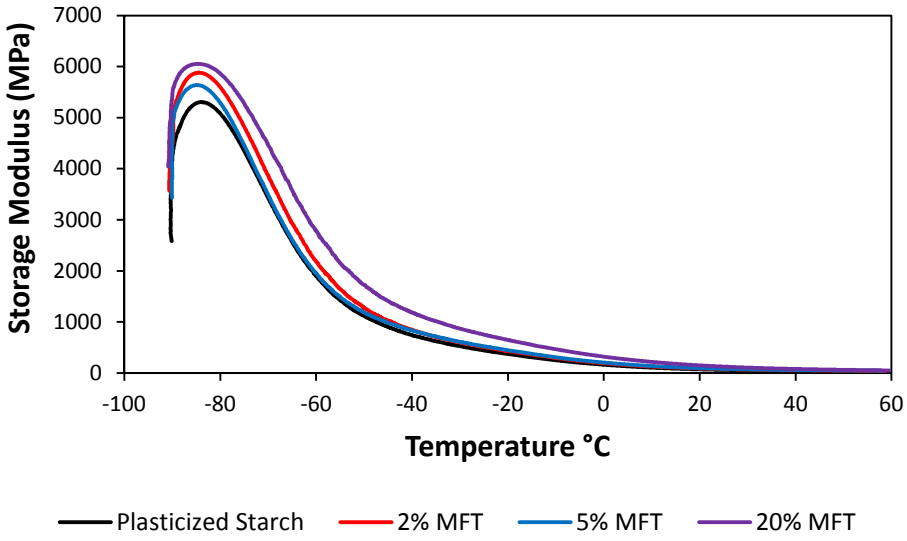

Figure 4.25 Storage Modulus of Plasticized Starch and MFT composites as a function of temperature.

Figure 4.25 shows that the storage modulus of plasticized starch (PS) and MFT composites decrease noticeably with increasing temperature. This decrease in storage modulus has been identified as the glass transition in various studies (Karimi, Abdulkhani, Tahir, and Dufresne, 2016; Vallejos et al., 2011), and is caused by energy dissipation achieved by the movement of large amorphous segments and rotation about single bonds in the polymer chains (Mathew, Thielemans, and Dufresne, 2008). Figure 4.26 shows how the loss modulus of the composites are at their maximum point in the same temperature range where the storage modulus starts to drop, after which both moduli decrease.

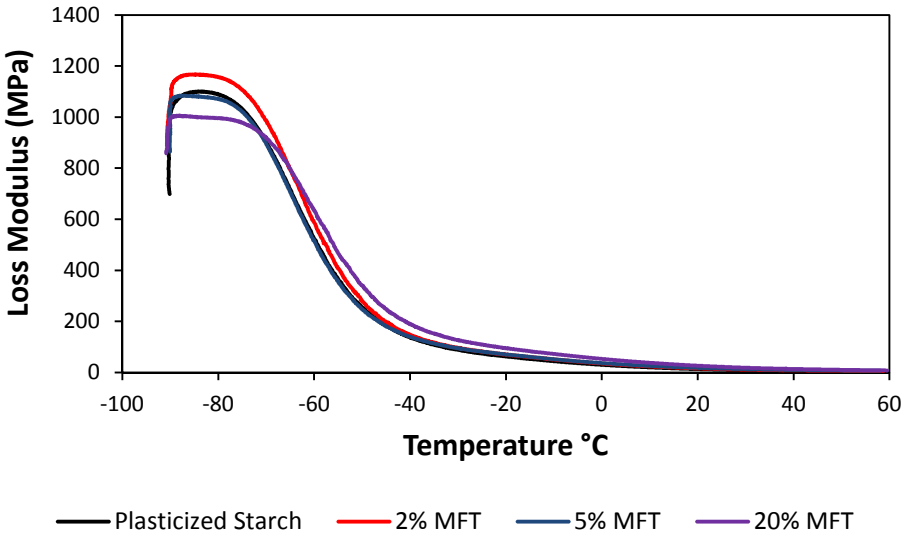

Figure 4.26. Loss modulus of Plasticized Starch and MFT composites as a function of temperature.

When comparing the storage modulus among different MFT composites, Figure 4.25 shows a similar trend for the storage modulus as the one showed for the tensile test. As the MFT content increases, there is also an increase in storage modulus, and the slope of the modulus decrease becomes less pronounced. This is because when more MFT is embedded in the matrix, there is more restriction to molecular motion.

Figure 4.27 shows the curve of the damping factor or loss factor Tan δ for MFT composites as a function of temperature. This factor, defined as the ratio between the energy lost and the energy stored in the material, is calculated by diving the loss modulus by the storage modulus at

each temperature point. The curve in Figure 4.27 has two peaks at different temperature ranges, indicating that the material is heterogeneous, having a glycerol rich domain with a thermal transition at lower temperatures (around -60 °C) and a starch rich domain at higher temperatures (Karimi et al., 2016; Mathew et al., 2008; Vallejos et al., 2011).

The glycerol-rich phase peak is around the same temperature for all MFT composites, but there is a decrease in the magnitude of the peak as the MFT content increases. This peak is related to the drop of storage modulus and is therefore associated with the molecular motion in the system (Karimi et al., 2016), behaving inversely to the storage modulus due to the decreased molecular motion as MFT content is increased.

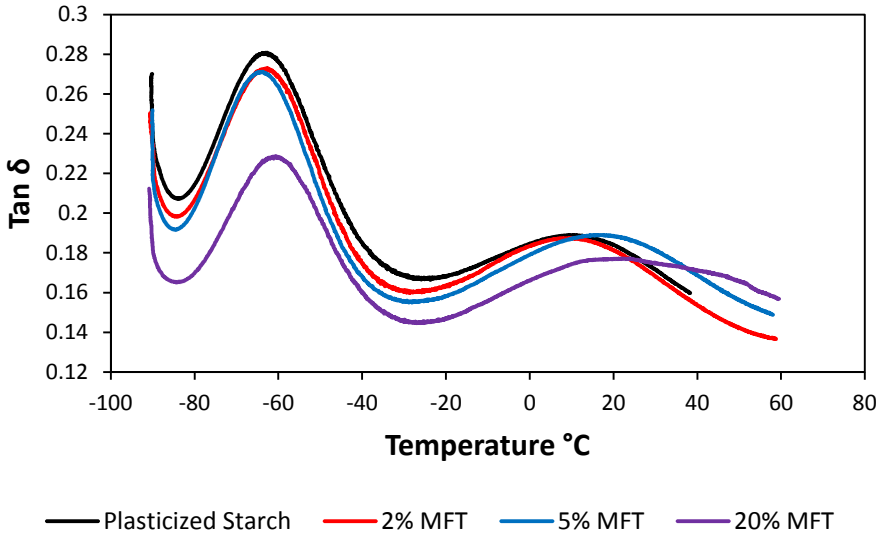

Figure 4.27. Loss Factor Tan δ of Plasticized Starch and MFT composites with temperature.

On the other hand, Figure 4.27 shows how for 5 and 20% MFT content there is shifting and broadening of the peaks in addition to the decrease in magnitude. As MFT content increases, there is a broader distribution of relaxation times of the amorphous starch chains in the presence of crystalline domains (Mathew et al., 2008).

The behavior for DS and MMT composites can be seen on Figures 4.28 and 4.29. The storage modulus shows the same drop in about the same temperature range as MFT composites, and the two thermals transitions in the Tan δ figures are also seen, with the differences in magnitude as the filler content increases and with a broadening of the second peak.

For a better understanding on how the different type of filler affects the behavior of the composites, a comparison of 2% and 5% composites is presented in Figures 4.30 (Storage Modulus) and 4.31 (Tan δ). It is shown that DS and MMT composites have a higher modulus than MFT composites, corresponding to the results obtained with tensile properties, but all the storage modulus curves come closer at room temperature.

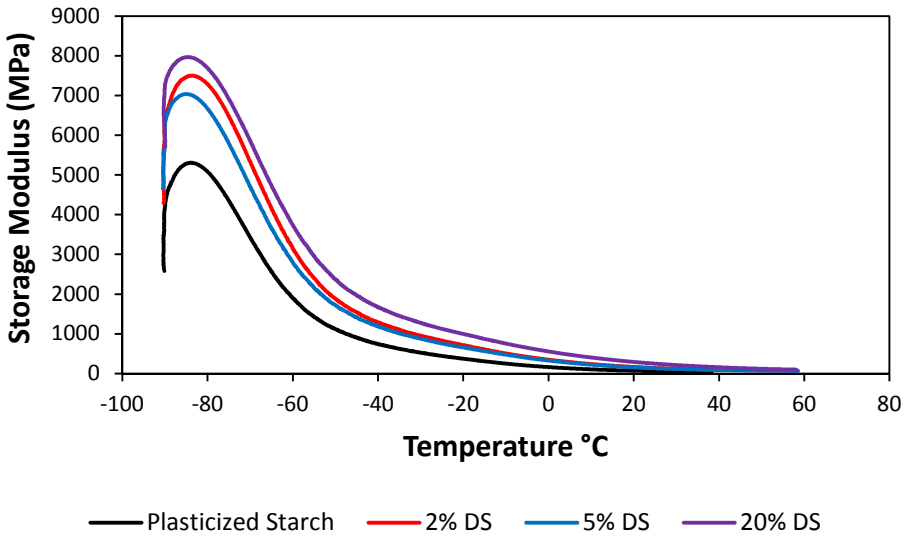

(a)

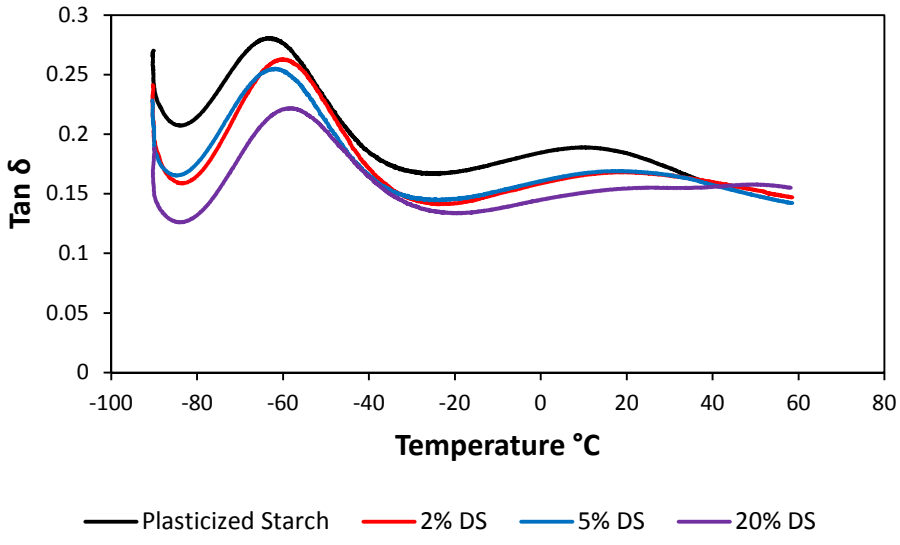

(b)

Figure 4.28. Storage modulus (a) and loss factor Tan δ (b) of Plasticized Starch and DS composites as a function of temperature.

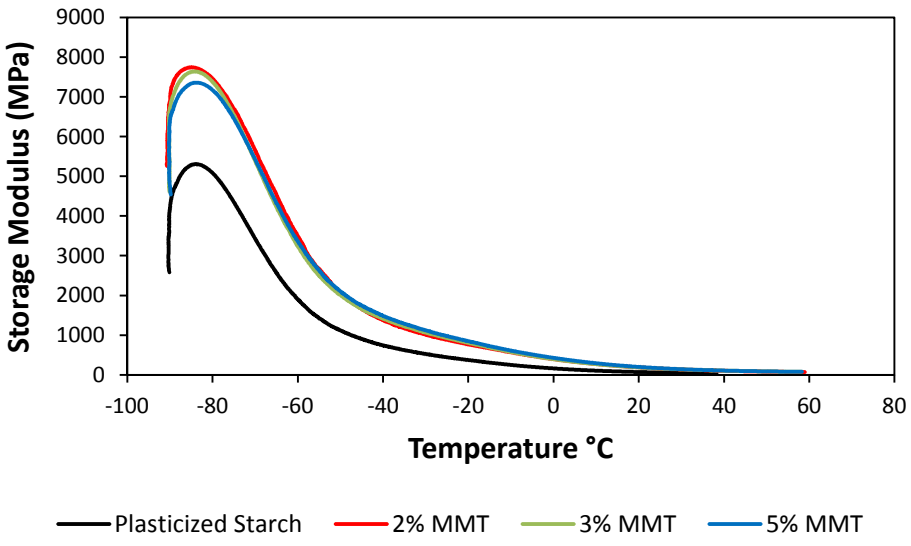

(a)

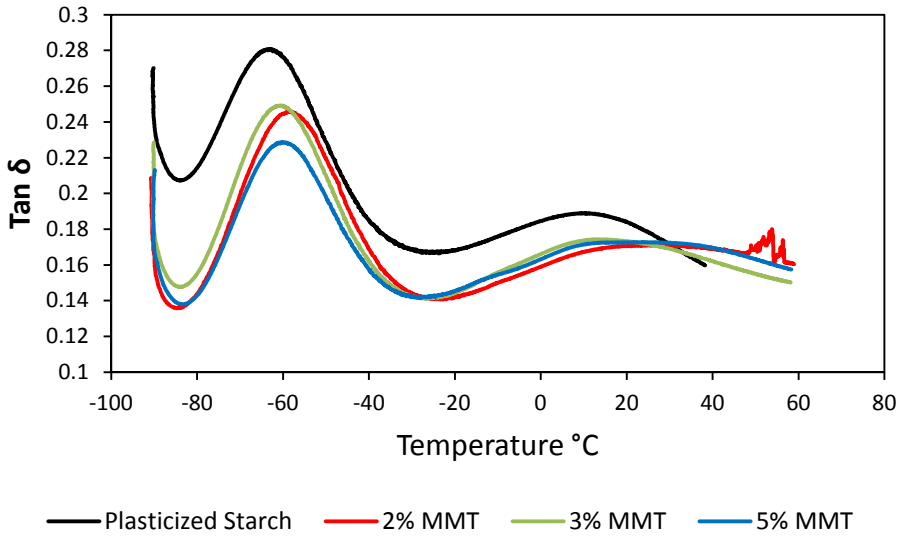

(b)

Figure 4.29. Storage modulus (a) and loss factor Tan δ (b) of Plasticized Starch and MMT composites as a function of temperature.

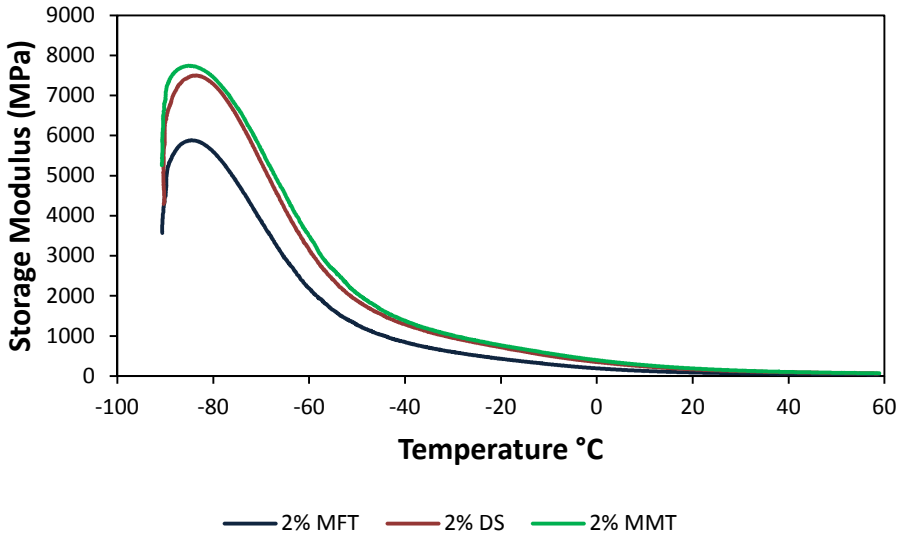

(a)

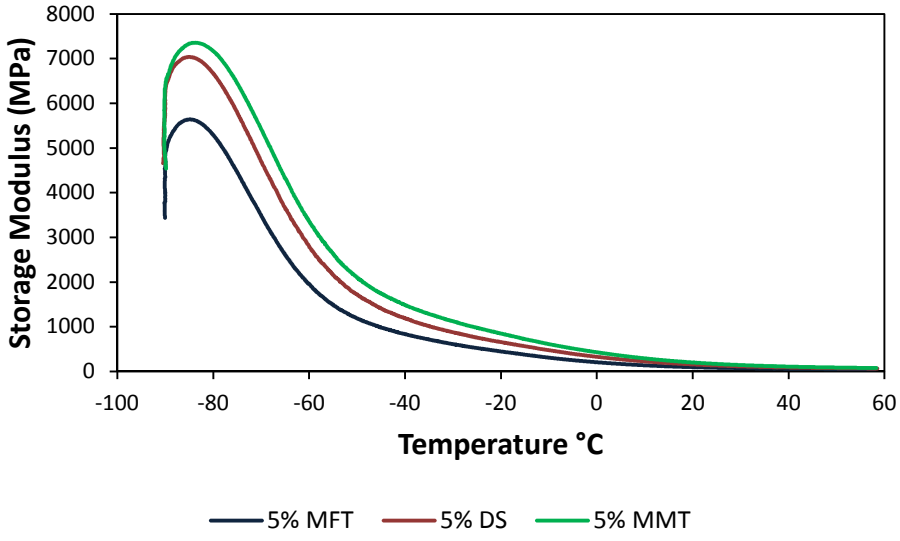

(b)

Figure 4.30. Storage modulus of (a) 2% MFT, DS and MMT composites and (b) 5% MFT, DS and MMT composites as a function of temperature.

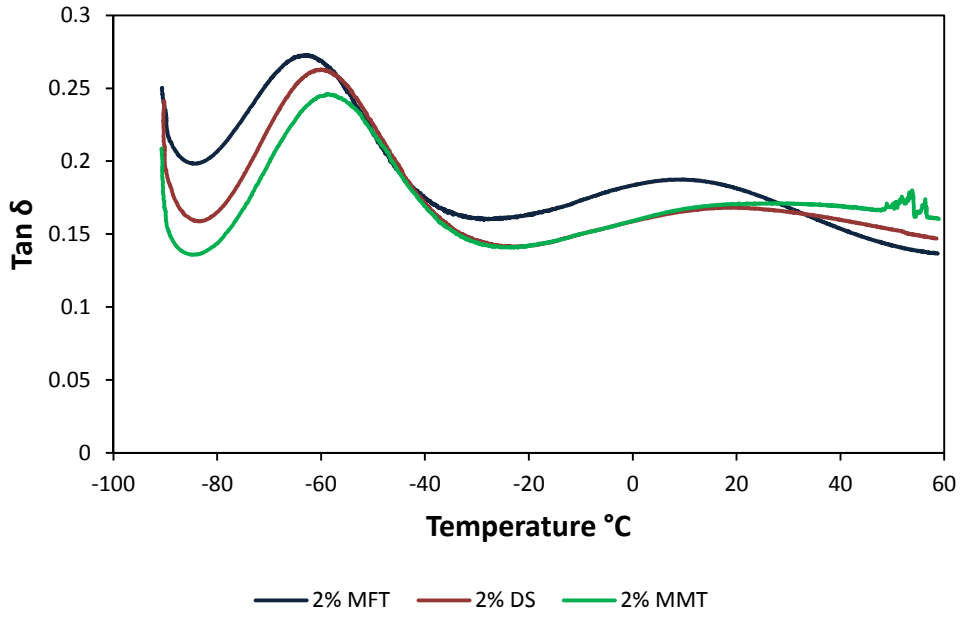

(a)

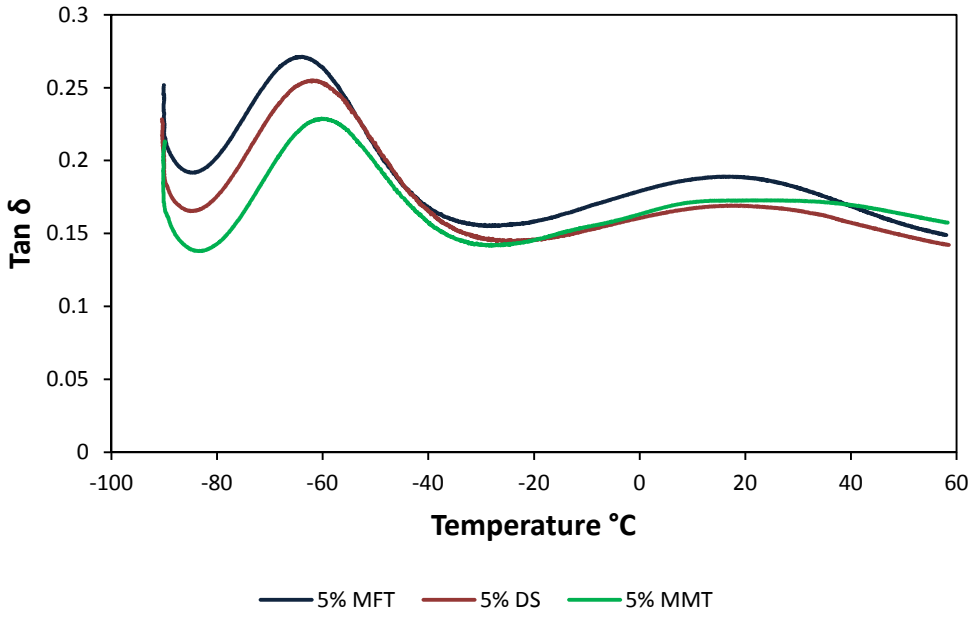

(b)

Figure 4.31. Loss factor Tan δ of (a) 2% MFT, DS and MMT composites and (b) 5% MFT, DS and MMT composites as a function of temperature.

The behavior of the Tan δ curves in Figure 4.31 also corresponds to the properties seen with the tensile tests, with higher magnitude for MFT composites and lower magnitudes for DS and

MMT composites, as well as a higher broadening of the starch-rich transition peak for DS and MMT composites. The higher broadening of the transition peak in DS and MMT composites suggests stronger clay-starch interactions than in MFT composites (Lu, Weng, and Cao, 2005), which means bitumen might be weakening this interaction in MFT composites.

4.9. Summary

This chapter showed how the properties of the starch-based composites vary with filler content and type. The composite morphology differed for each type of filler, and the structure of the composites changed as the filler content increased, contrary to what was observed for density, which remained relatively constant within a small range of values when changing filler type and content. The XRD patterns showed that MMT suffered some intercalation in the composites, which explains the superior tensile properties over MFT and DS composites. Differently, MMT composites have no water resistance, while MFT and DS composites had a slight decrease in water absorption as the filler content increased. The compression properties were slightly better for MFT and DS composites, and the dynamic mechanical analysis helped determined the heterogeneity of the materials and prove once more the reinforcement effect of the clays on the plasticized starch matrix.

References

Cyras, V. P., Manfredi, L. B., Ton-That, M.-T., and Vázquez, A. (2008). Physical and mechanical properties of thermoplastic starch/montmorillonite nanocomposite films. *Carbohydrate Polymers*, *73*(1), 55–63. https://doi.org/10.1016/j.carbpol.2007.11.014

Da Silva, A., Nievola, L. M., Tischer, C. A., Mali, S., and Faria-Tischer, P. C. S. (2013). Cassava starch-based foams reinforced with bacterial cellulose. *Journal of Applied Polymer Science*, *130*, 3043–3049. https://doi.org/10.1002/app.39526

Echeverria, C., Almeida, P. L., Feio, G., Figueirinhas, J. L., and Godinho, M. H. (2015). A cellulosic liquid crystal pool for cellulose nanocrystals: Structure and molecular dynamics at high shear rates. *European Polymer Journal*, *72*(November), 72–81.

https://doi.org/10.1016/j.eurpolymj.2015.09.006

Huang, M., Yu, J., and Ma, X. (2005). Ethanolamine as a novel plasticiser for thermoplastic starch. *Polymer Degradation and Stability*, *90*(3), 501–507. https://doi.org/10.1016/j.polymdegradstab.2005.04.005

Kaewtatip, K., Tanrattanakul, V., and Phetrat, W. (2013). Preparation and characterization of kaolin/starch foam. *Applied Clay Science*, *80–81*, 413–416. https://doi.org/10.1016/j.clay.2013.07.011

Karimi, S., Abdulkhani, A., Tahir, P. M., and Dufresne, A. (2016). Effect of cellulosic fiber scale on linear and non-linear mechanical performance of starch-based composites. *International Journal of Biological Macromolecules*, *91*, 1040–1044. https://doi.org/10.1016/j.ijbiomac.2016.06.061

Lin, C., and Tung, C. (2009). The Preparation of Glycerol Pseudo-Thermoplastic Starch (GTPS) via Gelatinization and Plasticization. *Polymer-Plastics Technology and Engineering*, *48*(5), 509–515. https://doi.org/10.1080/03602550902824309

Lu, Y., Weng, L., and Cao, X. (2005). Biocomposites of plasticized starch reinforced with cellulose crystallites from cottonseed linter. *Macromolecular Bioscience*, *5*(11), 1101–1107. https://doi.org/10.1002/mabi.200500094

Mathew, A. P., Thielemans, W., and Dufresne, A. (2008). Mechanical properties of nanocomposites from sorbitol plasticized starch and tunicin whiskers. *Journal of Applied Polymer Science*, *109*(6), 4065–4074. https://doi.org/10.1002/app.28623

Omotoso, O. (2004). High surface areas caused by smectitic interstratification of kaolinite and illite in Athabasca oil sands. *Applied Clay Science*, *25*(1–2), 37–47. https://doi.org/10.1016/j.clay.2003.08.002

Poletto, M., Pistor, V., and Zattera, A. J. (2013). Chapter 2 Structural Characteristics and Thermal Properties of Native Cellulose. In *Cellulose - Fundamental Aspects* (pp. 45–68). InTech. https://doi.org/10.5772/50452

Vallejos, M. E., Curvelo, A. A. S., Teixeira, E. M., Mendes, F. M., Carvalho, A. J. F., Felissia, F.

E., and Area, M. C. (2011). Composite materials of thermoplastic starch and fibers from the ethanol–water fractionation of bagasse. *Industrial Crops and Products*, *33*(3), 739–746. https://doi.org/10.1016/j.indcrop.2011.01.014

Zainuddin, S. Y. Z., Ahmad, I., and Kargarzadeh, H. (2013). Cassava starch biocomposites reinforced with cellulose nanocrystals from kenaf fibers. *Composite Interfaces*, *20*(3), 189–199. https://doi.org/10.1080/15685543.2013.766122

Zhou, M., and Xu, D. (2015). Starch-MMT composite films: Effects of bio-inspired modification on MMT. *Starch - Stärke*, *67*(5–6), 470–477. https://doi.org/10.1002/star.201400231

Zhou, M., Zhao, J., and Zhou, L. (2011). Utilization of starch and montmorrilonite for the preparation of superabsorbent nanocomposite. *Journal of Applied Polymer Science*, *121*(4), 2406–2412. https://doi.org/10.1002/app.33519

CHAPTER 5
Conclusions and Recommendations

5.1 Conclusions

The mature fine tailings (MFT) composites made in this investigation have a set of tunable properties comparable to those of composites made with montmorillonite (MMT) and cellulose nanocrystals (CNC), more expensive fillers that have been studied before for packing and agricultural applications. This investigation showed through SEM and XRD techniques that the starch grains are totally disrupted during the preparation of the composites, and that clays in MFT and DS solids are well dispersed in the composites but may agglomerate to a certain extent at higher loadings. In the case of MMT composites, the increasing interlayer spacing of the clays in the composites from 9.8 to 12.61 Å indicated intercalation of the clays by the starch matrix, leading to superior tensile properties up to 5% loading. However, the variation in morphology caused by filler type and content does not seem to significantly affect the density of the composites, since considering the uncertainties in density measurement, it stays in a range between 1.35 and 1.41 g/cm^3.

Water absorption measurements showed that organic matter and clays present in MFT and DS improve the water resistance of composites by about 6% over the water resistance of plasticized starch. The bitumen in MFT had no significant effect on water absorption, but MFT and DS composites performed better than MMT composites, in which water resistance worsened as the MMT content increased. This water resistance of MFT composites makes them good biodegradable candidates to replace polyethylene mulch, which usually ends up in landfills. The small amount of bitumen, being a percentage of a small percentage present in MFT, should be easily converted by bacteria, but further studies will have to prove this statement.

When it comes to mechanical properties, it can be said that there are similarities between MFT composites and MMT and CNC composites. The tensile properties of MFT composites showed that even though there is a small difference from DS composites caused by the presence of bitumen in the MFT composites, the modulus, strength and elongation at break stay in the same range of values. More interestingly, despite the increase in tensile modulus as a function of filler content (higher in MMT and CNC composites), the high viscosity of the initial mixture

used to prepare these composites did not allow to go further than 5% filler content, while MFT composites were made with up to 20% filler content, reaching the same tensile modulus achieved by MMT and CNC composites. Since one of the objectives of this work is to recycle as much MFT as possible in the form of useful composites, the ability to use more MFT to reach the same modulus can be seen as a positive feature of these composites. On the other hand, the compressive modulus followed a similar trend to the tensile modulus, but there was also a small improvement of the compressive strength at 5% MFT content that was not seen in the tensile strength. The overall compressive properties of MFT and DS composites were slightly better than the properties of MMT and CNC composites, but within a small range.

The dynamic mechanical analysis showed a decrease in storage modulus that started at temperatures as low as -80 °C for all composites, which indicated a glass-rubber transition. However, the loss factor Tan δ curve indicated the presence of a second transition at a temperature that varied between composites in a range from 10 to 23 °C. The two transitions appear because of the heterogeneity of the composites, with the first transition corresponding to a glycerol rich phase, and the second one to a starch rich phase. The magnitude of the Tan δ peaks and the broadening of the peak related to the starch-rich phase indicated a restricted molecular motion and a broader range of relaxation times when increasing the filler content, suggesting a better clay-starch interaction in MMT and DS composites than in MFT composites, but again in a very close range of modulus.

Although the presence of bitumen reduces the application range of MFT composites, these have similar mechanical properties as other composites already in use, which mean they can be suitable for making bags, boxes and other materials useful for packing applications once some improvements in water resistance and some mechanical properties are made. This means that the environmental effect caused by the MFT in ponds may be reduced by the production of MFT composites for the use in applications such as bags and boxes for non-edible foods, mulch, filler for carpets and insoles (with the aid of another materials), among others. However, some improvements in the properties have to be made, since for example, the tensile strength of high density polyethylene is around 15 MPa, a value significantly higher than the tensile strength of the MFT composites made in this work.

5.2. Recommendations

The improvement in MFT composites has to be aimed to mechanical properties and water resistance. Blending the starch and the fillers with other hydrophobic polymers is a good option to increase both properties, where polylactic acid and polycaprolactone appear as good options to maintain the biodegradability of the composites.

In terms of methodology, the specimen preparation methods for the determination of mechanical properties have to be improved to decrease the experimental error. Additionally, the number of number of specimens for density, water absorption and compression properties should be increased.

As good options for future work, the use of transmission scanning microscopy (TEM) to better study the interaction between filler and polymer chains is recommended, as well as the study of the thermal properties of MFT composite foams without water in their structure, and the study of the impact strength of MFT composites for potential high impact applications.

Bibliography

Alamgir, A., Harbottle, D., Masliyah, J., and Xu, Z. (2012). Al-PAM assisted filtration system for abatement of mature fine tailings. *Chemical Engineering Science*, *80*, 91–99. https://doi.org/10.1016/j.ces.2012.06.010

Botha, L., and Soares, J. B. P. (2015). The Influence of Tailings Composition on Flocculation. *The Canadian Journal of Chemical Engineering*, *93*(9), 1514–1523. https://doi.org/10.1002/cjce.22241

Cabrera, S. C. M., Bryan, J., Kantzas, A., and Tipm, C. (2010). Estimation of Bitumen and Solids Content in Fine Tailings Using Low-Field NMR Technique. *Journal of Canadian Petroleum Technology*, *49*(7), 8–19.

Cao, X., Chen, Y., Chang, P. R., Muir, A. D., and Falk, G. (2008). Starch-based nanocomposites reinforced with flax cellulose nanocrystals. *Express Polymer Letters*, *2*(7), 502–510. https://doi.org/10.3144/expresspolymlett.2008.60

Chen, B., and Evans, J. R. G. (2005). Thermoplastic starch–clay nanocomposites and their characteristics. *Carbohydrate Polymers*, *61*(4), 455–463. https://doi.org/10.1016/j.carbpol.2005.06.020

Coativy, G., Gautier, N., Pontoire, B., Buléon, A., Lourdin, D., and Leroy, E. (2015). Shape memory starch – clay bionanocomposites. *Carbohydrate Polymers*, *116*, 307–313. https://doi.org/10.1016/j.carbpol.2013.12.024

Cyras, V. P., Manfredi, L. B., Ton-That, M.-T., and Vázquez, A. (2008). Physical and mechanical properties of thermoplastic starch/montmorillonite nanocomposite films. *Carbohydrate Polymers*, *73*(1), 55–63. https://doi.org/10.1016/j.carbpol.2007.11.014

Da Silva, A., Nievola, L. M., Tischer, C. A., Mali, S., and Faria-Tischer, P. C. S. (2013). Cassava starch-based foams reinforced with bacterial cellulose. *Journal of Applied Polymer Science*, *130*, 3043–3049. https://doi.org/10.1002/app.39526

Echeverria, C., Almeida, P. L., Feio, G., Figueirinhas, J. L., and Godinho, M. H. (2015). A

cellulosic liquid crystal pool for cellulose nanocrystals: Structure and molecular dynamics at high shear rates. *European Polymer Journal*, *72*(November), 72–81. https://doi.org/10.1016/j.eurpolymj.2015.09.006

Eckhoff, S. R., and Watson, S. A. (2009). Chapter 9 Corn and Sorghum Starches: Production. In *Starch* (Third Edit, pp. 373–439). Elsevier Inc.

Fabunmi, O. O., Tabil, L. G., Panigrahi, S., and Chang, P. R. (2011). Effects of Incorporating Polycaprolactone and Flax Fiber into Glycerol-Plasticized Pea Starch, 841–848. https://doi.org/10.1007/s10924-011-0374-5

Glenn, G. M., and Irving, D. W. (1995). Starch-Based Microcellular Foams. *American Association of Cereal Chemists*, *72*(2), 155–161.

Huang, M., Yu, J., and Ma, X. (2005). Ethanolamine as a novel plasticiser for thermoplastic starch. *Polymer Degradation and Stability*, *90*(3), 501–507. https://doi.org/10.1016/j.polymdegradstab.2005.04.005

Imam, S. H., Wood, D. F., Abdelwahab, M. A., Chiou, B., Williams, T. G., Glenn, G. M., and Orts, W. J. (2012). Chapter 2 Starch Chemistry, Microstructure, Processing, and Enzymatic Degradation. In J. Ahmed, B. K. Tiwari, S. H. Imam, and M. A. Rao (Eds.), *Starch-Based Polymeric Materials and Nanocomposites* (pp. 5–32). CRC Press Taylor and Francis Group.

Jane, J. lin. (2009). *Chapter 6 Structural Features of Starch Granules II*. *Starch* (Third Edit). Elsevier Inc. https://doi.org/10.1016/B978-0-12-746275-2.00006-9

Jenkins, P. J., and Donald, A. M. (1998). Gelatinisation of starch: A combined SAXS/WAXS/DSC and SANS study. *Carbohydrate Research*, *308*(1–2), 133–147. https://doi.org/10.1016/S0008-6215(98)00079-2

Josmin P., J., Sant, K. M., Sabu, T., Kuruvilla, J., Koichi, G., and Meyyarappallil, S. S. (2012). Advances in Polymer Composites: Macro- and Microcomposites – State of the Art, New Challenges, and Opportunities. In *Polymer Composites: Volume 1* (Vol. 1, pp. 3–16). https://doi.org/10.1002/9783527645213

Kaewtatip, K., Tanrattanakul, V., and Phetrat, W. (2013). Preparation and characterization of

kaolin/starch foam. *Applied Clay Science*, *80–81*, 413–416. https://doi.org/10.1016/j.clay.2013.07.011

Kaisangsri, N., Kerdchoechuen, O., and Laohakunjit, N. (2014). Characterization of cassava starch based foam blended with plant proteins, kraft fiber, and palm oil. *Carbohydrate Polymers*, *110*, 70–77. https://doi.org/10.1016/j.carbpol.2014.03.067

Kaminsky, H., Etsell, T., Ivey, D. G., and Omotoso, O. (2006). Fundamental Particle Size of Clay Minerals in Athabasca Oil Sands Tailings. *Clay Science*, *12*(Supplement 2), 217–222.

Karimi, S., Abdulkhani, A., Tahir, P. M., and Dufresne, A. (2016). Effect of cellulosic fiber scale on linear and non-linear mechanical performance of starch-based composites. *International Journal of Biological Macromolecules*, *91*, 1040–1044. https://doi.org/10.1016/j.ijbiomac.2016.06.061

Kaufman, R. C., Wilson, J. D., Bean, S. R., Herald, T. J., and Shi, Y.-C. (2015). Development of a 96-well plate iodine binding assay for amylose content determination. *Carbohydrate Polymers*, *115*, 444–447. https://doi.org/10.1016/j.carbpol.2014.09.015

Lin, C., and Tung, C. (2009). The Preparation of Glycerol Pseudo-Thermoplastic Starch (GTPS) via Gelatinization and Plasticization. *Polymer-Plastics Technology and Engineering*, *48*(5), 509–515. https://doi.org/10.1080/03602550902824309

Liu, H., Yu, L., Xie, F., and Chen, L. (2006). Gelatinization of cornstarch with different amylose / amylopectin content, *65*, 357–363. https://doi.org/10.1016/j.carbpol.2006.01.026

Liu, J., Boo, W.-J., Clearfield, A., and Sue, H.-J. (2006). Intercalation and Exfoliation: A Review on Morphology of Polymer Nanocomposites Reinforced by Inorganic Layer Structures. *Materials and Manufacturing Processes*, *21*(2), 143–151. https://doi.org/10.1080/AMP-200068646

López, J. P., Mutjé, P., Carvalho, a. J. F., Curvelo, a. a S., and Gironès, J. (2013). Newspaper fiber-reinforced thermoplastic starch biocomposites obtained by melt processing: Evaluation of the mechanical, thermal and water sorption properties. *Industrial Crops and Products*, *44*, 300–305. https://doi.org/10.1016/j.indcrop.2012.11.020

Lu, D. R., Xiao, C. M., and Xu, S. J. (2009). Starch-based completely biodegradable polymer materials. *Express Polymer Letters*, *3*(6), 366–375. https://doi.org/10.3144/expresspolymlett.2009.46

Lu, Y., Weng, L., and Cao, X. (2005). Biocomposites of plasticized starch reinforced with cellulose crystallites from cottonseed linter. *Macromolecular Bioscience*, *5*(11), 1101–1107. https://doi.org/10.1002/mabi.200500094

Ma, X., Chang, P. R., and Yu, J. (2012). Chapter 4 Plasticized Starch. In J. Ahmed, B. K. Tiwari, S. H. Imam, and M. A. Rao (Eds.), *Starch-Based Polymeric Materials and Nanocomposites Chemistry, Processing and Applications* (pp. 69–83). CRC Press Taylor and Francis Group.

MacKinnon, M. D., Matthews, J. G., Shaw, W. H., and Cuddy, R. G. (2001). Water Quality Issues Associated With Composite Tailings (CT) Technology for Managing Oil Sands Tailings. *International Journal of Surface Mining, Reclamation and Environment*, *15*(4), 235–256. https://doi.org/10.1076/ijsm.15.4.235.7416

Masliyah, J. H., Czarnecki, J., and Xu, Z. (2011). *Handbook on Theory and Practice of Bitumen Recovery from Athabasca Oil Sands* (Vol. I). Kingsley Publishing.

Mathew, A. P., Thielemans, W., and Dufresne, A. (2008). Mechanical properties of nanocomposites from sorbitol plasticized starch and tunicin whiskers. *Journal of Applied Polymer Science*, *109*(6), 4065–4074. https://doi.org/10.1002/app.28623

Mcfarlane, A. J., and Bremmell, K. E. (2005). Optimising the dewatering behaviour of clay tailings through interfacial chemistry , orthokinetic flocculation and controlled shear, *160*, 27–34. https://doi.org/10.1016/j.powtec.2005.04.046

Mello, L. R. P. F., and Mali, S. (2014). Use of malt bagasse to produce biodegradable baked foams made from cassava starch. *Industrial Crops and Products*, *55*(2014), 187–193. https://doi.org/10.1016/j.indcrop.2014.02.015

Mikula, R. J., Kasperski, K. L., Burns, R. D., and MacKinnon, M. D. (1996). Nature and fate of oil sands fine tailings. *Suspensions: Fundamentals and Applications in the Petroleum Industry*, *251*, 677–723.

Nalin, T., Sperb-Ludwig, F., Venema, K., Derks, T. G. J., and Schwartz, I. V. D. (2015). Determination of amylose/amylopectin ratio of starches. *Journal of Inherited Metabolic Disease*, *38*(5), 985–986. https://doi.org/10.1007/s10545-015-9850-8

O'Shea, J. P., Qiao, G. G., and Franks, G. V. (2010). Solid-liquid separations with a temperature-responsive polymeric flocculant: Effect of temperature and molecular weight on polymer adsorption and deposition. *Journal of Colloid and Interface Science*, *348*(1), 9–23. https://doi.org/10.1016/j.jcis.2010.04.063

Odian, G. (2004). *Principles of polymerization*. *Principles of Polymerization* (Vol. 58). https://doi.org/10.1002/047147875X.ch3

Omotoso, O. (2004). High surface areas caused by smectitic interstratification of kaolinite and illite in Athabasca oil sands. *Applied Clay Science*, *25*(1–2), 37–47. https://doi.org/10.1016/j.clay.2003.08.002

Omotoso, O., Mikula, R. J., and Stephens, P. W. (2002). Surface Area of Interstratified Phyllosilicates in Athabasca Oil Sands From Synchrotron XRD. *Advances in X-Ray Analysis*, *45*, 391–396.

Painter, P., and Coleman, M. (2009). *Essentials of polymer science and engineering*. DEStech Publications, Inc.

Paul, D. R., and Robeson, L. M. (2008). Polymer nanotechnology: Nanocomposites. *Polymer*, *49*(15), 3187–3204. https://doi.org/10.1016/j.polymer.2008.04.017

Pavlidou, S., and Papaspyrides, C. D. (2008). A review on polymer–layered silicate nanocomposites. *Progress in Polymer Science*, *33*(12), 1119–1198. https://doi.org/10.1016/j.progpolymsci.2008.07.008

Perez, S., Baldwin, P. M., and Gallant, D. J. (2009). Chapter 5 Structural Features of Starch Granules I. In *Starch Chemistry and Technology* (Third Edit, pp. 149–192). Elsevier Inc. https://doi.org/10.1016/B978-0-12-746275-2.00005-7

Perotti, G. F., Tronto, J., Bizeto, M. A., Izumi, C. M. S., Temperini, M. L. A., Lugao, A. B., Parra, Duclerc F., and Constantino, V. R. L. (2014). Biopolymer-Clay Nanocomposites:

Cassava Starch and Synthetic Clay Cast Films. Journal of Brazilian Chemical Society, 25(2), 320–330. http://doi.org/http://doi.org/10.5935/0103-5053.20130300

Petzold, G., Mende, M., Lunkwitz, K., Schwarz, S., and Buchhammer, H. (2003). Higher efficiency in the flocculation of clay suspensions by using combinations of oppositely charged polyelectrolytes, *218*, 47–57. https://doi.org/10.1016/S0927-7757(02)00584-8

Polat, S., Uslu, M. K., Aygün, A., and Certel, M. (2013). The effects of the addition of corn husk fibre, kaolin and beeswax on cross-linked corn starch foam. *Journal of Food Engineering*, *116*(2), 267–276. https://doi.org/10.1016/j.jfoodeng.2012.12.017

Poletto, M., Pistor, V., and Zattera, A. J. (2013). Chapter 2 Structural Characteristics and Thermal Properties of Native Cellulose. In *Cellulose - Fundamental Aspects* (pp. 45–68). InTech. https://doi.org/10.5772/50452

Roy, S. B., Shit, D. S. C., Gupta, D. R. a Sen, and Shukla, D. P. R. (2014). A Review on Bio-Composites: Fabrication, Properties and Applications. *International Journal of Innovative Research in Science, Engineering and Technology*, *3*(10), 16814–16824. https://doi.org/10.15680/IJIRSET.2014.0310058

Rudin, A., and Choi, P. (2013). *The Elements of Polymer Science and Engineering* (Third). Academic Press - Elsevier.

Sak-bosnar, M., and Gvozdi, V. (2012). Determination of the botanical origin of starch using direct potentiometry and PCA, *87*, 2619–2623. https://doi.org/10.1016/j.carbpol.2011.11.038

Sargeant, J. G. (1982). Determination of Amylose: Amylopectin Ratios of Starches. *Starch - Stärke*, *34*(3), 89–92. https://doi.org/10.1002/star.19820340306

Sinha Ray, S. (2013). *Environmentally Friendly Polymer Nanocomposites*. *Environmentally Friendly Polymer Nanocomposites*. https://doi.org/10.1533/9780857097828.2.269

Song, K. H., and Kim, I. S. (2013). Effects of plasticizer on the mechanical properties of kenaf/starch bio-composites. *Fibers and Polymers*, *14*(12), 2135–2140. https://doi.org/10.1007/s12221-013-2135-7

Suncor Energy. (2016). Reclamation. Retrieved from http://sustainability.suncor.com/2011/en/responsible/1794.aspx

Syncrude. (2016). Water Capping. Retrieved from http://www.syncrude.ca/environment/tailings-management/tailings-reclamation/water-capping/

Tester, R. F., Karkalas, J., and Qi, X. (2004). Starch - Composition, fine structure and architecture. *Journal of Cereal Science*, *39*(2), 151–165. https://doi.org/10.1016/j.jcs.2003.12.001

Then, Y. Y., Ibrahim, N. A., and Wan Yunus, W. M. Z. (2011). Enhancement of Tensile Strength and Flexibility of Polycaprolactone/Tapioca Starch Blends by Octadecylamine Modified Clay. *Journal of Polymers and the Environment*, *19*(2), 535–539. https://doi.org/10.1007/s10924-011-0284-6

Vajihinejad, V., and Soares, J. B. P. (2016). Can We Make Better Polyurethane Composite Foams with Oil Sands Mature Fine Tailing? *Macromolecular Materials and Engineering*, *301*(4), 383–389. https://doi.org/10.1002/mame.201500396

Vallejos, M. E., Curvelo, A. A. S., Teixeira, E. M., Mendes, F. M., Carvalho, A. J. F., Felissia, F. E., and Area, M. C. (2011). Composite materials of thermoplastic starch and fibers from the ethanol–water fractionation of bagasse. *Industrial Crops and Products*, *33*(3), 739–746. https://doi.org/10.1016/j.indcrop.2011.01.014

Van Soest, J. J. G., and Vliegenthart, J. F. G. (1997). Crystallinity in starch plastics: Consequences for material properties. *Trends in Biotechnology*, *15*(6), 208–213. https://doi.org/10.1016/S0167-7799(97)01021-4

Vedoy, D. R. L., and Soares, J. B. P. (2015). Water-soluble polymers for oil sands tailing treatment: A Review. *Canadian Journal of Chemical Engineering*, *93*(5), 888–904. https://doi.org/10.1002/cjce.22129

Wang, S., Li, C., Copeland, L., Niu, Q., and Wang, S. (2015). Starch Retrogradation: A Comprehensive Review. *Comprehensive Reviews in Food Science and Food Safety*, *14*(5), 568–585. https://doi.org/10.1111/1541-4337.12143

Xie, F., Luckman, P., Milne, J., McDonald, L., Young, C., Tu, C. Y., … Halley, P. J. (2014). Thermoplastic Starch: Current development and future trends. *Journal of Renewable Materials*, *2*(2), 95–106. https://doi.org/10.7569/JRM.2014.634104

Xie, F., Yu, L., Su, B., Liu, P., Wang, J., Liu, H., and Chen, L. (2009). Rheological properties of starches with different amylose / amylopectin ratios. *Journal of Cereal Science*, *49*(3), 371–377. https://doi.org/10.1016/j.jcs.2009.01.002

Yang, Y., Tang, Z., Xiong, Z., and Zhu, J. (2015). Preparation and characterization of thermoplastic starches and their blends with poly(lactic acid). *International Journal of Biological Macromolecules*, *77*, 273–279. https://doi.org/10.1016/j.ijbiomac.2015.03.053

Yildirim, N., Shaler, S. M., Gardner, D. J., Rice, R., and Bousfield, D. W. (2014). Cellulose nanofibril (CNF) reinforced starch insulating foams. *Cellulose*, *21*(6), 4337–4347. https://doi.org/10.1007/s10570-014-0450-9

Yoon, S., and Deng, Y. (2004). Flocculation and reflocculation of clay suspension by different polymer systems under turbulent conditions, *278*, 139–145. https://doi.org/10.1016/j.jcis.2004.05.011

Zainuddin, S. Y. Z., Ahmad, I., and Kargarzadeh, H. (2013). Cassava starch biocomposites reinforced with cellulose nanocrystals from kenaf fibers. *Composite Interfaces*, *20*(3), 189–199. https://doi.org/10.1080/15685543.2013.766122

Zhou, M., and Xu, D. (2015). Starch-MMT composite films: Effects of bio-inspired modification on MMT. *Starch - Stärke*, *67*(5–6), 470–477. https://doi.org/10.1002/star.201400231

Zhou, M., Zhao, J., and Zhou, L. (2011). Utilization of starch and montmorrilonite for the preparation of superabsorbent nanocomposite. *Journal of Applied Polymer Science*, *121*(4), 2406–2412. https://doi.org/10.1002/app.33519

Zuraida, A., Yusliza, Y., Nurizan, O., Anuar, H., Zahurin, H., and Noorasikin, S. (2012). Properties of Montmorillonite-Reinforced Thermoplastic Sago Starch Composites, *445*, 469–474. https://doi.org/10.4028/www.scientific.net/AMR.445.469

APPENDIX A

Determination of amylose content of Starches – Modification of ISO 6647-1.

A.1 Reagents

- NaOH 99% purity
- Glacial Acetic Acid 99% purity
- Iodine (Lugol) solution
- Amylose from potato
- Amylopectin from maize

A.2 Molar Masses

- NaOH = 39.997 g/mol
- Acetic acid = 60.05 g/mol

A.3 Procedure

1. Preparation of 1M NaOH solution

$$1\frac{mol}{L} * \frac{1\ L}{1000\ mL} * 39.997\frac{g}{mol} * 100mL = 3.9997\ g\ in\ 100\ mL$$

2. Preparation of 0.1 M NaOH solution

$$0.1\frac{mol}{L} * \frac{1\ L}{1000\ mL} * 39.997\frac{g}{mol} * 100mL = 0.4000\ g\ in\ 100\ mL$$

3. Preparation of 1M acetic acid solution

$$1\frac{mol}{L} * \frac{1\ L}{1000\ mL} * 60.05\frac{g}{mol} * 100mL = 6.005\ g\ in\ 100\ mL$$

4. Preparation of standard potato amylose suspension (1 g/L)

    4.1. Weigh 100 mg ± 5mg of amylose in a 100-ml conical flask.
    4.2. Add 1 mL ethanol.
    4.3. Add 9 mL of 1M NaOH and mix.
    4.4. Heat mixture on boiling water bath for 10 min.
    4.5. Allow to cool to room temperature.
    4.6. Transfer to volumetric flask.
    4.7. Make up to the water mark.

5. Preparation of standard maize amylopectin suspension (1 g/L)

    5.1. Weigh 100 mg ± 5mg of amylopectin in a 100-ml conical flask.
    5.2. Add 1 mL ethanol.
    5.3. Add 9 mL 1M NaOH and mix.
    5.4. Heat mixture on boiling water bath for 10 min.
    5.5. Allow to cool to room temperature.
    5.6. Transfer to volumetric flask.
    5.7. Make up to the water mark.

6. Preparation of blank solution

    6.1. Pipette 5.0 mL of 0.1 M NaOH M solution into a 100-ml volumetric flask containing 50 mL of water.
    6.2. Add 1 mL of 1M acetic acid 1 and mix.
    6.3. Add 2 mL of iodine solution.
    6.4. Make up to the water mark and mix.
    6.5. Allow to stand for 10 minutes.

7. Preparation of calibration curve mixtures

7.1. Mix volumes of potato amylose suspension, maize amylopectin suspension and 0.1 M NaOH solution in 50 mL beakers in accordance with Table A-1.

Table A-1. Mixture of amylose and amylopectin solution for calibration curve

Amylose mass fraction (% dry matter basis)	Amylose Suspension (mL)	Amylopectin (mL)	NaOH 0.1 M (mL)
0	0	9	1
10	1	8	1
20	2	7	1
25	2.5	6.5	1
30	3	6	1
35	3.5	5.5	1
50	5	4	1
75	7.5	1.5	1
90	9	0	1

7.2. Pipette a 5.0 mL aliquot of each calibration solution into 100-ml volumetric flasks containing 50 mL of water.

7.3. Add 1 mL of 1M acetic acid and mix.

7.4. Add 2 mL of iodine solution.

7.5. Make up to the water mark and mix.

7.6. Allow to stand for 10 minutes.

8. Absorbance measurements and calibration curve

8.1. Measure the absorbance against the blank solution at 720 nm.

8.2. Draw a calibration curve with the measurements, absorbance versus amylose mass fraction.

9. Preparation of test solutions (1g/L)

9.1. Weigh 100 mg ± 5mg of the starch sample in a 100-ml conical flask.

9.2. Add 1 mL ethanol.

9.3. Add 9 mL 1M NaOH and mix.

9.4. Heat mixture on boiling water bath for 10 min.

9.5. Allow to cool to room temperature.

9.6. Transfer to volumetric flask.

10. Test solution absorbance determination

10.1. Pipette a 5.0 mL aliquot of each test solution into 100 mL volumetric flasks containing 50 mL of water.

10.2. Add 1 mL of 1 M acetic acid and mix.

10.3. Add 2 mL of iodine solution.

10.4. Make up to the water mark and mix.

10.5. Allow to stand for 10 minutes.

10.6. Measure Absorbance at 720 nm against the blank solution.

10.7. With the absorbance, determine amylose mass fraction using the calibration curve.

APPENDIX B

Data for Composites Characterization

B.1 Density

The sides and thickness of the specimens cut from thin sheets were measured at three different points to get an average of each, as shown on tables B.1 and B.2. After that, an average volume was calculated and each piece was weighed in a scale, obtaining the results shown on table B.2. Finally, an average density was calculated along with the standard deviation, as shown in table B.3.

Table B.1. Side dimensions of specimens for apparent density determination.

Sample		Side 1 (mm)				Side 2 (mm)			
		1	2	3	Avg Side 1	1	2	3	Avg Side 2
PS	1	12.760	12.770	12.730	12.753	35.300	35.240	-	35.270
	2	12.730	12.630	12.590	12.650	35.690	35.610	-	35.650
	3	13.480	13.430	13.490	13.467	35.880	35.780	-	35.830
	4	26.700	26.240	26.080	26.340	75.080	75.320	75.190	75.197
	5	26.130	26.170	26.170	26.157	75.300	75.110	75.220	75.210
	6	26.040	25.980	26.080	26.033	75.530	75.480	75.460	75.490
1% MFT	1	12.740	12.700	12.740	12.727	35.220	35.210	-	35.215
	2	12.680	12.660	12.510	12.617	34.820	35.070	35.170	35.020
	3	12.570	12.570	12.590	12.577	35.530	35.570	-	35.550
	4	25.700	26.080	26.450	26.077	75.560	75.600	76.140	75.767
	5	26.270	26.380	26.480	26.377	75.560	75.440	75.620	75.540
	6	25.930	25.790	25.720	25.813	75.870	75.610	75.610	75.697
2% MFT	1	12.510	12.530	12.440	12.493	35.660	35.650	35.520	35.610
	2	12.200	12.230	12.320	12.250	35.310	35.530	35.550	35.463
	3	12.710	12.710	12.640	12.687	35.300	35.130	35.330	35.253
	4	26.550	26.480	26.180	26.403	75.510	75.330	75.350	75.397
	5	26.260	25.870	25.700	25.943	75.960	75.710	76.010	75.893
	6	25.810	25.840	25.950	25.867	75.050	74.850	75.040	74.980

Table B.1 (Cont.). Side dimensions of specimens for apparent density determination.

Sample		Side 1 (mm)				Side 2 (mm)			
		1	**2**	**3**	**Avg Side 1**	**1**	**2**	**3**	**Avg Side 2**
3% MFT	1	12.640	12.670	12.720	12.677	35.730	35.610	35.750	35.697
	2	11.970	12.170	12.200	12.113	35.690	35.570	35.590	35.617
	3	12.610	12.570	12.550	12.577	35.560	35.300	35.470	35.443
	4	26.230	26.070	26.040	26.113	75.280	75.300	75.520	75.367
	5	27.010	26.720	26.670	26.800	75.270	75.060	75.100	75.143
	6	25.640	25.710	25.950	25.767	75.040	75.430	75.370	75.280
5% MFT	1	12.49	12.3	12.27	12.353	35.13	34.98	35.09	35.067
	2	12.86	12.8	12.75	12.803	35.67	35.32	35.56	35.517
	3	12.37	12.4	12.71	12.493	35.42	35.57	35.7	35.563
	4	28.32	27.86	27.59	27.923	76.08	76.09	76.03	76.067
	5	25.59	26.01	26.14	25.913	76.25	76.35	76.4	76.333
	6	26.57	26.56	26.64	26.590	75.98	75.68	76.02	75.893
10% MFT	1	12.68	12.61	12.62	12.637	35.54	35.28	35.51	35.443
	2	12.71	12.79	12.93	12.810	35.2	35.18	35.28	35.220
	3	12.22	12.42	12.47	12.370	35.49	35.43	35.38	35.433
	4	26.4	26.22	26.42	26.347	76.15	75.93	76.25	76.110
	5	26.74	26.61	26.38	26.577	75.9	75.7	75.76	75.787
	6	25.91	25.74	25.85	25.833	75.81	75.63	75.85	75.763
20% MFT	1	12.31	12.16	12.2	12.223	35.39	35.35	35.52	35.420
	2	12.75	12.62	12.74	12.703	35.58	35.47	35.59	35.547
	3	12.76	12.45	12.68	12.630	35.48	35.54	35.53	35.517
	4	12.49	12.39	12.49	12.457	35.34	35.36	35.41	35.370
	5	26.12	26.25	26.22	26.197	75.06	75.1	75.19	75.117
	6	25.98	26.03	25.83	25.947	75.39	75.49	75.49	75.457
	7	26.33	25.92	26.06	26.103	75.27	75.62	75.66	75.517
1% MMT	1	13.01	12.73	12.84	12.860	36.28	36.15	36	36.143
	2	12.86	12.87	12.91	12.880	35.26	35.17	35.3	35.243
	3	12.54	12.72	12.87	12.710	35.86	35.87	35.79	35.840
	4	25.85	25.83	25.81	25.830	75.81	75.89	75.94	75.880
	5	26.05	26.04	26.14	26.077	75.78	75.58	75.63	75.663
	6	26.38	26.34	26.45	26.390	75.87	75.51	75.66	75.680

Table B.1 (Cont.). Side dimensions of specimens for apparent density determination.

Sample		Side 1 (mm)				Side 2 (mm)			
		1	**2**	**3**	**Avg Side 1**	**1**	**2**	**3**	**Avg Side 2**
2% MMT	1	12.88	12.85	12.66	12.797	36.21	36.21	36.06	36.160
	2	12.72	12.74	12.71	12.723	35.74	35.83	35.75	35.773
	3	13.09	13.18	13.24	13.170	35.84	35.65	35.72	35.737
	4	26.05	25.97	26.14	26.053	75.53	75.48	75.33	75.447
	5	25.85	25.93	26.09	25.957	75.6	75.48	75.54	75.540
	6	26.19	26.16	26.53	26.293	75.12	75.91	75.83	75.620
3% MMT	1	12.88	12.99	12.99	12.953	35.81	35.54	35.67	35.673
	2	12.78	12.74	12.72	12.747	36.17	36.18	36.23	36.193
	3	13.81	13.8	13.68	13.763	35.77	35.58	35.72	35.690
	4	26.45	26.49	26.26	26.400	75.74	75.76	75.78	75.760
	5	26.21	25.99	25.98	26.060	76.3	76.07	76.22	76.197
	6	26.78	26.27	26.66	26.570	76.14	75.83	76.34	76.103
5% MMT	1	13.03	13.3	13.29	13.207	35.6	35.38	35.58	35.520
	2	12.62	12.65	12.79	12.687	35.89	35.89	35.94	35.907
	3	12.71	12.74	12.8	12.750	35.85	35.87	35.57	35.763
	4	25.71	25.81	26.02	25.847	75.65	75.78	75.86	75.763
	5	26.42	26.55	26.43	26.467	75.87	75.65	75.79	75.770
	6	25.77	25.78	25.68	25.743	75.77	75.61	75.95	75.777
1% DS	1	12.57	12.49	12.49	12.517	35.14	35.22	35.18	35.180
	2	12.49	12.3	12.25	12.347	35.31	35.59	35.58	35.493
	3	12.59	12.63	12.74	12.653	35.27	35.19	35.32	35.260
	4	25.83	25.77	25.67	25.757	75.12	75.11	75.13	75.120
	5	25.61	25.77	25.91	25.763	75.24	75.14	75.03	75.137
	6	25.85	25.6	25.37	25.607	75.05	75.04	75.2	75.097
2% DS	1	12.52	12.61	12.69	12.607	36.01	36.08	35.89	35.993
	2	12.62	12.73	12.82	12.723	35.43	35.36	35.43	35.407
	3	13.12	13.04	12.99	13.050	35.27	35.26	35.23	35.253
	4	25.64	25.69	25.71	25.680	75.69	76.39	76.13	76.070
	5	25.37	25.38	25.41	25.387	75.48	75.32	75.37	75.390
	6	25.18	25.23	25.17	25.193	75.81	75.45	75.79	75.683
3% DS	1	12.83	12.79	12.76	12.793	35.31	35.28	35.32	35.303
	2	12.8	12.78	12.69	12.757	35.45	35.41	35.39	35.417
	3	12.97	13.09	13.08	13.047	35.18	35.14	35.29	35.203
	4	25.8	25.79	25.89	25.827	75.46	75.62	75.66	75.580
	5	25.65	25.63	25.45	25.577	75.42	75.07	75.4	75.297
	6	25.65	25.6	25.63	25.627	74.79	75.18	75.2	75.057

Table B.1 (Cont.). Side dimensions of specimens for apparent density determination.

Sample		Side 1 (mm)				Side 2 (mm)			
		1	**2**	**3**	**Avg Side 1**	**1**	**2**	**3**	**Avg Side 2**
5% DS	1	12.84	12.86	12.96	12.887	35.52	35.35	35.38	35.417
	2	12.75	12.91	12.99	12.883	35.52	35.42	35.52	35.487
	3	13.08	13	12.77	12.950	35.45	35.3	35.34	35.363
	4	25.53	25.4	25.32	25.417	76.09	76.04	76.24	76.123
	5	25.96	25.8	25.83	25.863	75.25	75.13	75.23	75.203
	6	25.94	25.82	25.67	25.810	75.31	75.66	75.56	75.510
10% DS	1	12.89	12.82	12.89	12.867	35.57	35.47	35.57	35.537
	2	12.37	12.42	12.36	12.383	35.42	35.26	35.46	35.380
	3	12.65	12.7	12.56	12.637	35.48	35.49	35.43	35.467
	4	25.55	25.61	25.74	25.633	75.24	75.21	75.28	75.243
	5	25.72	25.65	25.62	25.663	74.87	74.67	74.77	74.770
	6	26.25	26.01	25.7	25.987	75.49	75.58	75.57	75.547
20% DS	1	13.14	13.2	13.22	13.187	35.85	35.89	35.74	35.827
	2	12.79	12.72	12.79	12.767	35.62	35.58	35.7	35.633
	3	12.98	12.92	12.93	12.943	35.47	35.35	35.36	35.393
	4	26.36	26.05	25.92	26.110	75.46	75.13	75.44	75.343
	5	25.98	26.19	26.51	26.227	75.82	75.18	75.87	75.623
	6	25.81	25.72	25.66	25.730	75.34	75.52	75.43	75.430
1% CNC	1	12.8	12.85	13	12.883	36.16	36.04	36.11	36.103
	2	13.39	13.69	13.62	13.567	35.06	35.32	35.27	35.217
	3	13.33	13.28	13.15	13.253	35.97	35.89	36.14	36.000
	4	13.62	13.34	13.3	13.420	35.51	35.42	35.44	35.457
	5	13.62	13.66	13.67	13.650	36.09	36.03	35.88	36.000
	6	13.42	13.44	13.51	13.457	36.2	36.3	36.47	36.323
2% CNC	1	12.77	12.85	12.71	12.777	35.76	35.78	35.67	35.737
	2	13.53	13.58	13.62	13.577	35.78	35.67	35.81	35.753
	3	13.35	13.34	13.27	13.320	35.83	35.76	35.99	35.860
	4	13.05	12.95	12.92	12.973	36.04	35.93	35.96	35.977
	5	13.19	13.19	13.13	13.170	36.28	36.13	36.14	36.183
	6	12.96	12.92	12.94	12.940	35.65	35.83	35.63	35.703
3% CNC	1	12.43	12.4	12.41	12.413	36.38	36.28	36.34	36.333
	2	12.84	13.28	13.18	13.100	36.27	36.24	36.26	36.257
	3	12.69	12.71	12.63	12.677	36.25	36.24	36.3	36.263
	4	12.66	12.73	13.11	12.833	35.89	36.06	36.09	36.013
	5	12.99	13	12.9	12.963	36.22	36.15	36.15	36.173
	6	13.41	13.54	13.4	13.450	36.04	36.1	36.06	36.067

Table B.1 (Cont.). Side dimensions of specimens for apparent density determination.

Sample		Side 1 (mm)				Side 2 (mm)			
		1	**2**	**3**	**Avg Side 1**	**1**	**2**	**3**	**Avg Side 2**
5% CNC	1	12.87	13.04	13.06	12.990	35.93	35.91	35.84	35.893
	2	13.16	12.93	13.09	13.060	36.12	35.95	36.05	36.040
	3	13.34	13.21	13.34	13.297	35.83	35.69	35.7	35.740
	4	13.21	13.18	13.2	13.197	35.46	35.48	35.44	35.460
	5	12.94	12.99	13.14	13.023	36.03	35.92	36.21	36.053
	6	12.92	13.03	13.12	13.023	35.79	35.51	35.68	35.660

Table B.2. Thickness, mass, and calculation of average volume of specimens for apparent density determination.

Sample		Thickness (mm)				Volume (cm^3)	Mass (g)
		1	**2**	**3**	**Avg Thickness**		
PS	1	2.790	2.770	2.780	2.780	1.250	1.721
	2	2.810	2.810	2.810	2.810	1.267	1.742
	3	2.800	2.780	2.790	2.790	1.346	1.836
	4	2.850	2.920	2.840	2.870	5.685	7.680
	5	2.800	2.940	2.800	2.847	5.600	7.686
	6	2.790	2.830	2.830	2.817	5.535	7.667
1% MFT	1	2.700	2.700	2.710	2.703	1.212	1.693
	2	2.700	2.690	2.700	2.697	1.191	1.658
	3	2.770	2.710	2.730	2.737	1.224	1.696
	4	2.950	2.930	2.940	2.940	5.809	8.051
	5	2.760	2.810	2.830	2.800	5.579	7.740
	6	2.870	2.800	2.930	2.867	5.601	7.738
2% MFT	1	2.770	2.760	2.780	2.770	1.232	1.682
	2	2.790	2.820	2.810	2.807	1.219	1.681
	3	2.780	2.770	2.800	2.783	1.245	1.715
	4	2.630	2.630	2.630	2.630	5.236	7.261
	5	2.850	2.850	2.860	2.853	5.618	7.745
	6	2.650	2.640	2.640	2.643	5.127	7.239

Table B.2 (Cont.). Thickness, mass, and calculation of average volume of specimens for apparent density determination.

Sample		Thickness (mm)				Volume (cm^3)	Mass (g)
		1	2	3	Avg Thickness		
3% MFT	1	2.810	2.790	2.810	2.803	1.269	1.741
	2	2.830	2.860	2.840	2.843	1.227	1.675
	3	2.900	2.870	2.880	2.883	1.285	1.730
	4	2.990	3.000	2.990	2.993	5.891	8.050
	5	2.700	2.680	2.670	2.683	5.404	7.387
	6	2.710	2.770	2.690	2.723	5.282	7.225
5% MFT	1	2.89	2.86	2.86	2.870	1.243	1.700
	2	2.87	2.86	3.06	2.930	1.332	1.821
	3	2.86	2.87	2.85	2.860	1.271	1.744
	4	2.86	2.87	2.97	2.900	6.160	8.361
	5	2.86	2.84	2.82	2.840	5.618	7.786
	6	2.89	2.87	2.87	2.877	5.805	8.036
10% MFT	1	2.92	2.91	2.9	2.910	1.303	1.782
	2	2.93	2.91	2.89	2.910	1.313	1.810
	3	3.02	3.02	3	3.013	1.321	1.833
	4	2.93	2.94	2.93	2.933	5.882	8.095
	5	3	3.02	3.02	3.013	6.069	8.309
	6	3	3.02	3	3.007	5.885	8.103
20% MFT	1	3.01	2.97	2.97	2.983	1.292	1.829
	2	2.99	2.96	2.96	2.970	1.341	1.901
	3	2.98	2.99	2.98	2.983	1.338	1.889
	4	3	3.01	3.01	3.007	1.325	1.866
	5	2.86	2.85	2.86	2.857	5.621	7.947
	6	2.99	2.99	2.99	2.990	5.854	8.310
	7	2.97	2.97	2.96	2.967	5.848	8.303
1% MMT	1	2.96	2.95	2.96	2.957	1.374	1.876
	2	3.04	3.04	3.04	3.040	1.380	1.878
	3	2.95	2.95	2.96	2.953	1.345	1.706
	4	3.02	3.03	3.04	3.030	5.939	8.105
	5	2.78	2.76	2.76	2.767	5.459	7.472
	6	2.95	2.96	2.99	2.967	5.925	8.103

Table B.2 (Cont.). Thickness, mass, and calculation of average volume of specimens for apparent density determination.

Sample		Thickness (mm)				Volume (cm^3)	Mass (g)
		1	2	3	Avg Thickness		
2% MMT	1	3	3.01	3.01	3.007	1.391	1.86
	2	2.74	2.75	2.76	2.750	1.252	1.702
	3	2.77	2.76	2.75	2.760	1.299	1.773
	4	2.77	2.76	2.75	2.760	5.425	7.449
	5	2.99	2.99	3.01	2.997	5.876	8.042
	6	2.76	2.79	2.85	2.800	5.567	7.621
3% MMT	1	3.03	3.02	3.02	3.023	1.397	1.895
	2	2.73	2.73	2.72	2.727	1.258	1.7
	3	2.73	2.75	2.75	2.743	1.348	1.827
	4	2.75	2.73	2.72	2.733	5.467	7.539
	5	2.74	2.75	2.74	2.743	5.447	7.511
	6	3.02	3.06	3	3.027	6.120	8.466
5% MMT	1	3.09	3.09	3.07	3.083	1.446	1.965
	2	2.81	2.81	2.81	2.810	1.280	1.77
	3	3.07	3.06	3.05	3.060	1.395	1.93
	4	3.09	3.27	3.08	3.147	6.162	8.261
	5	3.1	3.1	3.12	3.107	6.230	8.504
	6	2.77	2.79	2.84	2.800	5.462	7.442
1% DS	1	2.8	2.8	2.8	2.800	1.233	1.678
	2	2.83	2.83	2.83	2.830	1.240	1.685
	3	2.8	2.81	2.8	2.803	1.251	1.677
	4	2.8	2.83	2.83	2.820	5.456	7.506
	5	2.73	2.78	2.77	2.760	5.343	7.313
	6	2.8	2.81	2.81	2.807	5.397	7.384
2% DS	1	2.92	2.99	2.95	2.953	1.340	1.836
	2	2.79	2.8	2.81	2.800	1.261	1.75
	3	2.74	2.75	2.75	2.747	1.264	1.734
	4	2.94	2.97	2.95	2.953	5.769	7.974
	5	2.83	2.8	2.81	2.813	5.384	7.436
	6	2.74	2.75	2.73	2.740	5.224	7.278

Table B.2 (Cont.). Thickness, mass, and calculation of average volume of specimens for apparent density determination.

Sample		Thickness (mm)				Volume (cm^3)	Mass (g)
		1	2	3	Avg Thickness		
3% DS	1	2.9	2.87	2.86	2.877	1.299	1.797
	2	2.75	2.77	2.78	2.767	1.250	1.728
	3	2.65	2.65	2.65	2.650	1.217	1.69
	4	2.65	2.64	2.66	2.650	5.173	7.251
	5	2.88	2.88	2.87	2.877	5.540	7.752
	6	2.79	2.78	2.75	2.773	5.334	7.448
5% DS	1	2.98	2.98	2.98	2.980	1.360	1.866
	2	2.7	2.7	2.7	2.700	1.234	1.684
	3	2.85	2.87	2.86	2.860	1.310	1.779
	4	2.98	2.96	3.07	3.003	5.811	7.853
	5	2.89	2.88	2.87	2.880	5.602	7.643
	6	2.68	2.69	2.69	2.687	5.236	7.165
10% DS	1	2.85	2.85	2.85	2.850	1.303	1.838
	2	2.79	2.78	2.79	2.787	1.221	1.712
	3	2.78	2.76	2.76	2.767	1.240	1.739
	4	2.78	2.8	2.8	2.793	5.388	7.593
	5	2.8	2.8	2.8	2.800	5.373	7.539
	6	2.82	2.85	2.84	2.837	5.569	7.786
20% DS	1	2.77	2.8	2.78	2.783	1.315	1.893
	2	2.82	2.86	2.81	2.830	1.287	1.814
	3	2.86	2.87	2.87	2.867	1.313	1.886
	4	2.84	2.85	2.84	2.843	5.593	7.982
	5	2.82	2.78	2.75	2.783	5.520	7.842
	6	2.81	2.82	2.81	2.813	5.460	7.699
1% CNC	1	2.94	2.95	2.94	2.943	1.369	1.885
	2	2.95	2.93	2.94	2.940	1.405	1.9
	3	2.95	2.96	2.96	2.957	1.411	1.9
	4	2.96	2.95	2.94	2.950	1.404	1.87
	5	2.94	2.94	2.94	2.940	1.445	1.958
	6	2.94	2.98	2.96	2.960	1.447	1.956

Table B.2 (Cont.). Thickness, mass, and calculation of average volume of specimens for apparent density determination.

Sample		Thickness (mm)				Volume (cm^3)	Mass (g)
		1	2	3	Avg Thickness		
2% CNC	1	2.84	2.83	2.82	2.830	1.292	1.768
	2	2.83	2.83	2.84	2.833	1.375	1.878
	3	2.84	2.84	2.86	2.847	1.360	1.851
	4	2.83	2.84	2.85	2.840	1.326	1.798
	5	2.85	2.85	2.86	2.853	1.360	1.84
	6	2.83	2.83	2.83	2.830	1.307	1.77
3% CNC	1	2.81	2.81	2.81	2.810	1.267	1.717
	2	2.7	2.69	2.69	2.693	1.279	1.743
	3	2.71	2.71	2.71	2.710	1.246	1.685
	4	2.74	2.69	2.68	2.703	1.249	1.695
	5	2.95	2.95	2.99	2.963	1.390	1.862
	6	2.85	2.86	2.86	2.857	1.386	1.881
5% CNC	1	2.83	2.83	2.83	2.830	1.319	1.803
	2	2.8	2.78	2.78	2.787	1.312	1.787
	3	2.83	2.96	2.83	2.873	1.365	1.86
	4	2.84	2.84	2.84	2.840	1.329	1.833
	5	2.82	2.81	2.83	2.820	1.324	1.819
	6	2.83	2.82	2.84	2.830	1.314	1.811

Table B.3. Calculated apparent density of specimens, average density of composites, and standard deviation.

Sample		Apparent Density (g/ml)	Average Density (g/ml)	Standard Deviation
PS	1	1.376	1.371	0.012
	2	1.375		
	3	1.364		
	4	1.351		
	5	1.372		
	6	1.385		

Table B.3 (Cont.). Calculated apparent density of specimens, average density of composites, and standard deviation.

Sample		Apparent Density (g/ml)	Average Density (g/ml)	Standard Deviation
1% MFT	1	1.397	1.388	0.005
	2	1.392		
	3	1.386		
	4	1.386		
	5	1.387		
	6	1.381		
2% MFT	1	1.365	1.383	0.016
	2	1.379		
	3	1.378		
	4	1.387		
	5	1.379		
	6	1.412		
3% MFT	1	1.372	1.364	0.009
	2	1.365		
	3	1.346		
	4	1.366		
	5	1.367		
	6	1.368		
5% MFT	1	1.367	1.372	0.011
	2	1.367		
	3	1.372		
	4	1.357		
	5	1.386		
	6	1.384		
10% MFT	1	1.367	1.376	0.007
	2	1.379		
	3	1.388		
	4	1.376		
	5	1.369		
	6	1.377		

Table B.3 (Cont.). Calculated apparent density of specimens, average density of composites, and standard deviation.

Sample		Apparent Density (g/ml)	Average Density (g/ml)	Standard Deviation
20% MFT	1	1.416	1.415	0.004
	2	1.417		
	3	1.412		
	4	1.409		
	5	1.414		
	6	1.420		
	7	1.420		
1% MMT	1	1.365	1.349	0.040
	2	1.361		
	3	1.268		
	4	1.365		
	5	1.369		
	6	1.368		
2% MMT	1	1.337	1.362	0.013
	2	1.360		
	3	1.365		
	4	1.373		
	5	1.369		
	6	1.369		
3% MMT	1	1.356	1.367	0.014
	2	1.351		
	3	1.356		
	4	1.379		
	5	1.379		
	6	1.383		
5% MMT	1	1.359	1.365	0.016
	2	1.383		
	3	1.383		
	4	1.341		
	5	1.365		
	6	1.362		

Table B.3 (Cont.). Calculated apparent density of specimens, average density of composites, and standard deviation.

Sample		Apparent Density (g/ml)	Average Density (g/ml)	Standard Deviation
1% DS	1	1.361	1.362	0.012
	2	1.359		
	3	1.341		
	4	1.376		
	5	1.369		
	6	1.368		
2% DS	1	1.370	1.381	0.009
	2	1.387		
	3	1.372		
	4	1.382		
	5	1.381		
	6	1.393		
3% DS	1	1.383	1.392	0.008
	2	1.382		
	3	1.389		
	4	1.402		
	5	1.399		
	6	1.396		
5% DS	1	1.372	1.363	0.007
	2	1.364		
	3	1.358		
	4	1.351		
	5	1.364		
	6	1.368		
10% DS	1	1.410	1.404	0.005
	2	1.402		
	3	1.402		
	4	1.409		
	5	1.403		
	6	1.398		

Table B.3 (Cont.). Calculated apparent density of specimens, average density of composites, and standard deviation.

Sample		Apparent Density (g/ml)	Average Density (g/ml)	Standard Deviation
20% DS	1	1.440	1.424	0.013
	2	1.409		
	3	1.436		
	4	1.427		
	5	1.421		
	6	1.410		
1% CNC	1	1.377	1.353	0.014
	2	1.353		
	3	1.347		
	4	1.332		
	5	1.355		
	6	1.352		
2% CNC	1	1.368	1.360	0.006
	2	1.365		
	3	1.361		
	4	1.356		
	5	1.353		
	6	1.354		
3% CNC	1	1.355	1.354	0.008
	2	1.363		
	3	1.353		
	4	1.357		
	5	1.340		
	6	1.357		
5% CNC	1	1.366	1.370	0.008
	2	1.362		
	3	1.362		
	4	1.379		
	5	1.374		
	6	1.378		

B.2 Water Absorption

The water absorption characterization consisted in measuring, for each specimen prepared, the initial weight, the weight after completely drying the specimens for 24 hours, the weight after 2-hour immersion in water, and the weight after a final 24-hour drying after immersion. These values are shown in table B.4. Then, the initial moisture, water uptake and mass loss were calculated through equations 3.5 to 3.7, and are shown in table B.5 with their respective averages and standard deviations.

Table B.4. Initial weight, weight after first drying, weight after 2-hour immersion in water and final dry weight after immersion, measured according to ASTM D570-98.

Sample		Initial Weight (g)	Weight after Drying (g)	Weight After 2h Immersion (g)	Final Dry Weight (g)
PS	1	7.680	6.612	8.758	5.630
	2	7.686	6.624	8.797	5.651
	3	7.667	6.538	8.611	5.522
1% MFT	1	8.051	6.963	9.177	5.916
	2	7.740	6.731	8.897	5.773
	3	7.738	6.668	8.816	5.731
2% MFT	1	7.261	6.155	8.428	5.134
	2	7.745	6.591	8.693	5.656
	3	7.239	6.056	8.088	5.121
3% MFT	1	8.050	6.829	8.934	5.838
	2	7.387	6.226	8.354	5.267
	3	7.225	6.120	8.136	5.213
5% MFT	1	8.361	7.132	9.334	6.137
	2	7.786	6.629	8.743	5.696
	3	8.036	6.846	9.006	5.815
10% MFT	1	8.095	6.904	8.927	5.974
	2	8.309	7.109	9.147	6.193
	3	8.103	6.960	8.944	6.060
20% MFT	1	7.947	6.896	8.719	6.070
	2	8.310	7.219	9.072	6.369
	3	8.303	7.194	9.057	6.378

Table B.4 (Cont.). Initial weight, weight after first drying, weight after 2-hour immersion in water and final dry weight after immersion, measured according to ASTM D570-98

Sample		Initial Weight (g)	Weight after Drying (g)	Weight After 2h Immersion (g)	Final Dry Weight (g)
1% MMT	1	8.105	7.179	9.028	6.120
	2	7.472	6.576	8.306	5.583
	3	8.103	7.101	8.944	6.029
2% MMT	1	7.449	6.566	8.638	4.529
	2	8.042	7.102	10.892	5.032
	3	7.621	6.679	9.962	4.428
3% MMT	1	8.466	7.526	10.963	4.596
	2	7.511	6.706	10.152	4.233
	3	7.539	6.686	11.807	4.645
5% MMT	1	8.261	7.357	10.889	2.583
	2	8.504	7.607	9.890	3.403
	3	7.442	6.661	11.993	4.486
1% DS	1	7.506	6.536	8.524	5.563
	2	7.313	6.394	8.330	5.410
	3	7.384	6.437	8.367	5.456
2% DS	1	7.974	7.008	9.028	6.029
	2	7.436	6.564	8.501	5.581
	3	7.278	6.409	8.340	5.455
3% DS	1	7.251	6.481	8.468	5.472
	2	7.752	6.945	8.828	6.000
	3	7.448	6.667	8.581	5.742
5% DS	1	7.853	6.786	8.566	5.851
	2	7.643	6.608	8.363	5.657
	3	7.165	6.154	7.934	5.258
10% DS	1	7.593	6.609	8.323	5.705
	2	7.539	6.636	8.326	5.710
	3	7.786	6.864	8.568	5.963
20% DS	1	7.982	7.072	8.730	6.228
	2	7.842	6.957	8.628	6.054
	3	7.699	6.830	8.496	5.998

Table B.5. Initial moisture, water uptake, and mass loss of specimens with corresponding averages and standard deviations.

Sample		Initial Moisture (%)	Average Moisture	Std. Dev.	Water uptake (%)	Average Uptake	Std. Dev.	Mass Loss %	Average Mass loss	Std. Dev.
PS	1	13.91	14.15	0.50	32.46	32.32	0.56	14.85	15.03	0.45
	2	13.82			32.80			14.69		
	3	14.73			31.71			15.54		
1% MFT	1	13.51	13.46	0.40	31.80	32.06	0.23	15.04	14.44	0.52
	2	13.04			32.18			14.23		
	3	13.83			32.21			14.05		
2% MFT	1	15.23	15.49	0.76	36.93	34.12	2.57	16.59	15.40	1.20
	2	14.90			31.89			14.19		
	3	16.34			33.55			15.44		
3% MFT	1	15.17	15.39	0.29	30.82	32.65	1.70	14.51	14.91	0.45
	2	15.72			34.18			15.40		
	3	15.29			32.94			14.82		
5% MFT	1	14.70	14.79	0.08	30.87	31.44	0.52	13.95	14.36	0.61
	2	14.86			31.89			14.07		
	3	14.81			31.55			15.06		
10% MFT	1	14.71	14.42	0.30	29.30	28.83	0.42	13.47	13.10	0.33
	2	14.44			28.67			12.89		
	3	14.11			28.51			12.93		
20% MFT	1	13.23	13.24	0.11	26.44	26.00	0.39	11.98	11.70	0.32
	2	13.13			25.67			11.77		
	3	13.36			25.90			11.34		
1% MMT	1	11.43	11.93	0.47	25.76	26.01	0.28	14.75	14.98	0.20
	2	11.99			26.31			15.10		
	3	12.37			25.95			15.10		
2% MMT	1	11.85	11.97	0.35	31.56	44.69	11.57	31.02	31.29	2.29
	2	11.69			53.37			29.15		
	3	12.36			49.15			33.70		
3% MMT	1	11.10	11.05	0.30	45.67	57.88	16.45	38.93	35.45	4.38
	2	10.72			51.39			36.88		
	3	11.31			76.59			30.53		
5% MMT	1	10.94	10.66	0.24	48.01	52.69	25.34	64.89	50.94	16.55
	2	10.55			30.01			55.26		
	3	10.49			80.05			32.65		

Table B.5 (Cont.). Initial moisture, water uptake, and mass loss of specimens with corresponding averages and standard deviations.

Sample		Initial Moisture (%)	Average Moisture	Std. Dev.	Water uptake (%)	Average Uptake	Std. Dev.	Mass Loss %	Average Mass loss	Std. Dev.
1% DS	1	12.92	12.77	0.18	30.42	30.23	0.22	14.89	15.17	0.26
	2	12.57			30.28			15.39		
	3	12.83			29.98			15.24		
2% DS	1	12.11	11.93	0.19	28.82	29.49	0.65	13.97	14.61	0.56
	2	11.73			29.51			14.98		
	3	11.94			30.13			14.89		
3% DS	1	10.62	10.51	0.11	30.66	28.83	1.78	15.57	14.35	1.06
	2	10.41			27.11			13.61		
	3	10.49			28.71			13.87		
5% DS	1	13.59	13.75	0.32	26.23	27.24	1.47	13.78	14.24	0.41
	2	13.54			26.56			14.39		
	3	14.11			28.92			14.56		
10% DS	1	12.96	12.26	0.61	25.93	25.41	0.56	13.68	13.59	0.42
	2	11.98			25.47			13.95		
	3	11.84			24.83			13.13		
20% DS	1	11.40	11.32	0.07	23.44	23.95	0.48	11.93	12.37	0.55
	2	11.29			24.02			12.98		
	3	11.29			24.39			12.18		

B.3. Tensile Properties

The tensile test focused on measuring the tensile or Young's modulus, the tensile strength and the strain at break for each specimen. The measured tensile properties are shown in table B.6. Finally, with the values recorded for the specimens for each composite and each filler percentage, an average and a standard deviation was calculated for tensile modulus, tensile strength and strain at break, resulting in the values shown in table B.7.

Table B.6. Tensile modulus, tensile strength and strain at break.

Sample		Young modulus (Mpa)	Tensile Strength (Mpa)	Strain at Break (mm/mm)
PS	1	12.7469	2.2214	0.5967
	2	13.0350	2.1712	0.6046
	3	12.5892	2.1740	0.6379
	4	17.4057	2.3790	0.5684
	5	13.9435	2.1348	0.5956
	6	15.4908	2.2244	0.5669
	7	12.2587	1.9841	0.5064
	8	19.1928	2.5300	0.6405
	9	14.4122	2.1886	0.5295
	10	11.8213	2.0028	0.5239
	11	Damaged Specimen		
	12	18.1103	2.3846	0.5735
1% MFT	1	19.6417	2.3799	0.5649
	2	14.5046	2.1206	0.5225
	3	14.7031	2.1827	0.5548
	4	19.0899	2.3534	0.5445
	5	19.7811	2.4609	0.6111
	6	20.5479	2.4453	0.5611
	7	15.2498	2.3427	0.5863
	8	16.6319	2.3853	0.5322
	9	12.4562	2.0784	0.5018
	10	12.4730	2.0249	0.4787
	11	15.6597	2.2524	0.5812
	12	14.0386	2.1341	0.5113
2% MFT	1	18.2879	2.0947	0.4101
	2	17.7549	2.2079	0.4733
	3	Damaged Specimen		
	4	17.0820	2.1882	0.4935
	5	13.3043	1.9375	0.4852
	6	11.4291	1.7372	0.3993
	7	19.0037	2.1652	0.4534
	8	12.6890	1.8985	0.4668
	9	13.3419	2.0231	0.4790
	10	13.5597	2.0236	0.5055
	11	15.5973	2.1312	0.5391
	12	15.2229	2.0703	0.4776

Table B.6 (Cont.). Tensile modulus, tensile strength and strain at break.

Sample		Young modulus (Mpa)	Tensile Strength (Mpa)	Strain at Break (mm/mm)
3% MFT	1	14.2676	1.8922	0.4362
	2	17.8202	2.1507	0.4938
	3	15.3393	1.9872	0.4508
	4	14.3671	1.9903	0.4552
	5	16.4287	2.0946	0.4922
	6	16.7983	2.0665	0.4636
	7	15.1132	1.8830	0.4029
	8	18.3380	2.2443	0.5313
	9	12.7349	1.8733	0.4480
	10	13.2656	1.8660	0.4115
	11	19.0492	2.1294	0.4971
	12	19.5257	2.1993	0.5007
5% MFT	1	13.8502	1.9745	0.4175
	2	18.5986	2.1405	0.4265
	3	19.0661	2.1248	0.4455
	4	18.5824	2.1150	0.4650
	5	18.0610	2.1657	0.4500
	6	16.9449	1.9916	0.4303
	7	18.9646	2.0664	0.4112
	8	Damaged Specimen		
	9	14.8181	2.0302	0.4493
	10	18.6867	2.0901	0.4762
	11	19.2797	2.0737	0.4305
	12	18.8287	2.0080	0.4027
10% MFT	1	21.9202	2.0633	0.3765
	2	22.9766	2.0884	0.4153
	3	22.8287	2.0885	0.4436
	4	20.5776	1.9705	0.3833
	5	Damaged Specimen		
	6	21.6483	2.1618	0.4408
	7	18.4388	1.9866	0.4030
	8	23.1135	2.0158	0.3601
	9	21.9976	2.0247	0.3778
	10	21.9966	2.0097	0.3679
	11	18.8229	1.9516	0.3856
	12	19.1882	1.9766	0.3805

Table B.6 (Cont.). Tensile modulus, tensile strength and strain at break.

Sample		Young modulus (Mpa)	Tensile Strength (Mpa)	Strain at Break (mm/mm)
20% MFT	1	27.1311	2.0734	0.3285
	2	27.2041	2.1376	0.3613
	3	22.0095	1.9762	0.3451
	4	21.3242	1.9452	0.3141
	5	24.9818	2.0523	0.3232
	6	24.1522	2.1392	0.3638
	7	20.7337	1.9667	0.3549
	8	24.9557	1.9041	0.2776
	9	25.7692	2.0546	0.3513
	10	24.0592	2.0286	0.3495
	11	24.7189	2.0360	0.3267
	12	23.8101	1.9704	0.3124
1% DS	1	18.8578	2.6278	0.7314
	2	20.9683	2.7569	0.7618
	3	20.7091	2.7283	0.6816
	4	16.1680	2.5976	0.7465
	5	17.4412	2.6085	0.7277
	6	19.6205	2.6474	0.6279
	7	17.4547	2.5573	0.6563
	8	16.5136	2.5299	0.7016
	9	17.2497	2.3656	0.5268
	10	16.6776	2.5899	0.7308
	11	18.7125	2.5909	0.7044
	12	17.5937	2.6116	0.7223
2% DS	1	19.0246	2.6131	0.6497
	2	18.5852	2.6214	0.6896
	3	Damaged Specimen		
	4	18.1511	2.6486	0.7264
	5	21.6030	2.6723	0.5975
	6	21.1856	2.7933	0.6981
	7	18.8458	2.7307	0.6881
	8	19.6088	2.8198	0.7644
	9	19.2617	2.8020	0.7334
	10	18.9279	2.7328	0.6596
	11	16.7902	2.6363	0.7313
	12	17.6985	2.6607	0.7272

Table B.6 (Cont.). Tensile modulus, tensile strength and strain at break.

Sample		Young modulus (Mpa)	Tensile Strength (Mpa)	Strain at Break (mm/mm)
3% DS	1	19.2235	2.6777	0.6256
	2	19.2098	2.7157	0.6512
	3	21.2864	2.8017	0.6486
	4	22.0634	2.7669	0.6545
	5	21.5873	2.7464	0.6360
	6	21.2677	2.8254	0.6701
	7	Damaged Specimen		
	8	17.4711	2.6318	0.6495
	9	16.6006	2.6128	0.6636
	10	16.7034	2.6618	0.6946
	11	16.0307	2.5467	0.6318
	12	15.2089	2.5538	0.6750
5% DS	1	19.8935	2.4596	0.5531
	2	19.7613	2.4516	0.5298
	3	20.4934	2.4847	0.6000
	4	Damaged Specimen		
	5	18.4316	2.3798	0.5392
	6	18.7209	2.4725	0.5443
	7	17.7508	2.4415	0.5539
	8	14.4269	2.2455	0.5743
	9	15.0072	2.2726	0.5802
	10	15.8954	2.3536	0.5656
	11	15.4444	2.3286	0.5528
	12	18.1452	2.4497	0.5744
10% DS	1	19.2321	2.3921	0.5047
	2	18.0687	2.2978	0.4798
	3	18.4548	2.3312	0.4854
	4	19.3945	2.3988	0.4879
	5	19.7068	2.3794	0.4826
	6	24.4289	2.4543	0.5000
	7	20.8123	2.4744	0.4888
	8	21.6024	2.4415	0.5009
	9	21.1026	2.4394	0.4785
	10	Damaged Specimen		
	11	23.4013	2.5318	0.5204
	12	18.3382	2.3579	0.5112

Table B.6 (Cont.). Tensile modulus, tensile strength and strain at break.

Sample		Young modulus (Mpa)	Tensile Strength (Mpa)	Strain at Break (mm/mm)
20% DS	1	21.5243	2.3208	0.4204
	2	21.4113	2.3153	0.4345
	3	26.9987	2.4384	0.4238
	4	28.9671	2.4761	0.3891
	5	28.5534	2.3617	0.3246
	6	29.1864	2.2288	0.2939
	7	23.9238	2.3053	0.3774
	8	23.8712	2.4187	0.4190
	9	Damaged Specimen		
	10	23.1379	2.3536	0.4109
	11	23.4954	2.3348	0.3917
	12	26.3604	2.0649	0.2632
1% MMT	1	23.6383	2.5502	0.4839
	2	18.5428	2.4036	0.4572
	3	21.8779	2.4783	0.4428
	4	22.8044	2.4345	0.4465
	5	19.8326	2.4817	0.4493
	6	22.0794	2.4934	0.4568
	7	23.6397	2.6349	0.4891
	8	24.1681	2.6189	0.5074
	9	Damaged Specimen		
	10	19.1480	2.1316	0.3796
	11	21.8081	2.3303	0.4376
	12	16.8407	2.0296	0.3440
2% MMT	1	23.0537	2.2106	0.3374
	2	20.2684	2.1118	0.3550
	3	20.0622	2.1063	0.3565
	4	19.8972	2.0761	0.3568
	5	20.0612	2.0880	0.3491
	6	23.0439	2.2598	0.3426
	7	20.1775	2.2836	0.3786
	8	22.0643	2.2517	0.3774
	9	22.3890	2.2456	0.3741
	10	21.7069	2.2352	0.3544
	11	21.6705	2.2377	0.3610
	12	22.9530	2.3012	0.3507

Table B.6 (Cont.). Tensile modulus, tensile strength and strain at break.

Sample		Young modulus (Mpa)	Tensile Strength (Mpa)	Strain at Break (mm/mm)
3% MMT	1	17.7407	1.9935	0.3401
	2	27.6386	2.3388	0.3488
	3	25.7381	2.3212	0.3499
	4	22.5812	2.1449	0.3587
	5	26.1921	2.3559	0.3791
	6	29.0341	2.4193	0.3732
	7	30.0279	2.4745	0.3921
	8	25.6886	2.4205	0.3824
	9	25.2795	2.4002	0.3526
	10	25.7200	2.3210	0.3337
	11	26.7109	2.3493	0.3753
	12	19.8751	2.0472	0.3415
5% MMT	1	21.3740	1.3968	0.1744
	2	34.1853	2.5424	0.2946
	3	31.5484	2.0606	0.2065
	4	36.1399	1.6839	0.1373
	5	32.4435	2.1703	0.2106
	6	34.0048	2.4292	0.2667
	7	16.0990	1.4921	0.2004
	8	24.5469	1.7139	0.1972
	9	26.3309	2.1302	0.3092
	10	22.8460	2.1102	0.3138
	11	21.5517	1.7399	0.2469
	12	21.0008	1.6744	0.2293
2% CNC	1	12.9189	2.0356	0.7667
	2	12.5392	2.0242	0.7759
	3	13.9808	2.0894	0.7996
	4	14.5277	2.0898	0.7711
	5	14.5617	2.1022	0.8052
	6	14.9262	2.1021	0.8248
	7	14.6630	2.0806	0.8528
	8	15.6446	2.0935	0.8341
	9	15.9701	2.1199	0.8364
	10	16.7158	2.1279	0.8093
	11	Damaged Specimen		
	12	15.6254	2.1697	0.8540

Table B.6 (Cont.). Tensile modulus, tensile strength and strain at break.

Sample		Young modulus (Mpa)	Tensile Strength (Mpa)	Strain at Break (mm/mm)
3% CNC	1	16.5931	2.4743	1.0470
	2	19.2880	2.5037	1.0268
	3	Damaged Specimen		
	4	18.8193	2.5010	1.0937
	5	18.7242	2.4831	1.1140
	6	18.0952	2.4549	1.0742
	7	17.9180	2.3991	1.1098
	8	20.4652	2.5491	1.1165
	9	Damaged Specimen		
	10	16.9118	2.3921	1.0658
	11	19.5500	2.5362	1.0929
	12	18.2363	2.5211	1.0958
5% CNC	1	19.1909	2.3651	0.9708
	2	23.4512	2.2416	0.6924
	3	23.3519	2.3404	0.8465
	4	24.4116	2.2465	0.7041
	5	27.2752	2.5103	0.9655
	6	Damaged Specimen		
	7	24.7385	2.4683	1.0480
	8	24.9532	2.5025	1.0561
	9	22.8576	2.3552	0.8529
	10	25.1404	2.5016	0.9904
	11	25.8506	2.4949	0.9284
	12	24.3732	2.4416	0.8946

Table B.7. Average tensile modulus, tensile strength and strain at break for starch-based composites, with their respective standard deviation.

Sample	Avg. Young modulus (Mpa)	Std Dev	Avg. Tensile Strength (Mpa)	Std Dev	Avg. Strain at break (mm/mm)	Std Dev
Plasticized Starch						
PS	14.64	2.56	2.22	0.16	0.58	0.04

Table B.7 (Cont.). Average tensile modulus, tensile strength and strain at break for starch-based composites, with their respective standard deviation.

Sample	Avg. Young modulus (Mpa)	Std Dev	Avg. Tensile Strength (Mpa)	Std Dev	Avg. Strain at break (mm/mm)	Std Dev
MFT Composites						
1% MFT	16.23	2.62	2.26	0.15	0.55	0.04
2% MFT	15.21	2.93	2.04	0.14	0.47	0.04
3% MFT	16.09	2.78	2.03	0.13	0.47	0.04
5% MFT	17.79	2.72	2.07	0.06	0.44	0.02
10% MFT	21.23	2.90	2.03	0.06	0.39	0.03
20% MFT	24.24	0.90	2.02	0.07	0.33	0.03
DS Composites						
1% DS	18.16	1.61	2.60	0.10	0.69	0.06
2% DS	19.06	1.39	2.70	0.08	0.70	0.05
3% DS	18.79	2.50	2.69	0.09	0.65	0.02
5% DS	17.63	2.12	2.39	0.08	0.56	0.02
10% DS	20.41	2.09	2.41	0.07	0.49	0.01
20% DS	25.22	2.90	2.33	0.11	0.38	0.06
MMT Composites						
1% MMT	21.31	2.39	2.42	0.19	0.44	0.05
2% MMT	21.45	1.28	2.20	0.08	0.36	0.01
3% MMT	25.19	3.55	2.30	0.15	0.36	0.02
5% MMT	26.84	6.57	1.93	0.36	0.23	0.06
CNC Composites						
2% CNC	14.73	1.26	2.09	0.04	0.81	0.03
3% CNC	18.46	1.18	2.48	0.05	1.08	0.03
5% CNC	24.14	2.05	2.41	0.10	0.90	0.12

B.4. Compressive Properties

The measurement of compressive properties recorded the compressive modulus, compressive strength and compression at break for each specimen of each composite. The obtained values are shown in table B.8. As with tensile properties, an average and a standard

deviation were calculated for each filler percentage and each type of filler, generating the values shown in table B.9.

Table B.8. Compressive modulus, compressive strength and compression at break.

Sample		Compressive Modulus (Mpa)	Compressive Strength (Mpa)	Compression at break (mm/mm)
PS	1	480.8900	2123.0440	6.2930
	2	473.0930	2312.4008	6.7660
	3	479.7745	2214.3875	6.0490
	4	471.5164	2215.2044	6.2640
1% MFT	1	498.3394	2257.1764	6.1990
	2	488.1050	2240.6582	6.6460
	3	463.0869	2194.6451	6.8560
2% MFT	1	460.3920	2010.0153	6.2210
	2	407.9500	1988.8798	6.4320
	3	402.4150	1863.6030	6.1910
	4	408.2026	1955.0079	6.2650
5% MFT	1	543.4268	2421.8960	7.6790
	2	526.5429	2465.9415	7.9300
	3	531.5120	2753.0780	8.6870
	4	563.6950	2671.8100	8.4750
	5	530.6607	2749.6530	8.1790
10% MFT	1	522.7233	1847.9604	5.8960
	2	495.8869	1920.4628	6.8470
	3	529.0146	1954.7102	6.5020
20% MFT	1	570.7384	1867.4799	5.939
	2	603.3030	2079.7044	6.1740
	3	552.9781	2114.0661	6.8330
	4	665.9447	2173.7404	6.6980
1% DS	1	492.5934	2694.5531	7.5640
	2	455.8927	2624.4998	7.6780
	3	499.0600	2795.6044	7.8720
2% DS	1	416.6888	2160.6932	6.9780
	2	459.0210	2185.1361	7.4310
	3	500.6724	2220.3896	7.3300
	4	478.0917	2227.6050	7.3480

Table B.8 (Cont.). Compressive modulus, compressive strength and compression at break.

Sample		Compressive Modulus (Mpa)	Compressive Strength (Mpa)	Compression at break (mm/mm)
5% DS	1	661.1776	2068.0275	6.6070
	2	483.9438	2104.2427	7.2490
	3	549.7922	2208.1444	7.5760
	4	591.3582	1950.0210	6.7180
10% DS	1	650.0050	2031.5351	6.7600
	2	546.0785	2007.6154	6.7340
	3	617.1765	1797.5749	6.5190
	4	606.2162	1925.9729	6.4360
20% DS	1	458.1045	1848.3461	6.8550
	2	730.2032	1943.1807	6.0250
	3	571.4385	1657.6494	5.9930
	4	744.0232	1929.4651	6.3760
1% MMT	1	475.6349	1960.3687	6.4690
	2	414.9407	1958.9534	6.3670
	3	506.9979	1747.5336	5.6110
	4	484.0961	2094.0448	6.4260
2% MMT	1	502.0018	1502.5745	5.8350
	2	521.1123	1574.4589	6.0560
	3	543.5836	1602.9680	5.9700
	4	535.2740	1537.5282	5.9160
5% MMT	1	474.9158	901.7313	3.4380
	2	407.6297	757.1677	2.7720
	3	483.1476	966.0295	4.3590
	4	491.9450	832.5663	3.5770
1% CNC	1	339.9443	1478.9993	5.2290
	2	369.7510	1613.0899	4.9440
	3	370.3168	1509.8776	5.1850
	4	378.5602	1445.4116	4.9100
2% CNC	1	344.2307	1508.5568	6.7410
	2	341.8175	1454.0690	5.7240
	3	364.3321	1601.2883	6.6290
	4	318.3569	1357.6097	5.6080
5% CNC	1	204.0750	1063.9318	7.6700
	2	211.6369	843.9644	6.4620
	3	215.8477	1023.2407	6.5360
	4	180.1756	738.5412	5.6290

Table B.9. Average compressive modulus, compressive strength and compression at break for starch-based composites, with their respective standard deviation.

Sample	Avg. Compressive Modulus (Mpa)	Std Dev	Avg. Compressive Strength (Mpa)	Std Dev	Avg. Compression at break (mm/mm)	Std Dev
Plasticized Starch						
PS	476.32	4.70	2216.26	77.32	6.34	0.30
MFT Composites						
1% MFT	483.18	18.14	2230.83	32.40	6.57	0.34
2% MFT	419.74	27.23	1954.38	64.62	6.28	0.11
5% MFT	539.17	15.08	2612.48	158.03	8.19	0.41
10% MFT	515.87	17.59	1907.71	54.51	6.42	0.48
20% MFT	598.24	49.71	2058.75	133.30	6.41	0.42
DS Composites						
1% DS	482.52	23.28	2704.89	86.02	7.70	0.16
2% DS	463.62	35.62	2198.46	31.27	7.27	0.20
5% DS	571.57	74.33	2082.61	106.49	7.04	0.46
10% DS	604.87	43.39	1940.67	105.56	6.61	0.16
20% DS	625.94	136.57	1844.66	131.51	6.31	0.40
MMT Composites						
1% MMT	470.42	39.29	1940.23	143.23	6.22	0.41
2% MMT	525.49	18.20	1554.38	43.71	5.94	0.09
5% MMT	464.41	38.49	864.37	89.88	3.54	0.65
CNC Composites						
1% CNC	364.64	16.95	1511.84	72.45	5.07	0.16
2% CNC	342.18	18.82	1480.38	101.94	6.18	0.59
5% CNC	202.93	15.93	917.42	152.81	6.57	0.84

Appendix C
Thermal Conductivity Measurement of MFT composites

C.1 General

Since one of the possible applications for the starch composites was as an insulation material, the measurement of thermal conductivity of the specimens was required to determine how effective these composites were as insulators. Unfortunately, the thermal conductivity results were not comparable to those of other insulation materials because for starch-composites to compete with insulation materials, they would have to be turned into foams, which was not the initial objective of this work.

In this appendix, we describe the method and equipment used to measure the thermal conductivity and the related results, as a guideline for future work on starch-composite foams.

C.2 Method and Equipment

A Thermtest 2500 thermal constants analyzer measured the thermal conductivity of 1.5 in x 1.5 in x 0.5 in pieces cut from thick sheets of polymer composite with a knife and a ruler. For each measurement, two pieces were put together with the sensor in the middle and kept tight with a screw while the machine measured the thermal conductivity of the samples.

C.3 Thermal Conductivity Results

Figure C.1 shows that thermal conductivity of MFT, DS, and MMT composites increases for higher filler contents, which disqualifies their use as thermal insulators. Vajihinejad and Soares (2016) explained that the thermal conductivity of foams happens by conduction through the polymer phase, by radiation and by gas, and since foams have cells, the number and size affect the thermal conductivity. In the case of the starch composites made in this work there are no cells as in foams, therefore the main mechanism is conduction, which is increased with the addition of solid fillers.

A positive point for these composites is the fact that as water is lost, the thermal conductivity decreases, but further studies in thermal conductivity should be centered in starch-based composite foams with no water in their structure.

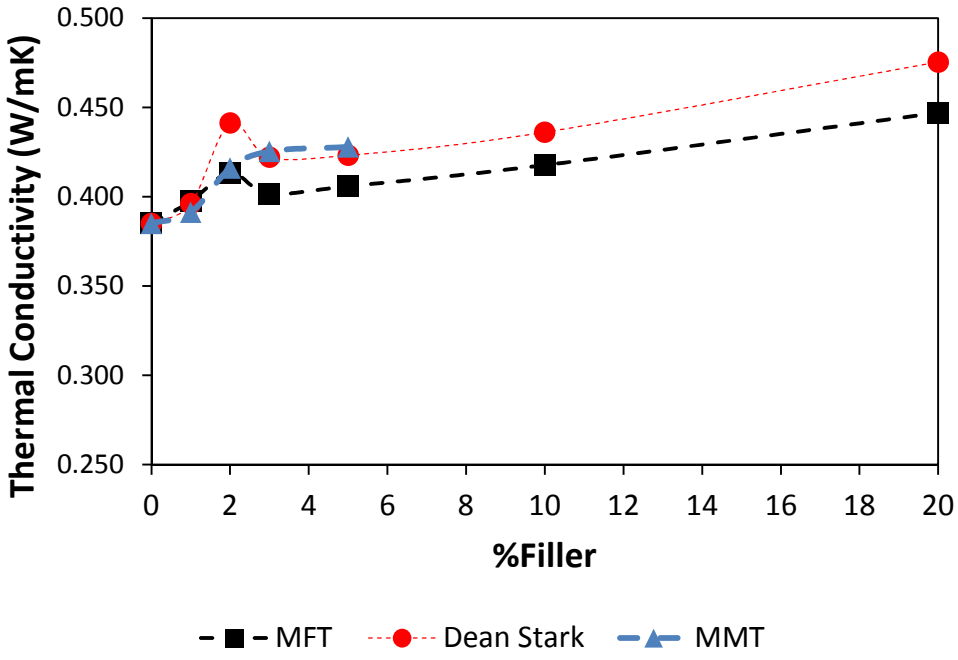

Figure C.1. Thermal conductivity of MFT, DS, and MMT composites as a function of filler content.

References

Vajihinejad, V., & Soares, J. B. P. (2016). Can We Make Better Polyurethane Composite Foams with Oil Sands Mature Fine Tailing? *Macromolecular Materials and Engineering*, *301*(4), 383–389. http://doi.org/10.1002/mame.201500396